Orbital

The Electronic Journal of Chemistry

Pd
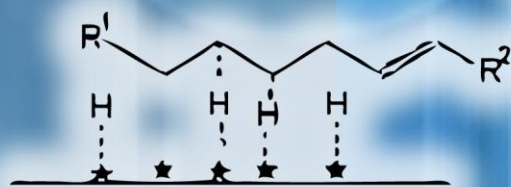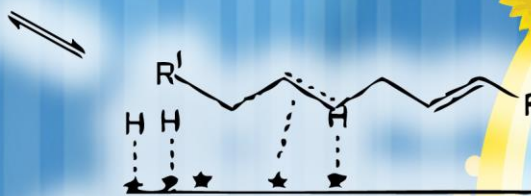
UFMS

Orbital - Vol. 2 No. 2 - April-June 2010

Table of Contents

FULL PAPERS

Full Paper

Removal of malachite green from aqueous solution by activated carbon prepared from the *Annona squmosa* seed *by adsorption*

T. Santhi[a]*, S. Manonmani[b], T. Smith[a]

[a]Department of Chemistry, Karpagam University, Coimbatore-641021, India
[b]Department of Chemistry, PSG College of Arts and Science, Coimbatore-641014, India

ABSTRACT: *The use of low -cost, locally available, highly efficient and eco-friendly adsorbents has been investigated as an ideal alternative to the current expensive methods of removing dyes from wastewater. This study investigates the potential use of activated carbon prepared from the Annona squmosa seed for the removal of malachite green (MG) dye from simulated wastewater. The effects of different system variables, adsorbent dosage, initial dye concentration, pH and contact time were investigated and optimal experimental conditions were ascertained. The results showed that as the amount of the adsorbent is increased, the percentage of dye removal increase accordingly. Optimum pH value for dye adsorption was 7.0. Maximum dye was sequestered within 50 min from the start of every experiment. The adsorption of malachite green followed the pseudo-second –order rate equation and fits the Langmuir, Freundlich, Dubinin-Radushekevich (D-R) and Tempkin equations well. The maximum removal of MG was obtained at pH 7 as 86.11% for adsorbent dose of 0.2 g/ 50 mL and 25 mg L $^{-1}$ initial dye concentration at room temperature. Furthermore, adsorption kinetics of MG was studied and the rate of adsorption was found to conform to pseudo-second –order kinetics with a good correlation ($R^2 > 0.99$) with intraparticle diffusion as one of the rate determining steps. Activated carbon developed from the Annona squmosa seed can be an attractive option for dye removal from diluted industrial effluents since test reaction made on simulated dyeing wastewater showed better removal percentage of MG.*

Keywords: *Annona squmosa*; *adsorption*; *wastewater*; *malachite green*; *kinetics*; *activated carbon*

Introduction

---

* Corresponding author. E-mail: ssnilasri@yahoo.co.in

Industrial effluents are one of the major causes of environmental pollution because effluents discharged from dyeing industries are highly colored with a large amount of suspended organic solids [1]. Untreated disposal of this colored water into the receiving water body either causes damage to aquatic life or to human beings by their mutagenic and carcinogenic effect. The discharge of such effluents is worrying for both toxicological and environmental reasons [2, 3].

Conventional wastewater treatment methods for removing dyes include physicochemical, chemical and biological methods, such as coagulation and flocculation [4], adsorption [5], ozonation [6], electrochemical techniques [7], and fungal decolonization [8]. Among these methods adsorption has gained favors in recent years due to proven efficiency in the removal of pollutants from effluents. Activated carbon, as an adsorbent has been widely investigated for the adsorption of dyes [9], but its high cost limits its commercial application. In recent years, there has been growing interest in finding inexpensive and effective alternatives to carbon, such as rice husk [10], chitin [11], orange waste [12], lemon peel [13], granular kohlrabi peel [14], raw barley straw [15] , eggshell [16].

Annona squmosa is a commonly available hedge plant, which is used in fencing property perimeter in Kenerapallam, Palaghat Dt, Kerala. Foliage of the plant is thick and fruits are in abundance during the season. The inner core of the ripe fruit is delicious and of nutritive value and commonly consume. The seeds are nonedeble and available free of cost, only the carbonization of its involved for the waste water treatment. Therefore the main objective of this study was to evaluate the possibility of using dried *Annona squmosa* seed to develop a new low –cost activated carbon and study its application to remove malachite green from simulated wastewater. Granulized *Annona squmosa* seed was previously investigated to adsorb cationic dyes [17]. The parameters such as pH, adsorbent dose, adsorbent particle size, initial dye concentration and time are systematically evaluated.

Material and Methods

Preparation of activated carbon from the Annona squmosa seed (CAS)

The *Annona squmosa* seed was air-dried and powdered in a grinder. It was soaked in concentrated H_2SO_4 for 12 hours and washed thoroughly with distilled water until it attained neutral pH and soaked in two percent $NaHCO_3$ overnight. Then the material was washed with distilled water and dried at 110 ± 2 ^0C. The dry biomass was crushed into granules, sieved to different particle sizes, and then preserved in desiccators for use.

A stock solution of 500 mgL^{-1} was prepared by dissolving the appropriate amount of MG (obtained from s. d. Fine Chemicals, Mumbai, India) in 100 mL and made to 1000

102

Orbital Elec. J. Chem*., Campo Grande, 2(2): 101-117, 2010*

mL with distilled water. Different concentrations ranged between 25 and 200 mgL^{-1} of MG were prepared from the stock solution. All the chemicals used throughout this study were of analytical-grade reagents. Double-distilled water was used for preparing all of the solutions and reagents. The initial pH was adjusted with 0.1 M HCl or 0.1 M NaOH. All the adsorption experiments were carried out at room temperature (27 ±2 ^{0}C).

Batch adsorption studies

Effect of pH on MG adsorption

The effect of pH on the equilibrium uptake of dyes was investigated by employing an initial concentration of MG (100mg/L) and 0.2 g/50 mL of CAS. The initial pH values were adjusted with 0.1 M HCl or NaOH to form a series of pH from 2 to 10. The suspensions were shaken at room temperature (27 ±2 ^{0}C) using agitation speed (150 rpm) , the minimum contact time required to reach the equilibrium (100 min) and the amount of MG adsorbed determined.

Effect of CAS dose on MG adsorption

The effect of adsorbent dose on the equilibrium uptake of MG (100 mgL^{-1}) was investigated with CAS concentrations of 0.2, 0.4 and 0.6 g/ 50mL. The experiments were performed by shaking a known MG concentration with the different CAS concentrations to the equilibrium uptake (100 min) and the amount of MG adsorbed was determined.

Kinetics studies

Adsorption studies were conducted in 250 mL-shaking flasks with a solution of pH 7.0. CAS (0.2g/50 mL) was thoroughly mixed individually with 50 mL of MG solution (100 mg/L) and the suspensions were shaken at room temperature. Samples of 1.0 mL were collected from the duplicate flasks at required time intervals viz. 10, 20, 30, 40, 50, 60, 70, 80, 90 and 100 min. and were centrifuged for 5 min. The clear solutions were analyzed for residual MG concentration in the solutions.

Adsorption isotherm

Batch adsorption experiments were carried out in a rotary shaker at 150 rpm using 250 mL-shaking flasks at room temperature for 100 min. The CAS (0.2 g) was thoroughly mixed with 50 mL of MG solutions. The isotherm studies were performed by varying the initial MG concentrations from 25 to 200 mg/L at pH 7.0, which was adjusted using 0.1 M HCl or 0.1 M NaOH before addition of CAS and maintained throughout the experiment. After shaking the reaction mixture was analyzed for the residual MG concentration.

The concentration of MG in solution was measured by using direct UV-vis spectrophotometric method using a Systronic Spectrophotometer-104. All the

103

Orbital Elec. J. Chem., Campo Grande, 2(2): 101-117, 2010

experiments were duplicated and only the mean values are reported. The maximum deviation observed was less than ±4%.

Adsorption of MG from simulated wastewater was studied using 0.2g/50 mL of CAS and MG concentrations 100 mg/L at initial pH 7.0. The amount of dye adsorbed at equilibrium onto carbon, q_e (mg/g), was calculated by the following mass balance relationship:

$$q_e = (C_0 - C_e) V/W \qquad (1)$$

where C_0 and C_e (mg/L) are the initial and the equilibrium liquid–phase concentration of MG, respectively, V the volume of the solution(L), and W is the weight of the CAS used(g).

Results and Discussion

Effect of system pH on MG Uptake

The pH of the system exerts profound influence on the adsorptive uptake of adsorbate molecules presumably due to its influence on the surface properties of the adsorbent and ionization/dissociation of the adsorbate molecule. Fig. 1 shows the variations in the removal of dye from wastewater at different system pH. From the figure, it is evident that the maximum removal of MG color is observed at pH 7. Similar trend of pH effect was observed for the adsorption of malachite green on activated carbon prepared from fly ash [18] and tuncbilek lignite [19]. Which may be attributed to the hydrophobic nature of the developed carbon which led to absorb hydrogen ions (H^+) onto the surface of the carbon when immersed in water and made it positively charged. Low pH value (1.0 to 3.0) leads to an increase in H^+ ion concentration in the system and the surface of the activated carbon acquires positive charge by absorbing H^+ ions. On the other hand, increase of the pH value (7) led to increase of the number of negatively charged sites. As the CAS surface is negatively charged at high pH, a significantly strong electrostatic attraction appears between the negatively charged carbon surface and cationic dye molecule leading to maximum adsorption of MG [20] from waste water. The lowest adsorption occurred at pH 2.0 and the highest adsorption occurred at pH ~6.0. Adsorbents surface would be positively charged up to pH<4, and heterogeneous in the pH range 4–6. Thereafter, it should be negatively charged. Moreover, the increasing in the adsorption of MG with increasing of pH value is also due to the attraction between cationic dye and excess OH^- ions in the solution.

Effect of contact time and initial MG concentration

The relation between removal of MG and reaction time were studied to see the rate of dye removal. The results of percentage removal of MG at pH 7.0 with increase of

104

Orbital Elec. J. Chem*., Campo Grande*, 2(2): 101-117, 2010

contact time using CAS are presented in Fig. 2. It was found that more than 50% removal of MG concentration occurred in the first 30 min, and thereafter the rate of adsorption of the MG onto CAS was found to be slow. The rapid adsorption at the initial contact time is due to the highly negatively charged surface of the CAS for adsorption of cationic MG in the solution at pH 7. Later slow rate of MG adsorption is probably due to the electrostatic hindrance or repulsion between the adsorbed positively charged adsorbate species onto the surface of CAS and the available cationic adsorbate species in the solution as well as the slow pore diffusion of the solute ions into the bulk of the adsorbent. The equilibrium was attained at 100 min when the maximum MG adsorption onto CAS was reached.
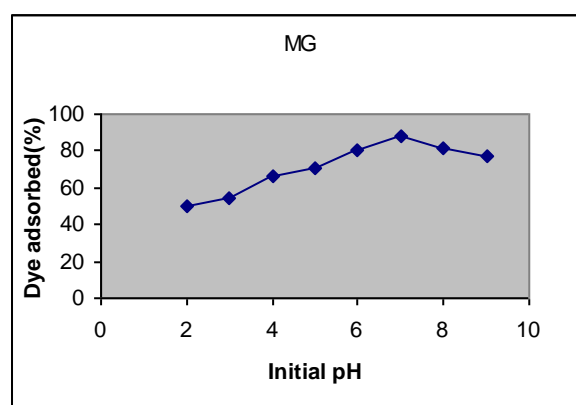
Figure 1. Effect of system pH on adsorption of MG (100 mg L^{-1}) onto CAS (0.2 g/50mL) at room temperature (27±2 °C), agitation speed 150 rpm for the minimum contact time required to reach the equilibrium (100 min).
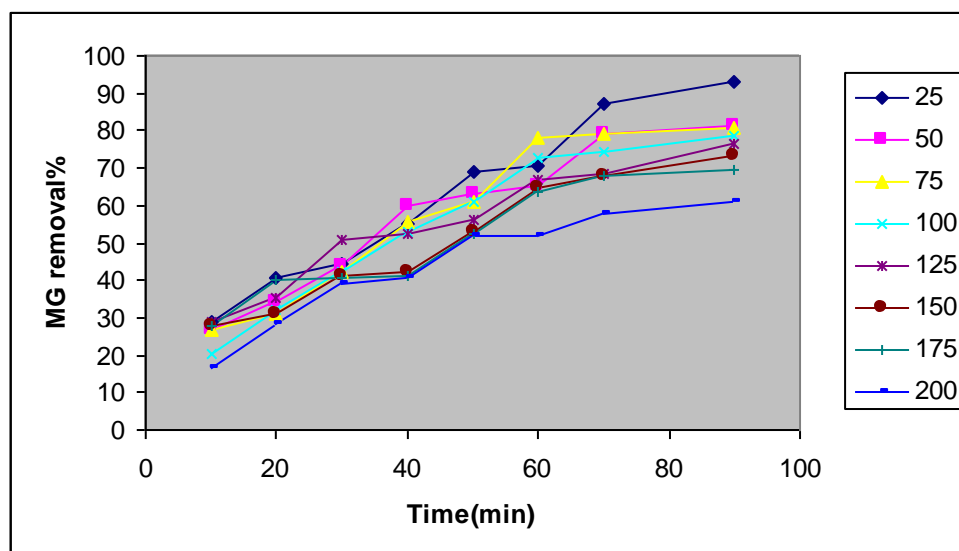
Figure 2. Effect of contact time on the removal of different initial concentrations of MG using CAS (0.2 g/50mL) at pH 7.0.

Also, the effect of initial concentration of MG in the solution on the capacity of

105

Orbital Elec. J. Chem*., Campo Grande, 2(2): 101-117, 2010*

adsorption onto CAS was studied and is shown in Fig. 2. The experiments were carried out at fixed adsorbent dose (0.2 g/50 mL) in the test solution at room temperature (27±2 °C), pH 7 and at different initial concentrations of MG (25, 50, 75, 100, 125, 150, 175 and 200 mgL^{-1}) for different time intervals (10, 20, 30, 40, 50, 60, 70, 80, 90 and 100 min.). Fig. 2 shows that the percentage of adsorption efficiency of CAS decreased with the increase of initial MG concentration in the solution. Though the percent adsorption decreased with increase in the initial dye concentration, the actual amount of MG adsorbed per unit mass of adsorbent increased with increase in MG concentration in the test solution. It is evident from Fig. 2 that the amount adsorbed on the solid phase CAS at a lower initial concentration of MG was smaller than the corresponding amount when higher initial concentrations were used. However, the percentage of removal of MG was greater at lower initial concentrations and smaller at higher initial concentrations. The adsorption capacity for CAS was increased from 5.38 to 31.15mg g^{-1} as the MG concentration increased from 25 to 200 mgL^{-1}. In the process of MG adsorption initially dye molecules have to first encounter the boundary layer effect and then it has to diffuse from boundary layer film onto adsorbent surface and then finally, it has to diffuse into the porous structure of the adsorbent. This phenomenon will take relatively longer contact time.

Effect of adsorbent mass on MG adsorption

The adsorption of MG on CAS was studied by changing the quantity of adsorbent (0.2, 0.3, 0.4, 0.5 and 0.6 g/50 mL) in the test solution while keeping the initial MG concentration (100 mgL^{-1}), temperature (27±2 °C) and pH (7.0) constant at contact times for 100 min (Fig. 3). The adsorption increased from 79.79% to 82.69%, as the CAS dose increased from 0.2 g to 0.6 g/50 mL at equilibrium time (100 min). Maximum MG removal was achieved within 10–50 min after which MG concentration in the reaction solution was almost constant. Increase in the adsorption with adsorbent dose can be attributed to the increase of MG surface area and availability of more adsorption sites, while the unit adsorbed of MG decrease with increase in CAS dose.

Isotherm data analysis

The relationship between the amount of a substance adsorbed at constant temperature and its concentration in the equilibrium solution is called the adsorption isotherm. The adsorption isotherm is important from both a theoretical and a practical point of view. In order to optimize the design of an adsorption system to remove the dye, it is important to establish the most appropriate correlations of the equilibrium data of each system. Equilibrium isotherm equations are used to describe the experimental adsorption data. The parameters obtained from the different models provide important information on the adsorption mechanisms and the surface properties and affinities of the

106

Orbital Elec. J. Chem., Campo Grande, 2(2): 101-117, 2010

adsorbent. The most widely accepted surface adsorption models for single-solute systems are the Langmuir and Freundlich models. The correlation with the amount of adsorption and the liquid-phase concentration was tested with the Langmuir, Freundlich, Tempkin and Dubinin–Radushkevich (D–R) isotherm equations. Linear regression is frequently used to determine the best-fitting isotherm, and the applicability of isotherm equations is compared by judging the correlation coefficients.
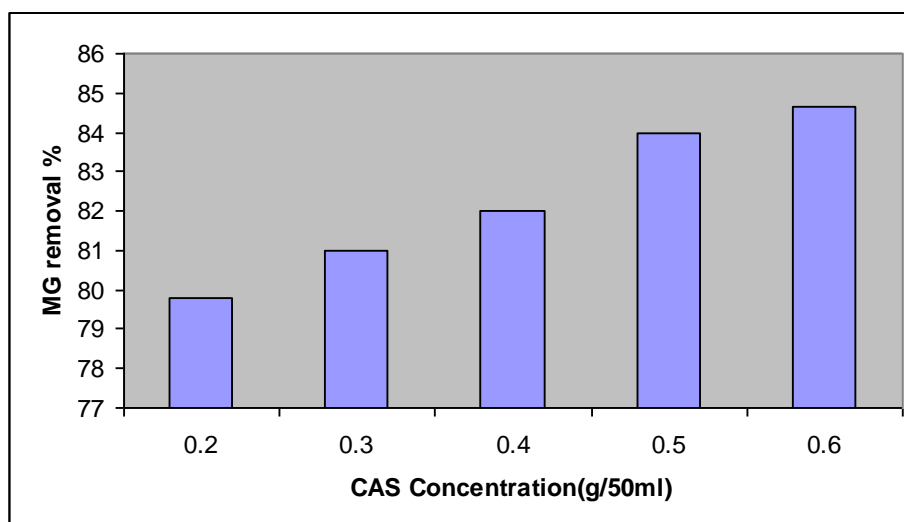
Figure 3. Effect of adsorbent concentration on MG removals (C_0: 100 mgL^{-1}, pH 7.0, agitation speed: 150 rpm, temperature: 27±2 °C).

Langmuir isotherm

The theoretical Langmuir isotherm [21] is valid for adsorption of a solute from a liquid solution as monolayer adsorption on a surface containing a finite number of identical sites. Langmuir isotherm model assumes uniform energies of adsorption onto the surface without transmigration of adsorbate in the plane of the surface [22]. Therefore, the Langmuir isotherm model was chosen for estimation of the maximum adsorption capacity corresponding to complete monolayer coverage on the adsorbent surface. The Langmuir non-linear equation is commonly expressed as followed:

$$q_e = \frac{Q_m K_a C_e}{1 + K_a C_e} \qquad (2)$$

In Eq. (2), C_e and q_e are defined as before in Eq. (1), Q_m is a constant and reflect a complete monolayer (mgg^{-1}); K_a is the adsorption equilibrium constant (Lmg^{-1}) that is related to the apparent energy of sorption. The Langmuir isotherm Eq. (2) can be linearized into the following form [23, 24].

Langmuir-1 $$\frac{C_e}{q_e} = \frac{1}{K_a Q_m} + \frac{1}{Q_m} \times C_e \qquad (3)$$

107

Orbital Elec. J. Chem*., Campo Grande*, 2(2): 101-117, 2010

A plot of C_e/q_e versus C_e should indicate a straight line of slope $1/Q_m$ and an intercept of $1/(K_aQ_m)$.

The results obtained from the Langmuir model for the removal of MG onto CAS are shown in Table 1. The correlation coefficients reported in Table 1 shown strong positive evidence on the adsorption of MG onto CAS follows the Langmuir isotherm. The applicability of the linear form of Langmuir model to CAS was proved by the high correlation coefficients $R^2 > 0.96$. This suggests that the Langmuir isotherm provides a good model of the sorption system. The maximum monolayer capacity Q_m obtained from the Langmuir is 25.91 mgg^{-1}.

The Freundlich isotherm

The Freundlich isotherm model [25] is the earliest known equation describing the adsorption process. It is an empirical equation and can be used for non-ideal sorption that involves heterogeneous adsorption. The Freundlich isotherm can be derived assuming a logarithmic decrease in the enthalpy of adsorption with the increase in the fraction of occupied sites and is commonly given by the following non-linear equation:

$$q_e = K_F C_e^{1/n} \tag{4}$$

where K_F is a constant for the system, related to the bonding energy. K_F can be defined as the adsorption or distribution coefficient and represents the quantity of dye adsorbed onto adsorbent for unit equilibrium concentration. $1/n$ is indicating the adsorption intensity of dye onto the adsorbent or surface heterogeneity, becoming more heterogeneous as its value gets closer to zero. A value for $1/n$ below 1 indicates a normal Langmuir isotherm while $1/n$ above 1 is indicative of cooperative adsorption. Eq. (4) can be linearized in the logarithmic form (Eq.(5)) and the Freundlich constants can be determined:

$$\log q_e = \log K_F + \frac{1}{n}\log C_e \tag{5}$$

The applicability of the Freundlich adsorption isotherm was also analyzed, using the same set of experimental data, by plotting $\log(q_e)$ versus $\log(C_e)$. The data obtained from linear Freundlich isotherm plot for the adsorption of the MG onto CAS is presented in Table 1. The correlation coefficients (>0.904) showed that the Freundlich model is comparable to the Langmuir model. The $1/n$ is lower than 1.0, indicating that MG is favorably adsorbed by CAS.

The Tempkin isotherm

Tempkin adsorption isotherm model was used to evaluate the adsorption potentials of the CAS for MG. The derivation of the Tempkin isotherm assumes that the

fall in the heat of adsorption is linear rather than logarithmic, as implied in the Freundlich equation. The Tempkin isotherm has commonly been applied in the following form [26-28]:

$$q_e = \frac{RT}{b}\ln(AC_e) \tag{6}$$

The Tempkin isotherm Eq. (6) can be simplified to the following equation:

$$q_e = \beta \ln a + \beta \ln C_e \tag{7}$$

where $\beta = (RT)/b$, T is the absolute temperature in Kelvin and R is the universal gas constant, 8.314 J (mol K)$^{-1}$. The constant b is related to the heat of adsorption [29-30].

Table 1. Comparison of the coefficients isotherm parameters for MG adsorption onto CAS.

Isotherm model	CAS concentrations (g/50mL)
	0.2 (g /50mL)
Langmuir	
Q_m (mg g^{-1})	25.91
K_a (L mg^{-1})	0.1545
R^2	0.9602
Freundlich	
$1/n$	0.4916
K_F (mg g^{-1})	3.7879
R^2	0.9039
Tempkin	
a (L g^{-1})	0.5537
β (mg L^{-1})	7.9805
b	312.54
R^2	0.9667
Dubinin−Radushkevich	
Q_m (mg g^{-1})	25.287
K (×10-5 mol^2 kJ^{-2})	0.7
E (kJ mol^{-1})	0.2673

The adsorption data were analyzed according to the linear form of the Tempkin isotherm equation (7). Examination of the data shows that the Tempkin isotherm fitted well the MG adsorption data for CAS. The linear isotherm constants and coefficients of determination are presented in Table 1. The correlation coefficients R^2 obtained from Tempkin model were comparable to that obtained for Langmuir and Freundlich equations, which explain the applicability of Tempkin model to the adsorption of MG onto CAS.

The Dubinin−Radushkevich (D−R) isotherm

The D−R model was also applied to estimate the porosity apparent free energy

Orbital Elec. J. Chem., Campo Grande, 2(2): 101-117, 2010

109

and the characteristics of adsorption [31-33]. The D–R isotherm dose not assumes a homogeneous surface or constant adsorption potential. The D–R model has commonly been applied in the following Eq. (8) and its linear form can be shown in Eq. (9):

$$q_e = Q_m \exp(-K\varepsilon^2) \tag{8}$$

$$\ln q_e = \ln Q_m - K\varepsilon^2 \tag{9}$$

where K is a constant related to the adsorption energy, Q_m the theoretical saturation capacity, ε the Polanyi potential, calculated from Eq. (10).

$$\varepsilon = RT \ln \left(1 + \frac{1}{C_e} \right) \tag{10}$$

The slope of the plot of $\ln q_e$ versus ε^2 gives K (mol^2 (kJ^2)$^{-1}$) and the intercept yields the adsorption capacity, Q_m (mg g^{-1}). The mean free energy of adsorption (E), defined as the free energy change when one mole of ion is transferred from infinity in solution to the surface of the solid, was calculated from the K value using the following relation [34]:

$$E = \frac{1}{\sqrt{2K}} \tag{11}$$

The calculated value of D–R parameters is given in Table 1. The saturation adsorption capacity Q_m obtained using D–R isotherm model for adsorption of MG onto CAS is 25.29 mgg^{-1} at 0.2g/50 mL adsorbent dose, which is close to that obtained (25.91 mgg^{-1}) from the Langmuir isotherm model (Table 1). The values of E calculated using Eq. (11) is 0.2673 kJ mol^{-1} which indicates that the physical-sorption process plays a significant role in the adsorption of MG onto CAS.

Kinetic models applied to the adsorption of MG onto CAS

Several steps can be used to examine the controlling mechanism of adsorption process such as chemical reaction, diffusion control and mass transfer; kinetic models are used to test experimental data from the adsorption of MG onto CAS. The kinetics of MG adsorption onto CAS is required for selecting optimum operating conditions for the full-scale batch process. The kinetic parameters, which are helpful for the prediction of adsorption rate, give important information for designing and modeling the adsorption processes. Thus, the kinetics of MG adsorption onto CAS were analyzed using pseudo-first-order [35], pseudo-second-order [36], Elovich [37-39] and intraparticle diffusion [40-41] kinetic models. The conformity between experimental data and the model-predicted values was expressed by the correlation coefficients (R^2, values close or equal to 1). The relatively higher value is the more applicable model to the kinetics of MG adsorption onto CAS.

110

Orbital Elec. J. Chem., Campo Grande, 2(2): 101-117, 2010

Pseudo-first-order equation

The adsorption kinetic data were described by the Lagergren pseudo-first-order model [35], which is the earliest known equation describing the adsorption rate based on the adsorption capacity. The differential equation is generally expresses a follows:

$$\frac{dq_t}{dt} = k_1(q_e - q_t) \tag{12}$$

where q_e and q_t are the adsorption capacity at equilibrium and at time t, respectively (mg g^{-1}), k_1 is the rate constant of pseudo-first-order adsorption (Lmin^{-1}). Integrating Eq. (12) for the boundary conditions $t = 0–t$ and $q_t = 0–q_t$ gives:

$$\log\left(\frac{q_e}{q_e - q_t}\right) = \frac{k_1}{2.303}t \tag{13}$$

Eq. (13) can be rearranged to obtain the following linear form:

$$\log(q_e - q_t) = \log(q_e) - \frac{k_1}{2.303}t \tag{14}$$

In order to obtain the rate constants, the values of $\log(q_e-q_t)$ were linearly correlated with t by plot of $\log(q_e-q_t)$ versus t to give a linear relationship from which k_1 and predicted q_e can be determined from the slope and intercept of the plot, respectively (Fig. 4). The variation in the rate should be proportional to the first power of concentration for strict surface adsorption. However, the relationship between initial solute concentration and rate of adsorption will not be linear when pore diffusion limits the adsorption process. Fig. 4 shows that the pseudo-first-order equation fits well for the first 50 min and thereafter the data deviate from theory. Thus, the model represents the initial stages where rapid adsorption occurs well but cannot be applied for the entire adsorption process. Furthermore, the correlation coefficient R^2 was relatively low and adsorption constant (Qm) was different from experimental value (Table 2). This shows that the adsorption of MG onto CAS cannot be applied and the reaction mechanism is not a first-order reaction.

Pseudo-second-order equation

The adsorption kinetic may be described by the pseudo-second-order model [36]. The differential equation is generally given as follows:

$$\frac{dq_t}{dt} = k_2(q_e - q_t)^2 \tag{15}$$

where k_2 (g (mg min)$^{-1}$) is the second-order rate constant of adsorption. Integrating Eq. (15) for the boundary conditions $q_t = 0–q_t$ at $t = 0–t$ is simplified as can be rearranged

111

Orbital Elec. J. Chem., Campo Grande, 2(2): 101-117, 2010

and linearized to obtain:

$$\left(\frac{t}{q_t}\right) = \frac{1}{k_2 q_e^2} + \frac{1}{q_e}(t) \tag{16}$$

The second-order rate constants were used to calculate the initial sorption rate, given by the following equation:

$$h = k_2 q_e^2 \tag{17}$$

If the second-order kinetics is applicable, then the plot of t/q_t versus t should show a linear relationship. Values of k_2 and equilibrium adsorption capacity q_e were calculated from the intercept and slope of the plots of t/q_t versus t (Fig. 5). The linear plots of t/q_t versus t show good agreement between experimental and calculated q_e values at 100 mg/L initial MG and 0.2 mg/50 mL adsorbent concentrations (Table 2). The correlation coefficients for the second-order kinetic model are greater than 0.995 and the adsorption constant (Qm) was close to experimental value, which led to believe that the pseudo-second-order kinetic model provided good correlation for the bioadsorption of MG onto CAS.

Figure 4. Pseudo-first-order kinetics for MG (100 mg L^{-1}) adsorption onto CAS. Conditions: adsorbent dosage 0.2 g/50 mL, pH 7.0, temperature 27 ± 2 °C.

Table 2. Comparison of the first- and second-order adsorption rate constants and calculated and experimental q_e values for fixed initial MG and CAS (0.2g/50mL)

Parameter		First-order kinetic model			Second-order kinetic model		
	q_e	k_1	q_e	R^2	k_2	q_e	h
R^2	(experimental)	(calculated)			(calculated)		
MG (mgL^{-1})							
100	18.91	0.024	6.85	0.8757	0.0074	21.74	3.49 0.995

k_1 (min^{-1}), k_2 (g (mg min)$^{-1}$), q_e (mg g^{-1}), h (mg (g min)$^{-1}$).

112

Orbital Elec. J. Chem., Campo Grande, 2(2): 101-117, 2010

The values of initial sorption (h) that represents the rate of initial adsorption, is 3.4879 mg (g min)$^{-1}$ with 100 mg/L MG concentrations onto CAS dose 0.2 gmL^{-1} (Table 2).

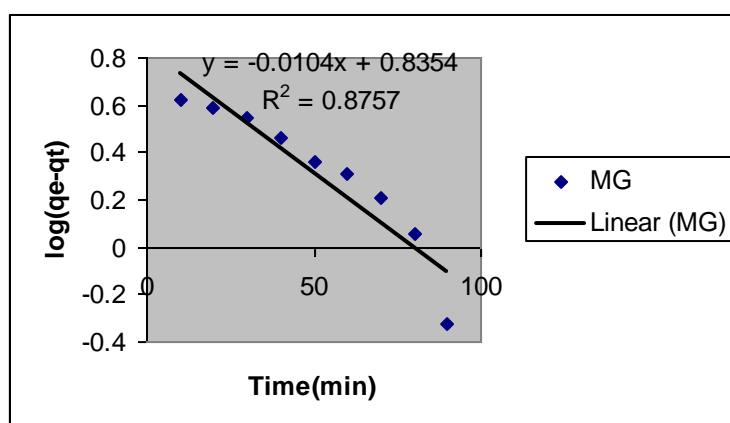**Figure 5**. Pseudo-second-order kinetics for MG (100 mgL^{-1}) adsorption onto CAS. Conditions: adsorbent dosage 0.2 g/50 mL, pH 7.0, temperature 27±2 °C.

Elovich equation

The Elovich equation is another rate equation based on the adsorption capacity generally expressed as following [37-39]:

$$\frac{dq_t}{dt} = B_E \exp(-A_E q_t) \tag{18}$$

where B_E is the initial adsorption rate (mg (g min)$^{-1}$) and A_E is the de-sorption constant (g mg^{-1}) during any experiment. It is simplified by assuming $A_E B_E t \gg t$ and by applying the boundary conditions $q_t = 0$ at $t = 0$ and $q_t = q_t$ at $t = t$ Eq. (18) becomes:

$$q_t = \frac{1}{A_E} \ln(B_E A_E) + \frac{1}{A_E} \ln(t) \tag{19}$$

If MG adsorption by CAS fits the Elovich model, a plot of q_t versus $\ln(t)$ should yield a linear relationship with a slope of ($1/A_E$) and an intercept of ($1/A_E$) ln ($A_E B_E$) (Fig. 6). Thus, the constants can be obtained from the slope and the intercept of the straight line (Table 3). The initial adsorption rate was 1181.35 mg (g min) $^{-1}$ for the initial MG concentration of 100 mgL^{-1} on CAS dose of 0.2 gmL^{-1}. Similar pattern is mentioned above for the initial adsorption rate, h, obtained from pseudo-second-order model. The desorption constant, A_E was 0.5437 g mg^{-1} for initial MG concentration 100 mgL^{-1} over CAS dose of 0.2 gmL^{-1} (Table 3).

The intraparticle diffusion model

The adsorbate species are most probably transported from the bulk of the solution

113

Orbital Elec. J. Chem., Campo Grande, 2(2): 101-117, 2010

into the solid phase through intraparticle diffusion/transport process, which is often the rate-limiting step in many adsorption processes, especially in a rapidly stirred batch reactor [42]. Since the MG is probably transported from its aqueous solution to the CAS by intraparticle diffusion, so the intraparticle diffusion is another kinetic model that should be used to study the rate of MG adsorption onto CAS. The possibility of intraparticle diffusion was explored by using the intraparticle diffusion model, which is commonly expressed by the following equation:

$$q_t = K_{dif}t^{1/2} + C \qquad (20)$$

where C (mgg^{-1}) is the intercept and K_{dif} is the intraparticle diffusion rate constant (in mgg^{-1}min$^{-1/2}$).

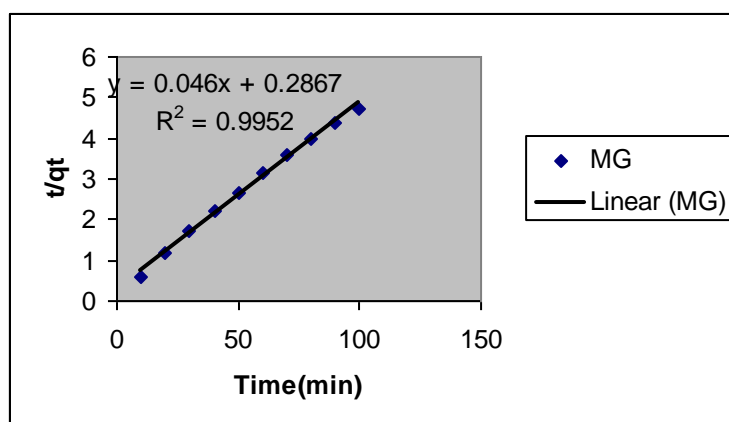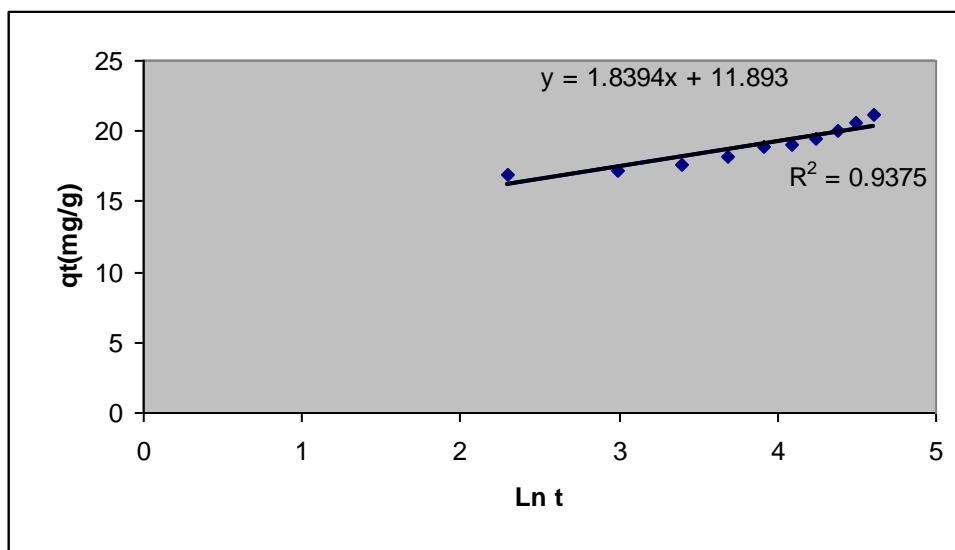**Figure 6**. Elovich model plot for MG (100 mgL^{-1}) adsorption onto CAS. Conditions: adsorbent dosage 0.2 g/50 mL, pH 7.0, temperature 27±2 °C.

Table 3. The parameters obtained from Elovich kinetics model and intraparticle diffusion model .

Parameter		Elovich			Intraparticle diffusion		
	A_E	B_E	R^2		K_{dif}	C	R^2
MG (mgL^{-1})							
100	0.54	1181.35	0.938		0.63	14.438	0.964

The values of q_t were found to be linearly correlated with values of $t^{1/2}$ (Fig. 7) and the rate constant K_{dif} directly evaluated from the slope of the regression line (Table 3). The values of intercept C (Table 3) provide information about the thickness of the

114

Orbital Elec. J. Chem.*, Campo Grande, 2(2): 101-117, 2010*

boundary layer, the resistance to the external mass transfer increase as the intercept increase. The constant C was found to be 14.438 for the dye concentration 100 mgL^{-1} indicating the increase of the thickness of the boundary layer and decrease of the chance of the external mass transfer and hence increase of the chance of internal mass transfer. The R^2 values given in Table 3 are close to unity indicating the application of this model. This may confirm that the rate-limiting step is the intraparticle diffusion process. The intraparticle diffusion rate constant, K_{dif}, was 0.629 mgg^{-1}min$^{-1/2}$. The linearity of the plots demonstrated that intraparticle diffusion played a significant role in the uptake of the adsorbate by adsorbent. However, as still there is no sufficient indication about it, Ho [43] has shown that if the intraparticle diffusion is the sole rate-limiting step, it is essential for the q_t versus $t^{1/2}$ plots to pass through the origin, which is not the case in Fig. 7, it may be concluded that surface adsorption and intraparticle diffusion were concurrently operating during the MG and CAS interactions.
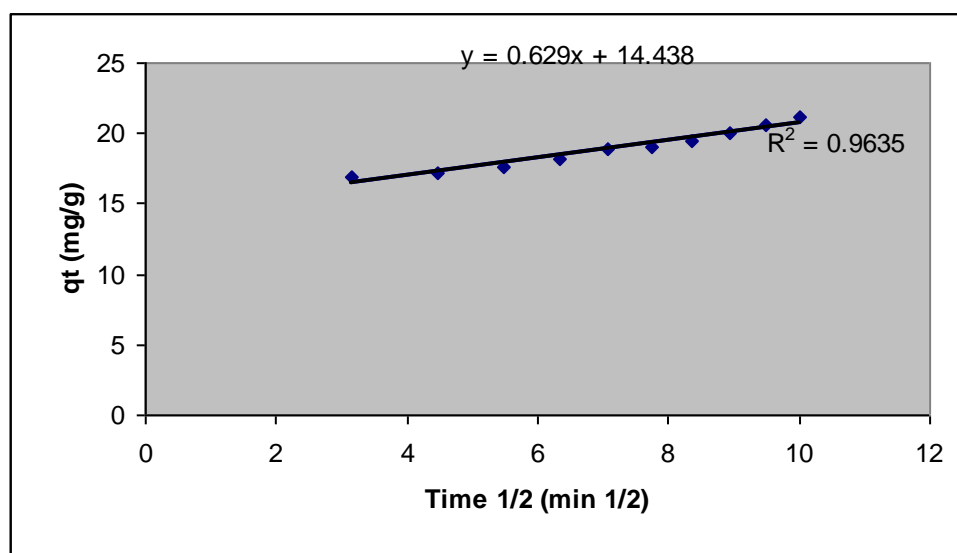
Figure 7. Intraparticle diffusion plot for MG (100 mgL^{-1}) adsorption onto CAS. Conditions: adsorbent dosage 0.2 g/50 mL, pH 7.0, temperature 27±2 °C.

Conclusion

The results of this investigation show that activated carbon developed from *Annona squmosa* seed has a suitable adsorption capacity for the removal of MG from aqueous solutions. The equilibrium adsorption is practically achieved in 100 min. The experimental results were analyzed by using Langmuir, Freundlich, Tempkin and Dubinin–Radushkevich isotherm models and the correlation coefficients for Langmuir, Freundlich, Tempkin and Dubinin–Radushkevich equations are well fitted. Adsorption behavior is described by a monolayer Langmuir-type isotherm. The kinetic study of MG on CAS was performed based on pseudo-first-order, pseudo-second-order, Elovich and intraparticle diffusion equations. The data indicate that the adsorption kinetics follow the

115

Orbital Elec. J. Chem., Campo Grande, 2(2): 101-117, 2010

pseudo-second-order rate with intraparticle diffusion as one of the rate determining steps. The present study concludes that the CAS could be employed as low-cost adsorbents as alternatives to commercial activated carbon for the removal of color and dyes from water and wastewater.

References and Notes

[1] Crini, G.; *Bioresour. Technol.* **2006**, *97*, 1061.

[2] Robinson, T.; McMullan, G.; Marchant R.; Nigam, P.; *Bioresour. Technol.* **2001**, *77*, 247.

[3] Aksu, Z.; *Process Biochem.* **2005**, *40*, 997.

[4] Han, R. P.; Zhang, J. H.; Zou, W. H ; Shi, J.; Liu, H. M.; *J. Hazard. Mater.* **2005**, *125*, 266.

[5] Gupta, V. K.; Ali, I.; Suhas D.; Mohan, *J. Colloid Interface Sci.* **2003**, *265*, 257.

[6] Ho, Y. S.; Chiu, W. T.; Wang, C. C. *Bioresour. Technol.* **2005**, *96*, 1285.

[7] Kumar, K. V.; *J. Hazard. Mater.* **2006**, *136*, 197.

[8] Ho, Y. S.; *Water Res.* **2006**, *40*, 119.

[9] Han, R. P.; Wang, Y.; Zou, W. H.; Wang, Y. F.; Shi, J. *J. Hazard. Mater.* **2007**, *145*, 331.

[10] Kumar, U.; Bandyopadhyay, M.; *Biores. Technol*. **2006**, *97*, 104.

[11] Ghimire, K. N.; Inoue, K.; Miyajima, T.; Yoshizuka, K.; Shoji, T. *Chitin Res*. **2001**, *7*, 61.

[12] Dhakal, R. P.; Ghimire, K. N.;.Inoue, K.; Yano, M .;.Makino, K . *Sep. Pur. Technol*. **2005**, *42*, 219.

[13] Vasanth Kumar, K. *Dyes and Pigments* **2007**, *74*, 595.

[14] Renmin, G.; Xiaoping, Z.; Huijun, L.; Yingzhi, S.; Birong, L. *Biores. Technol*. **2007**, *98*, 1319.

[15] Husseien, M.; Amer, A. A.; Azza, E. M.; Nahla, A. *J. Applied sciences Research.* **2007**, *3*, 1352.

[16] Nuttawan, P.; Nuttakan, N. *J. Nat. Sci.* **2006**, *40*, 192.

[17] Santhi, T.; Manonmani, S.; *E-Journal of Chemistry* **2009**, *6*, 1260.

[18] Tabrez, A. K.; Imran, A.; Ved, V.S.; Sangeeta, S.; *J. Envirn. Production Science* **2009**, *3*, 11.

[19] Onal, Y.; Akmil-Basar, C.; Didem, E.; Cigdem, S. O.; Tolga, D. *J. Hazard. Mater. B* **2006**, *128*, 150.

[20] Ahmed, E. N.; Ola, A.; Amany, E. S.; Azza, K. *J. Hazard. Mater* **2009**, *161***,** 102.

[21] Langmuir, I. *J. Am. Chem. Soc.* **1916**, *38*, 2221.

[22] Doğan, M.; Alkan, M.; Onganer, Y. *Water Air Soil Pollut.* **2000**, *120*, 229.

[23] Kinniburgh, D. G. *Environ. Sci. Technol.* **1986**, *20***,** 895.

[24] Longhinotti, E.; Pozza, F.; Furlan, L.; Sanchez, M. D. N. D.; Klug, M.; Laranjeira, M. C. M.; Favere, V. T. *J. Brazil. Chem. Soc.* **1998**, *9***,** 435.

[25] Freundlich, H. M. F. *Z. Phys. Chem. (Leipzig)* **1906**, *57A,* 385.

116

Orbital Elec. J. Chem., Campo Grande, 2(2): 101-117, 2010

[26] Aharoni, C.; Sparks, D. L. *Rate of Soil Chemical Processes*, Soil Science Society of America, Madison: WI **1991**, 1–18.

[27] Aharoni, C.; Ungarish, M.; *J. Chem. Soc., Faraday Trans.* **1977**, *73*, 456.

[28] Wang, X. S.; Qin, Y. *Process Biochem.* **2005**, *40*, 677.

[29] Akkaya, G.; Ozer, A. *Process Biochem.* **2005**, *40***,** 3559.

[30] Pearce, C. I.; Lioyd, J. R.; Guthrie, J. T. *Dyes Pigments* **2003**, *58***,** 179.

[31] Dubinin, M. M. *Chem. Rev.* **1960**, *60*, 235.

[32] Dubinin, M. M; *Zhurnal Fizicheskoi Khimii* **1965**, *39*, 1305.

[33] Radushkevich, L. V. *Zhurnal Fizicheskoi Khimii* **1949**, *23*, 1410.

[34] Kundu, S.; Gupta, A. K. *Colloid Surf. A: Physicochem. Eng. Aspects* **2006**, *273***,** 121.

[35] Lagergren, S. *Handlingar* **1898**, *24*, 1.

[36] Ho, Y. S.; McKay, G.; Wase, D. A. J.; Foster, C. F. *Adsorp. Sci. Technol.* **2000**, *18,* 639.

[37] Chien, S. H.; Clayton, W. R. *Soil Sci. Soc. Am. J.* **1980**, *44*, 265.

[38] Sparks, D. L.; CRC Press, Boca Raton **1986**.

[39] Zeldowitsch, J. *Acta Physicochim. URSS* **1934**, *1,* 364.

[40] Weber, W. J.; Morris, J. C. *J. Sanity Eng. Div. Am. Soc. Civil Eng.* **1963**, *89*, 31.

[41] Srinivasan, K.; Balasubramanian, N.; Ramakrishan, T. V. *Indian J. Environ. Health* **1988**, *30*, 376.

[42] McKay, G. *Chem. Eng. J.* **1983**, *27*, 187.

[43] Ho, Y. S. *Water Res.* **2003**, *37*, 2323.

[44] Kumar, K. V.; Sivanesan, S. *Dyes and Pigments*, **2007**, *72*, 124.

[45] Mittal, Alok. *Journal of Hazardous Materials*, **2006**, *133*, 196.

[46] Mittal, A.; Krishnan, L.; Gupta, V.K.; *Separation and Purification Technology*, **2005**, *43*, 125.

[47] Zhang, J.; Li, Y.; Zhang, C.; Jing, Y. *Journal of Hazardous Materials*, **2008**, *150*, 774.

[48] Kumar, K. *Dyes and Pigments*, **2007**, *74*, 595.

117

Orbital Elec. J. Chem., Campo Grande, 2(2): 101-117, 2010

Full Paper

Kinetics and mechanism of *N*-chlorosaccharin oxidation of malic acid

Sanjay K. Singh[a]*, Hari D. Gupta[a], Mohammad U. Khan[b], Santosh S. Baghel[c]

[a]Department of Chemistry, Govt. T. R. S. College, Rewa 486001 (M.P.), India
[b]Govt. College Umaria (M.P.) India
[c]Department of Chemistry, Govt. College Rampur Naikin, Sidhi (M.P.) India

ABSTRACT: *Kinetic study of N-chlorosaccharin (NCSA) oxidation of malic acid (MA) in aqueous acetic acid medium in presence of perchloric acid has been investigated. The reactions exhibit first-order dependency in oxidant and $HClO_4$ while order varies from one to zero in substrate. The reactions are acid catalyzed and retarded by the addition of saccharin, a byproduct of reaction. The rate of oxidation decreases with decrease in dielectric constant of the medium. The effect of temperature on the reaction has been investigated in the temperature range 313-333 K. The stochiometric studies revealed 1:1 mole ratio. Various thermodynamic parameters have been computed and a possible operative mechanism is proposed.*

Keywords: *malic acid; mechanism; N-chlorosaccharin; bifunctional; hydroxy acid*

Introduction

The prime aim of the authors is to probe the hitherto unreported results on the mechanistic routes of N-chlorosaccharin [1, 2] oxidation of malic acid. Recently reactions involving NCSA received limited attention. Although a variety of compounds like alcohol]3, 4], hydroxy acids [5, 6], acid [7], aldehyde [8], ketones [9, 10], benzaldehyde [11], amino acids [12, 13], keto acid [14] etc. has been oxidized employing this oxidant. Malic acid is an aliphatic hydroxy acid. It is a bi-functional compound with hydroxy and carboxyl function having active electron attracting species. Due to inductive effect of these groups, a negative center is created for the attack of HOCl and H_2O^+Cl, which is active species of NCSA. It has been found despite of great diversity in structure of

---

hydroxy acids, the reactivity and rate are often markedly affected by changes in the carbon skeleton. Aliphatic hydroxy acids have been oxidized by a numerous oxidants namely Os (VII) [15], $KMnO_4$ [16], NBSA [17] etc. The peculiar properties of this oxidant are limited and therefore in view of widening the dimension of understanding, the present task has been probed kinetically. The investigation aimed to study the newer areas with broad vision by employing the hidden potentiality of NCSA as an oxidant and malic acid as the substrate.

Material and Methods

The sample of NCSA employed in this study was prepared in acetic acid (E. Merck). All other chemicals were of Analytical grade. The solutions used were standardized iodometrically. Demineralized distilled water was used for preparing the solution of hypo and others. Malic acid (E. Merck) was prepared in the requisite amount of acetic acid and water mixture. The kinetic measurements were initiated by mixing appropriate volumes of two solutions containing NCSA solution and the malic acid in aqueous acetic acid in presence of perchloric acid. The progress of the reaction was monitored by estimating unconsumed NCSA iodometrically. The stochiometric results indicated consumption of mole ratio 1:1.

$$C_4H_6O_5 \ + \ NCSA \ \rightleftharpoons \ CH_3CHO \ + \ 2\,CO_2 \ + \ HCl \ + \ Saccharin$$

After complete oxidation of the system, the end product so obtained was detected by means of chromatography, and existing conventional methods [18, 19].

Results and Discussion

Oxidation kinetics has been carried out in binary solvent mixture of the acetic acid and water under the reaction condition [NCSA] << [Malic Acid] $[H^+]$.

Dependence of rate on oxidant

In a typical kinetic run, for the reaction ([NCSA] = 2.5 mol dm^{-3}, $[H^+]$ = 0.05 $moldm^{-3}$ and [MA] =5 .0 x 10^2 $moldm^{-3}$), a plot of log (a-x) *versus* time (Fig. 1) gave a straight line, which indicates that reaction under the chosen condition follows pseudo first order kinetics. The order with respect to NCSA is unity (Table 1).

Effect of concentration of substrate

On varying malic acid concentration from 1.0 to 10.0 $moldm^{-3}$, there is an increase in rate of reaction. The plots of log k_1 *verses* log [MA] (Fig. 2) gave straight line at lower concentration but bend at higher concentration, suggesting that order with respect to malic acid is fractional. A double reciprocal plot between k^{-1} *verses* $[MA]^{-1}$ (Fig. 3) has been found to be straight line with positive intercept at y-axis. That leads to follow

119

Orbital Elec. J. Chem., Campo Grande, 2(2): 118-126, 2010

Michaelis-Menten kinetics indicating evidence for the intermediate complex formation between the species of oxidant and the substrate in a pre-equilibrium step. This kinetic evidence of complex formation between the substrate and the oxidant, further support the first order dependence.
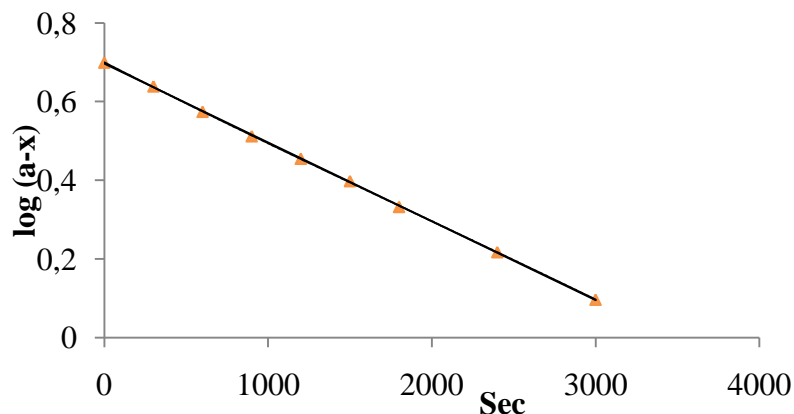
Figure 1. Plot of log (a-x) *versus* time.

Table 1. Effect of variation of [NCSA] on the rate constant k_1 [MA]$x10^2$, (moldm^{-3})= 5.0; [H$^+$] (moldm^{-3})=0.05 ; HOAc-H$_2$O, (%vol.)=20; temperature (K)=318.

[NCSA] x 10^3(mol dm^{-3})	$\leftarrow$ k_1x 10^4 (s^{-1}) $\rightarrow$
1.0	4.671
2.0	4.669
2.5	4.683
4.0	4.682
5.0	4.662

Table 2. Dependence of rate on the variation of the concentration of malic acid. [NCSA] x 10^3, (moldm^{-3}) = 2.5; [H$^+$] (moldm^{-3}) = 0.05; HOAc-H$_2$O, (%vol.)=20; temperature (K)=318.

[MA] x 10^2 (moldm^{-3})	$\leftarrow$ k_1x 10^4 (s^{-1}) $\rightarrow$
1.0	1.619
2.0	2.673
2.5	3.279
4.0	4.304
5.0	4.683
8.0	5.021
10.0	5.068

The effect of variation of hydrogen ion

On varying perchloric acid concentration from 0.1 to 0.5 moldm^{-3} the negative catalyzed

120

Orbital Elec. J. Chem*., Campo Grande, 2(2): 118-126, 2010*

kinetics was observed by the addition of $HClO_4$ and first-order was evaluated (Table 3). The plots of $1/k_1$ verses log $[H^+]$ (Fig. 4) gave straight line with positive intercept, suggesting that acid plays a complex role in the reaction system. The retardation by $[H^+]$ may be mainly attributed to the conversion of the more reactive neutral species of malic acid to less reactive protonated form.
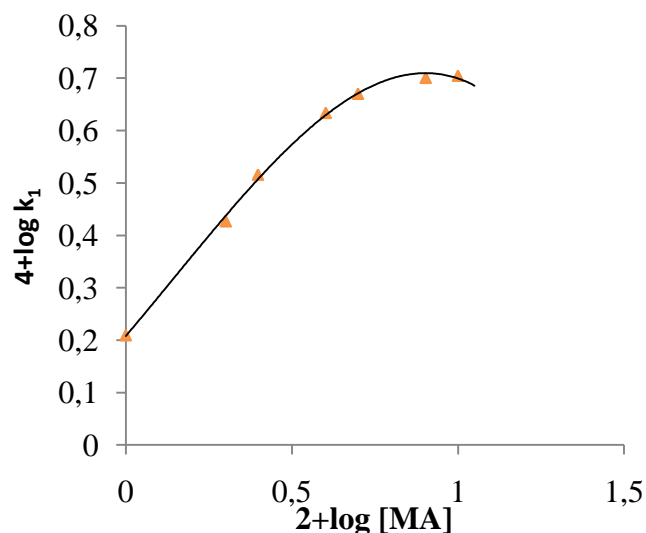
Figure 2. Plot of log k_1 versus log [MA].
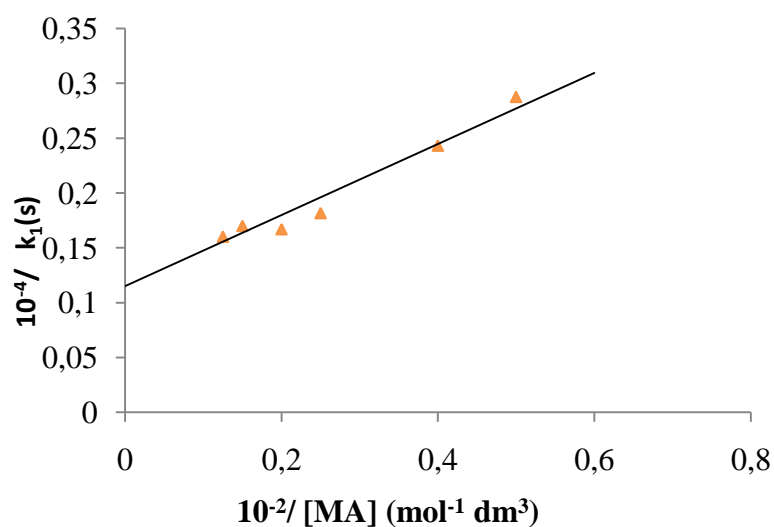
Figure 3. Plot of $1/k_1$ versus $1/$[MA].

Table 3. Effect of change of concentration of H^+. $[NCSA] \times 10^3$, $(moldm^{-3})$ = 2; $[MA] \times 10^2$ $(moldm^{-3})$ = 5.0; $HOAc-H_2O$, (% vol.) = 20; temperature (K) = 318.

$[HClO_4]$ $(moldm^{-3})$	$\leftarrow$ $k_1 \times 10^4$ (s^{-1}) $\rightarrow$
0.10	1.619
0.20	2.673
0.25	3.279
0.40	4.304
0.50	4.683

121

Orbital Elec. J. Chem., Campo Grande, 2(2): 118-126, 2010
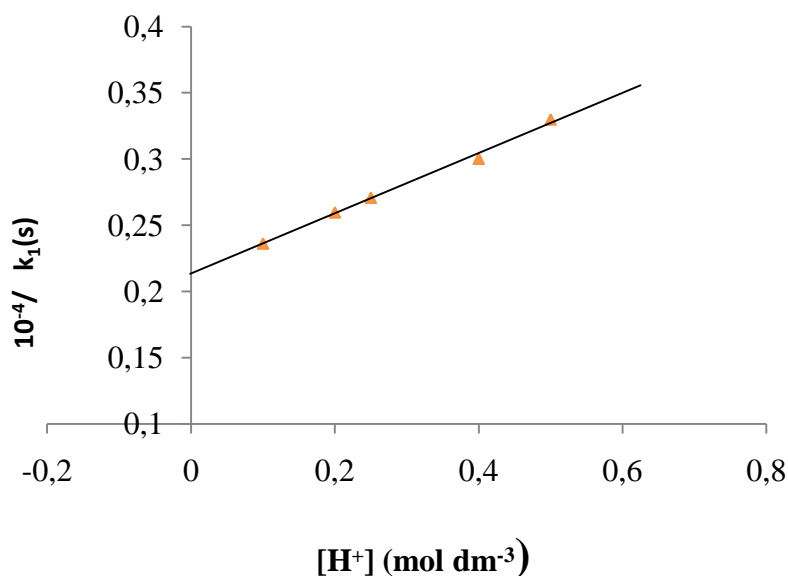
Figure 4. Plot of $1/k_1$ versus $[H^+]$.

Effect of variation of ionic strength, dielectric constant and saccharin

It was found that there is no substantial change in the reaction rate on varying the ionic strength from 1 to 10 moldm^{-3} by the addition of neutral sodium per chlorate. The small salt effect suggests the participation of neutral species in rate determining step i.e., the substrate molecule and HOCl. This assumption further got support from effect of change in dielectric constant of the reaction medium. The effect of dielectric constant in reaction medium has been studied by adding acetic acid (10-60%) in the reaction medium at constant concentration of other reactants. The rate of reaction decreases by increasing the proportion of acetic acid in solvent medium; this supports the involvement of neutral species in the rate determining step. Addition of saccharin, one of the reaction products, from 0.0005 to 0.001 moldm^{-3} at constant NCSA and malic acid concentration, decreases the rate of reaction. This supports that HOCl is the main oxidizing species. The oxidation of malic acid by NCSA failed to induce polymerization of acrylonitrile. Hence a free radical mechanism is ruled out.

Effect of temperature

By increasing temperature the rate of the reaction increases. The plot of log k verses 1/T (Fig. 5) is a straight line in the temperature range 313-333 K. This shows Arrhenius equation is valid for this reaction. From the linear Arrhenius plot activation parameters for overall reaction were evaluated (Table 4).

Reaction Mechanism

Before highlighting the mechanism of the oxidation reaction it is worthwhile at this

Orbital Elec. J. Chem., Campo Grande, 2(2): 118-126, 2010

122

stage to have an idea regarding the reacting species of NCSA in aqueous acetic acid medium in the presence of perchloric acid. Thus the formation of different reactive oxidizing species may be assumed in the following manners:

$$NCSA + H^+ \rightleftharpoons NCSAH^+ \tag{1}$$

$$NCSA + H^+ \rightleftharpoons Saccharin + Cl^+ \tag{2}$$

$$NCSA + H_2O \rightleftharpoons HOCl + Saccharin \tag{3}$$

$$HOCl + H^+ \rightleftharpoons H_2O^+Cl \tag{4}$$

$$NCSAH^+ + H_2O \rightleftharpoons H_2O^+Cl + Saccharin \tag{5}$$

$$NCSA + CH_3COOH \rightleftharpoons Saccharin + CH_3COOCl \tag{6}$$

$$CH_3COOCl + H^+ \rightleftharpoons CH_3COO^+HCl \tag{7}$$
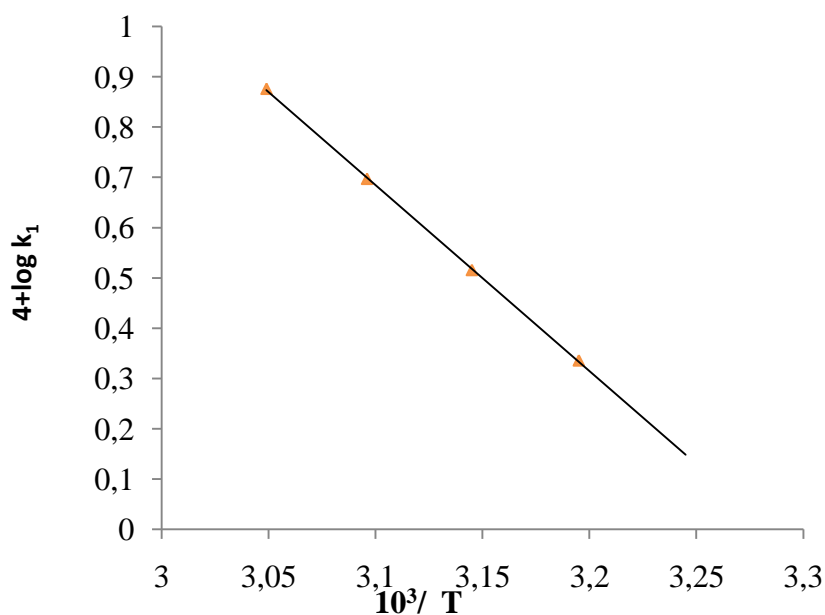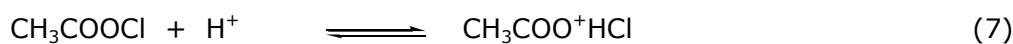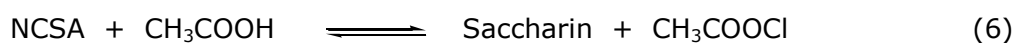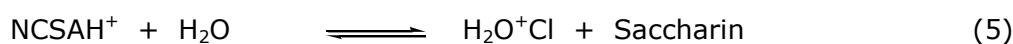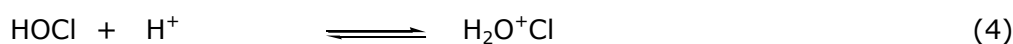
Figure 5. Arrhenius plot.

Table 4. Thermodynamic parameters of malic acid-NCSA system

Hydroxy acid	E_a (kJ mol^{-1})	A (s^{-1})	ΔH^* (kJ mol^{-1})	ΔG^* (kJ mol^{-1})	$-\Delta S^*$ (JK^{-1} mol^{-1})
Malic acid	68.359 ±0.677	6.745 ±0.671x10^7	64.060 ±0.599	89.668 ±0.433	0.813 ±0.006

The choice of species actively participated in initiation of the oxidation can be

Orbital Elec. J. Chem., Campo Grande, 2(2): 118-126, 2010

123

explained on the basis of the following kinetic results as:

(a) The retardation trend observed in reaction velocity, when the reduction product of oxidant, i.e. saccharin, is added. That is ruled out NCSA as an active oxidant species;

(b) The large negative reaction constant suggest a high carbocationic reaction centre exist this eliminates the possibility of Cl^+ as a reactive species;

(c) The possibility of CH_3COOCl and CH_3COO^+HCl, the acetate complex of NCSA (equations 6 and 7) may also be ruled out as inhibition in the rate of oxidation was observed with an increase in the percentage composition of CH_3COOH and H_2O. Kinetically it is not possible to, distinguish equation (1) and (4) from equation (5);

(d) NCSA and HOCl undergo protonation in the presence of $HClO_4$ (equation 1, 4) which inhibit the rate of oxidation and therefore clearly ruling out that these cannot be assumed as the remote profile reacting species. The derecognition of activities is also due to the fact that H^+ does not involve in transformation of NCSA;

(e) Thus the only choice and possibility is left that HOCl or H_2O^+Cl [20] is a remote and prime active species.

Mechanistic paths involve the electrophillic attack of remote prime species of HOCl or H_2O^+Cl on malic acid. On the basis of results the following oxidation kinetic mechanistic reaction scheme for malic acid-NCSA system is proposed.

$$NCSA + H_2O \xrightleftharpoons{k_1} HOCl + Saccharin \qquad (8)$$

$$HOCl + H^+ \xrightleftharpoons{k_2} H_2O^+Cl \qquad (9)$$

$$MA + HOCl \xrightleftharpoons{k_3} Complex\ (C) + H_2O \qquad (10)$$

$$Complex\ (C) \xrightarrow{k_1} Products \qquad (11)$$
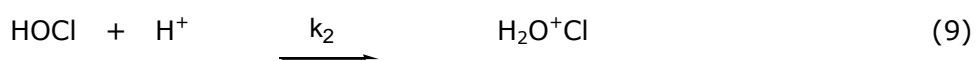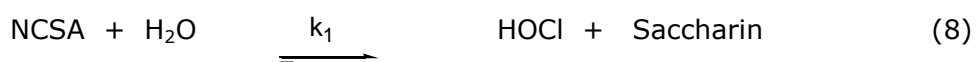
On the basis of the aforementioned steps involved in the proposed mechanism and at steady state approximation condition, the final rate law is derived as:

$$k_{obs}^{-1} = \frac{1}{[HA]} \left[\frac{[S]}{k_1 K_1 K_3} + \frac{1}{k_1 K_3} + \frac{K_2 [H^+]}{k_1 K_3} \right] + \frac{1}{k_1} \qquad (12)$$

124

Orbital Elec. J. Chem., Campo Grande, 2(2): 118-126, 2010

According to the equation (12), a plot of kobs^{-1} against [HA]$^{-1}$ (double reciprocal) should give a straight line with a positive intercept at y-axis. This supports the validity of the rate law (12) and hence confirms the proposed complex reaction mechanism.

Conclusion

The kinetic results and thermodynamic parameters support the C-C bond fission in the rate determining step. The flip of C-H bond is actually not involved in the rate determining step due to loss of translation and rotational freedom in the process. The mechanism involving C-C fission in the system is further supported by Bakore et al. [21].

Acknowledgements

References and Notes

[1]   Chattaway, F. D. *J. Chem.Soc.* **1905**, 87, 1884.

[2]   Bacchawat, J.M.; Mathur, N. C. *Indian J. Chem*. **1971**, *9*, 1335.

[3]   Vijay, M. K.; Raghunath, R. P.; Sundaram, E. V. *Proc. N. Acad. Sc. India* **1988**, *58*, 137.

[4]   Khan, M. U.; Tiwari, R. K.; Verma, J. K.; Gupta, H. D. *Oxid. Commun*. **1997**, *20*, 124.

[5]   Khan, M. U.; Sharma, V. K.; Verma, J. K.; Dwivedi, H. P. *Oxid. Commun.* **1991**, *14*, 60.

[6]   Khan, M. U.; Verma, J. K.; Singh, V. R.; Dwivedi, H. P. *Oxid. Commun*. **1993**, *16*, 235.

[7]   Khan, M. U.; Nigam, S. K.; Nigam, A.; Verma, J. K.; Chauhan, R. P. S. *Oxid. Commun*. **1995**, *18*, 304.

[8]   Khan, M. U.; Verma, J. K.; Parihar, S. S.; Dwivedi, H. P. *Oxid. Commun*. **1998**, 21, 362.

[9]   Khan, S.; Khan, M. U.; Singh, S. K.; Gupta, H. D.; Singh, P. K. *Asian J. Chem*. **2003**, 15, 595.

[10] Khan, S.; Nigam, S. K.; Khan, M. U.; Dwivedi, H. P.; Singh, P. K. *Asian J. Chem*. **2004**, *16*, 751.

[11] Nigam, S. K.; Khan, M. U.; Tiwari, S.; Dwivedi, H. P.; Singh, P. K. *Asian J. Chem.* **2004**, *16*, 362.

[12] Farook, N. A. M.; Seyed, D. G. A.; Murugesan, A.; Kanagaraj, M. *E. J. Chem*. **2004**, *1*, 132.

[13] Farook, N. A. M.; Kanagaraj, M. *E. J. Chem*. **2004**, *1*, 1.

[14] Farook, N. A. M. *Journal of Solution Chemistry* **2007,** *36*, 345.

[15 Singh, N. P.; Singh, V. N.; Singh, H. S.; Singh, M. P. *Aust. J. Chem*. **1970**, *23*, 921.

125

Orbital Elec. J. Chem., Campo Grande, 2(2): 118-126, 2010

[16] Jain, A. N.; Banerji, K. K. *J. Indian Chem. Soc*. **1982**, *59*, 654.

[17 Sharma, V. K.; Sharma, K.; Mishra, U. *J. Indian Chem. Soc.*, **1986**, *63*, 586.

[18] Barkat, M. Z.; Abdelwahab, M. F. *Analyt. Chem*. **1954**, *26*, 1973.

[19] Fegl, F. *Spot-test in Organic Analysis*. Elsevier: New York, **1996**, 12.

[20] Sharma,V. K.; Sharma, K.; Mishra, U. *Oxid. Commun*.**1988**, *11*, 275.

[21] Bakore, G. V.; Narain, S. *Z. Phys. Chem.* **1964**, *8*, 227.

126

Orbital Elec. J. Chem*., Campo Grande,* 2(2): 118-126, 2010

Full Paper

Kinetics of oxidation of D-arabinose and D-xylose by vanadium (V) in the presence of manganese II as homogeneous catalyst

Ezekiel O. Odebunmi[a], Adeniyi S. Ogunlaja*[b] and Samson O. Owalude[a]

[a]Department of Chemistry, University of Ilorin, P.M.B. 1515, Ilorin, Nigeria
[b]Department of Chemical Sciences, Bells University of Technology, PMB 1015, Ota, Ogun State, Nigeria

ABSTRACT: *Kinetics of oxidation of D-arabinose and D-xylose by acidic solution of vanadium (V) ions in the presence of manganese (II) has been reported. First-order dependence of the reaction rate was observed on [sugars] and [H^+] at low concentrations throughout the oxidation reaction and a zero-order dependence on [sugar] and [H^+] was observed at high concentrations. First-order kinetics with respect to [Mn (II)] was also observed throughout the oxidation for both sugars. The results indicate the effect of Cl^- concentration is negligible. The reaction rates increase with the ionic strength of the medium. Various activation parameters were evaluated and provide further support to the proposed mechanism. Formic acid was reported as one of the oxidation products of these sugars.*

Keywords: *kinetics; vanadium (V); oxidation; arabinose; xylose; manganese (II) chloride catalysis; perchloric acid*

Introduction

The biological and economic importance of carbohydrates has been largely responsible for the interest in the study of their biochemical and physiochemical properties along with their reactivity. Studies have been carried out on the structural elucidation, chemical degradation, and oxidation reactions. The catalytic oxidation of sugars has been carried out both in acidic and alkaline media, using such oxidants as transition metal ions, inorganic acids, organometallic complexes, and enzymes [1-10]. Recently Mn (II) was reported to catalyze the oxidation of arabinose and xylose by

---

chromium VI [10]. In view of the biological importance of carbohydrate and the limited research carried out using Mn (II) as catalyst, this study seeks to report the catalytic importance of Mn (II) in the oxidation of arabinose and xylose using vanadium V as oxidant.

The aim of this study is to determine the kinetic orders with respect to each reactant of the reactions, as well as to present a suitable reaction mechanism for the oxidation of the reducing sugars under investigation.

Material and Methods

All chemicals were of analytical reagent grade and were used as received. Vanadium (V) (BDH) was prepared by dissolving 3 g of NH_4VO_3 in 40 cm^3 of 2 M NaOH and 80 cm^3 of 1M H_2SO_4 were added to the mixture. A yellow solution indicates Vanadium (V) [11].

In preparation of the required concentration a dilution factor was employed and its concentration was checked iodometrically. A solution of $MnCl_2$ (Uchem limited) was prepared by dissolving the sample in known strength of very dilute hydrochloric acid (0.001 M). The standard solutions of arabinose and xylose (A. R. grade) were freshly prepared with double-distilled water. The standard solution of $HClO_4$ (E. Merck) was used to maintain the required acidity. KCl (Analar) was prepared by dissolving its required amount in doubly distilled water to fix the Cl^- ion concentration; and $NaClO_4$ (Analar) was used to maintain the required ionic strength of the medium.

Kinetic Measurements

Appropriate quantities of the solutions of V (V), $HClO_4$, $MnCl_2$, KCl, and $NaClO_4$ were placed in separate glass vessels and kept for at least one hour in a thermostated water bath after reaching the temperature of 40 $^{\circ}C$; then, the calculated amount of each reaction mixture was added together into a particular glass vessel, followed by the required amount of double-distilled water mixed together. The reaction mixture was then placed in a thermostated water bath maintained at a constant temperature of 40 $^{\circ}C$ (±0.5 $^{\circ}C$) and the reaction was initiated by adding the required amount of oxidant solution placed separately in the same bath. The reaction progress was followed by estimating the decrease in the absorbance of V (V) spectrophotometrically at 525 nm in regular time intervals.

Polymerization Test

To test for the presence of free radicals in the reaction a 20% acrylamide solution was added to reaction mixtures containing the substrate and the vanadium (V) solution and then placed in an inert atmosphere for 24 hours. When the reaction mixture was

diluted with methanol, a precipitate was formed in the reaction mixture. This confirms the formation of free radicals in the redox reactions under investigation.

Stoichiometry and product analysis

Reaction mixtures, in which the concentration of V (V) presented a large excess of the reducing sugars, were kept in the presence of appropriate quantities of KCl, $NaClO_4$, $MnCl_2$, and $HClO_4$ at room temperature for 72 hours. Estimation of the unreacted V (V) showed that 1 mol of each sugar consumes 1 mol of V (V) for oxidation to take place, on the assumption that all the sugars are consumed under this condition. Formic acid was confirmed as one of the oxidation products of these two sugars using spot test [12].

$$V_2O_5 + H_2O + C_5H_{10}O_5 \xrightarrow{\text{Mn(II) / H}^+} \underset{\text{Formic acid}}{HCOOH} + \underset{\text{erythronic acid}}{RCOOH} + V_2O_4 + H_{2\,g}$$

$$\text{where, R= } C_3H_7O_3$$
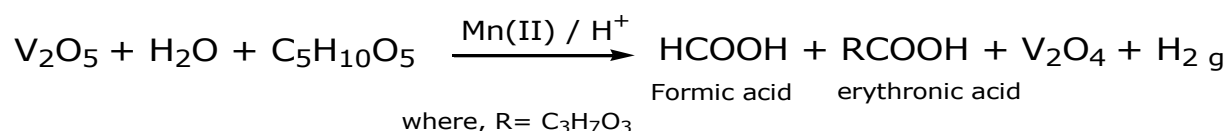
Results and Discussion

The progress of the reaction was followed by measuring the decrease in absorbance of the vanadium (V) ions at regular time interval, using a UNISPEC SM7504UV spectrophotometer. The pseudo first-order rate constants (k_{obs}) were determined from the linear portion of the plots of log (absorbance) versus time [16].

Table 1. Effect of variation of [sugars] and [$HClO_4$] of the medium on pseudo first-order rate constant k_{obs} in the oxidation of arabinose and xylose at 40°C.

[$HClO_4$] M	[Sugar] M	$k_{obs} \times 10^5\ s^{-1}$	
		D-arabinose	D-xylose
0.03	0.01	0.17	0.09
0.15	0.01	0.68	0.36
0.21	0.01	0.98	0.40
0.27	0.01	1.12	0.50
0.33	0.01	1.32	0.60
0.39	0.01	1.47	0.80
0.45	0.01	1.53	1.20
0.51	0.01	1.55	1.30
0.57	0.01	1.59	1.40
0.15	0.002	1.21	0.35
0.15	0.008	1.63	0.83
0.15	0.010	2.15	1.33
0.15	0.012	2.72	1.67
0.15	0.014	3.19	1.80
0.15	0.016	3.55	2.17
0.15	0.018	3.87	2.15
0.15	0.020	3.92	2.22
0.15	0.022	3.97	2.23

Solution conditions: [V (V)] = 1×10^{-3} M, [$MnCl_2$] = 6×10^{-4} M; [KCl] = 5×10^{-4} M; [$NaClO_4$] = 0.1 M.

From the observation of Table 1 one may conclude that the concentrations of [sugars] and [$HClO_4$] varied; this table indicates the rate of oxidation increases as the

129

Orbital Elec. J. Chem*., Campo Grande,* 2(2): 127-139, 2010

[sugar] and [HClO$_4$] increases. It suggests the reaction is acid-dependent concerning [HClO$_4$] [10].

Table 2. Effect of the variation of [NaClO$_4$] and [MnCl$_2$] of the medium on pseudo first-order rate constant k$_{obs}$ in the oxidation of arabinose and xylose at 40°C

[NaClO$_4$] M	[V (V)] ×10^3 M	[MnCl$_2$]×10^4 M	k$_{obs}$×10^5 s^{-1}	
			D-arabinose	**D-xylose**
0.05	1.0	6.0	0.65	0.50
0.08	1.0	6.0	0.73	0.67
0.13	1.0	6.0	0.86	0.83
0.15	1.0	6.0	1.23	1.00
0.16	1.0	6.0	1.36	1.17
0.20	1.0	6.0	1.46	1.34
0.25	1.0	6.0	1.58	1.78
0.1	1.0	1.0	0.38	0.30
0.1	1.0	3.0	1.15	0.91
0.1	1.0	5.0	1.85	1.41
0.1	1.0	7.0	2.70	1.90
0.1	1.0	9.0	3.45	2.80
0.1	1.0	11.0	3.98	3.20

Solution conditions: [sugar] = 1.00 × 10^{-2} M, [HClO$_4$] = 0.15 M, [KCl] = 5 × 10^{-4} M.

Table 2 displays the effect of varying the concentrations of [NaClO$_4$] and the catalyst [MnCl$_2$]. This table indicates the reaction rate increases as the sodium perchlorate concentration increases, indicating that reactions take place between ions of similar charges [18]. The rate of reaction also increases as the catalyst concentration increases, indicating that the reaction is catalyst-dependent [10].

The reactions were also studied at four different temperatures: 40, 50, 60, and 70 $^{\circ}$C and the observed values of pseudo first-order rate constant, k$_{obs}$, were used to calculate the activation parameters of the various sugars, including their entropy of activation reported in Tables **3a** and **b**. The Arrhenius activation energies, E$_a$, for the uncatalyzed path were 98.83 and 99.90 kJmol^{-1} for xylose and arabinose, respectively, while the Arrhenius activation energies for the catalyzed path were 45.16 and 44.52 kJmol^{-1} for arabinose and xylose, respectively. The difference in the Arrhenius activation energies for the uncatalyzed and catalyzed reactions concerning the different sugars indicates the reaction is catalyzed.

Table 3. Energy of activation and other activation parameters observed for the oxidation of D-arabinose and D-xylose at 40∘C.
(a) For the catalyzed path

SUGARS	*E$_{act}$* *kJmol^{-1}*	*ΔH$^{\#}$* *kJmol^{-1}*	*ΔS$^{\#}$* *Jmol^{-1}K^{-1}*	*ΔG$^{\#}$* *kJmol^{-1}*	*K$_{obs}$(s^{-1})* *×10^5*	*A (mol^{-2}dm^{6}s^{-1})*
Xylose	44.52	41.92	-154.63	90.32	1.33	5.42 × 10^4
Arabinose	45.16	42.55	-150.48	89.65	2.15	8.93× 10^4

(b) For the uncatalyzed path

130

Orbital Elec. J. Chem*., Campo Grande,* 2(2): 127-139, 2010

SUGARS	E_{act} $kJmol^{-1}$	$\Delta H^{\#}$ $kJmol^{-1}$	$\Delta S^{\#}$ $Jmol^{-1}K^{-1}$	$\Delta G^{\#}$ $kJmol^{-1}$	$k_s(s^{-1})$ $\times 10^5$	A $(mol^{-2}dm^6s^{-1})$
Xylose	98.83	96.23	8.34	93.62	0.85	1.76×10^{13}
Arabinose	99.90	97.30	14.17	92.86	0.95	3.55×10^{13}

Average linear regression coefficients, r ≥ 0.89, were observed for all activation parameters.

Mechanism: Reaction Scheme

In our study comparing the oxidation of xylose and arabinose by V (V) in the presence of Mn (II) chloride as homogeneous catalyst, the entropy of activation was negative; this suggests the reaction proceeds through a hydride transfer process for complex formation. Thus, when vanadate is acidified by a perchloric acid the yellow pervanadyl ion, VO_2^+, is formed as the initial species [14].

$$VO_3^- + 2H^+ \rightleftharpoons VO_2^+ + H_2O \tag{1}$$
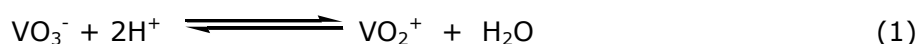
This may exist in hydrated form V (OH) $_4^+$ [15]. In a stronger perchloric acid ($H^+ >$ 2 M) the species becomes protonated to form VO (OH) $^{2+}$ [13].

A reaction mechanism based on the observed kinetic results and the spectral information collected for the formation of complex presents itself as proposed in the reaction scheme below [17]:

$$R = C_3H_7O_3 \tag{2}$$
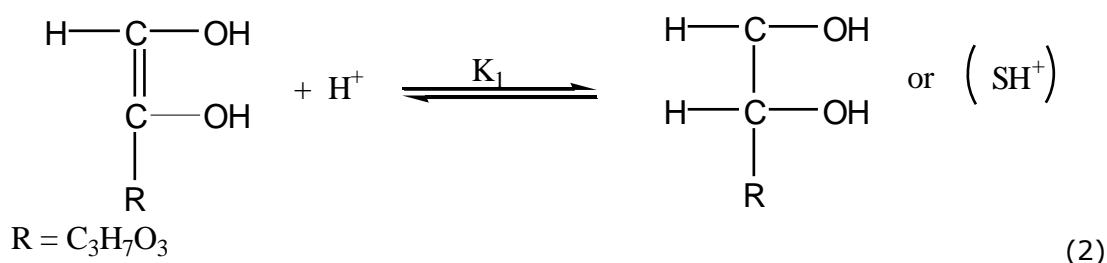
Where SH $^+$ represents the protonated form of the sugars.

The protonated sugar then reacts with the catalyst Mn (II), according to the equation (3) below to give the first complex labelled C_1.

$$(3)$$
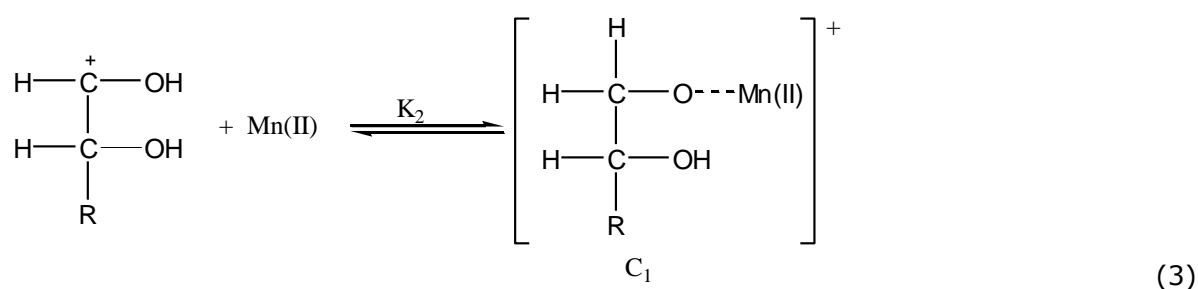
The positively charged complex then reacts further with the protonated vanadium

131

Orbital Elec. J. Chem., Campo Grande, 2(2): 127-139, 2010

in the slow and rate determining step.

Equation (4) is supported by the positive effect of the addition of sodium perchlorate to the rate of the reactions; it indicates that reactions take place between ions of similar charges [18]. The lower aldose undergoes further oxidation with the protonated chromic acid to yield the erythronic acid.

$$(4/5)$$

From the proposed mechanism, the rate of the reaction in terms of decrease in the concentration of V (V) was derived as:

$$- \frac{d\,[VO_2^+]}{dt} = k_3\,[\,C\,]\,[\,VO_2^+\,]$$

$$6)$$

From the reaction mechanism the total Mn (II), i.e., Mn (II)$_T$, is given below:

$$Mn(II)_T = Mn(II) + C$$

where $Mn(II) = Mn(II)_T - C$

$$K_1[\,S\,]\,[\,H^+] = [\,SH^+]$$

$$(7)$$

Substituting equation 7 into the equation below:

$$K_2 = \frac{C}{[\,SH^+\,]\,[\,Mn(II)\,]}$$

$$K_2 = \frac{C}{K_1[\,S]\,[H^+]\,[\,Mn(II)\,]}$$

Making the complex 'C" subject of the formulae:

132

Orbital Elec. J. Chem., Campo Grande, 2(2): 127-139, 2010

$$C = K_2 K_1 [S] [H^+] [Mn(II)]$$

$$C = K_2 K_1 [S] [H^+] \left[Mn(II)]_T - C \right]$$

$$C = K_2 K_1 [S] [H^+] [Mn(II)]_T - K_2 K_1 [S] [H^+] C$$

$$C = \frac{K_2 K_1 [S] [H^+] [Mn(II)]_T}{1 + K_2 K_1 [S] [H^+]} \tag{8}$$

Substituting eq. 8 into eq. 6 gives:

$$Rate = \frac{-d[VO_2^+]}{dt} = \frac{k_3 K_2 K_1 [S] [H^+] [VO_2^+] [Mn(II)]_T}{1 + K_2 K_1 [S] [H^+]} \tag{9}$$

The inverse reaction gives:

$$Mn(II)_T * \frac{1}{Rate} = \frac{1}{k_3 K_2 K_1 [S] [H^+] [VO_2^+]} + \frac{1}{k_3 [VO_2^+]} \tag{10}$$

From the double reciprocal plot of the graph Mn (II)/rate against 1/[S] and Mn (II)/rate against 1/ [H$^+$] the values of $k_3 K_2 K_1$ and k_3 were obtained as the slope and intercept respectively. From the respective plots of the data a straight line was obtained with a positive intercept, which confirms the validity of equation (10).

For xylose the values presented in figures 1 and 3, obtained from the plots of Mn (II)/rate against 1/[S] and Mn (II)/rate against 1/ [H$^+$] were, respectively, 2.123 moldm^{-3}s^{-1} and 0.0483 moldm^{-3}s^{-1}; the value k_3 obtained from the intercepts of the above plots are 0.308 s^{-1} and 0.033 s^{-1}, respectively.

A similar plot was also made for arabinose, and it also supports the validity of the equation (figures 5 and 7) and the values of the plot were found to be 0.416 moldm^{-3}s^{-1} and 0.092 moldm^{-3}s^{-1} and the value of k_3 obtained from the intercepts of the above plots are 0.280 s^{-1} and 0.072 s^{-1}.

At low concentration of [S] and [H$^+$] the whole 1 >> $K_2 K_1$[S][H$^+$] will be valid, so the rate = $k_3 K_2 K_1$[S][H$^+$][VO$_2^+$].

The graph of rate/Mn (II) vs. [S] and a graph of rate/Mn (II) vs. [H$^+$] were plotted; the values of $k_3 K_2 K_1$ obtained for xylose (figures 2 and 4) are 2.045 moldm^{-3}.s and 0.040 moldm^{-3}.s respectively.

133

Orbital Elec. J. Chem., Campo Grande, 2(2): 127-139, 2010
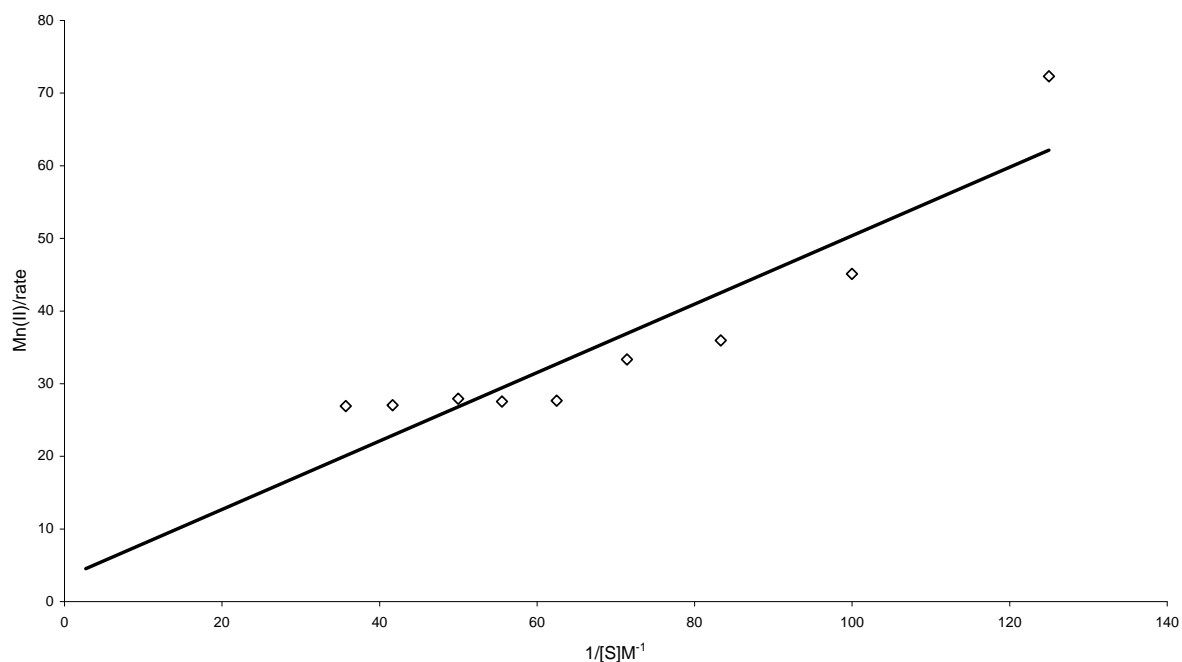
Figure 1. Plot of Mn (II)$_T$/k$_{obs}$ against 1/[xylose] at 40°C. [V (V)] = 1 × 10^{-3} M, [MnCl$_2$] = 6 × 10^{-4} M; [KCl] = 5 × 10^{-4} M; [NaClO$_4$] = 0.1 M, [HClO$_4$] = 0.15 M.

Figure 2: Plot of rate/Mn (II)$_T$ against [xylose] at 40°C . [V (V)] = 1 × 10^{-3} M, [MnCl$_2$] = 6 × 10^{-4} M; [KCl] = 5 × 10^{-4} M; [NaClO$_4$] = 0.1 M, [HClO$_4$] = 0.15 M.

134

Orbital Elec. J. Chem., Campo Grande, 2(2): 127-139, 2010

Figure 3: Plots of Mn (II)$_T$/k$_{obs}$ against 1/[H$^+$] for xylose at 40°C: [xylose]= 0.01 M [V (V)] = 1 × 10^{-3} M, [MnCl$_2$] = 6 × 10^{-4} M; [KCl] = 5 × 10^{-4} M; [NaClO$_4$]= 0.1 M.
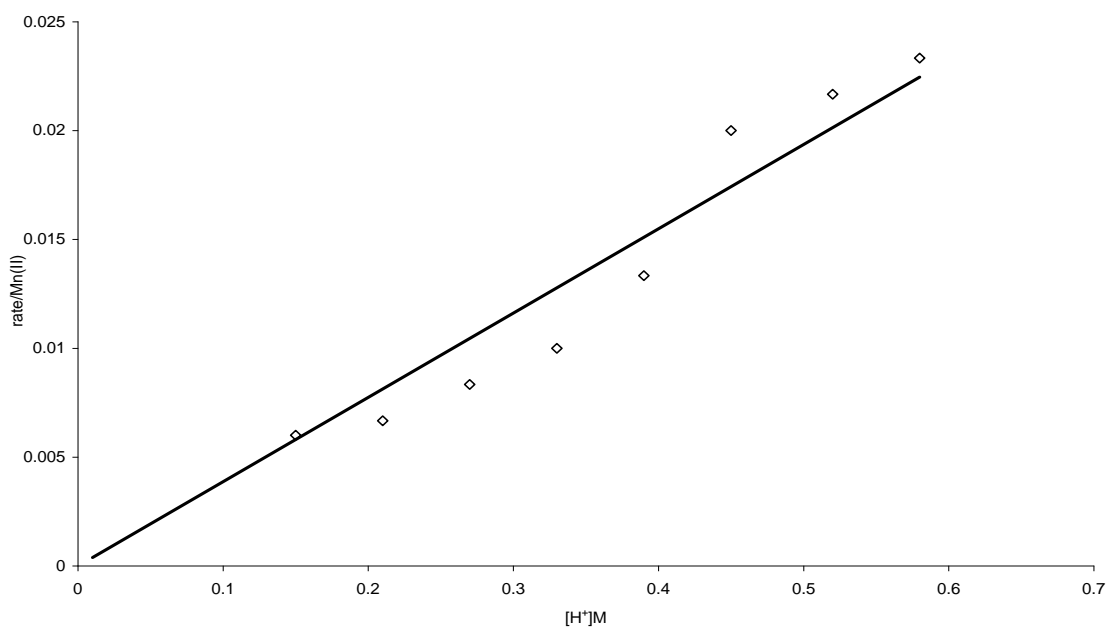
Figure 4. Plot of rate/Mn (II)$_T$ against [H$^+$] for xylose at 40°C.[xylose]= 0.01 M, [V (V)] = 1 × 10^{-3} M, [MnCl$_2$] = 6 × 10^{-4} M; [KCl] = 5 × 10^{-4} M; [NaClO$_4$] = 0.1 M.

135

Orbital Elec. J. Chem., Campo Grande, 2(2): 127-139, 2010
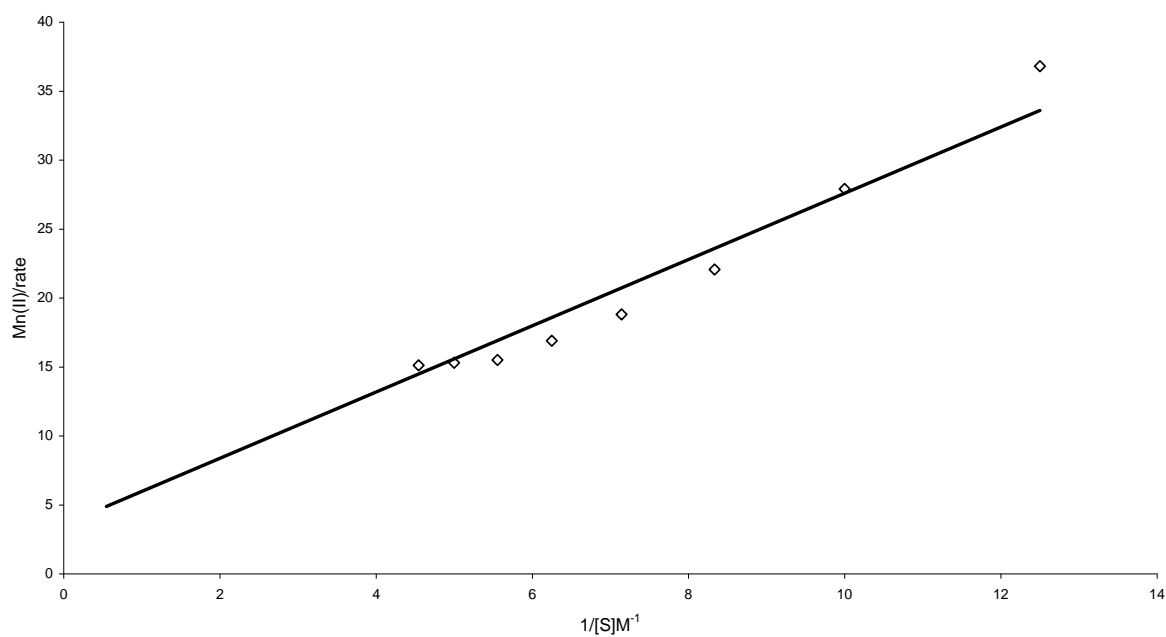
Figure 5. Plot of Mn $(II)_T$/rate against 1/[arabinose]: [V (V)] = 1 × 10^{-3} M, [MnCl$_2$] = 6 × 10^{-4} M; [KCl] = 5 ×10^{-4} M; [NaClO$_4$] = 0.1 M, [HClO$_4$] = 0.15 M.
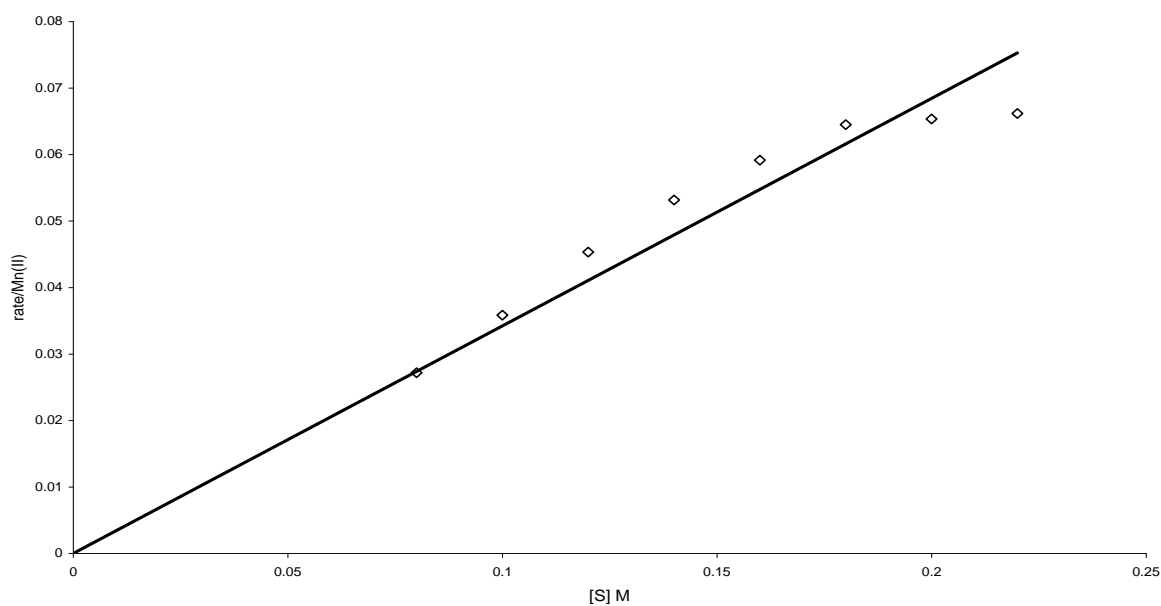
Figure 6. Plot of rate/Mn $(II)_T$ against 1/[arabinose] at 40°C [V (V)] = 1 × 10^{-3} M, [MnCl$_2$] = 6 × 10^{-4} M; [KCl] = 5 ×10^{-4} M; [NaClO$_4$]= 0.1 M, [HClO$_4$] = 0.15 M

136

Orbital Elec. J. Chem., Campo Grande, 2(2): 127-139, 2010
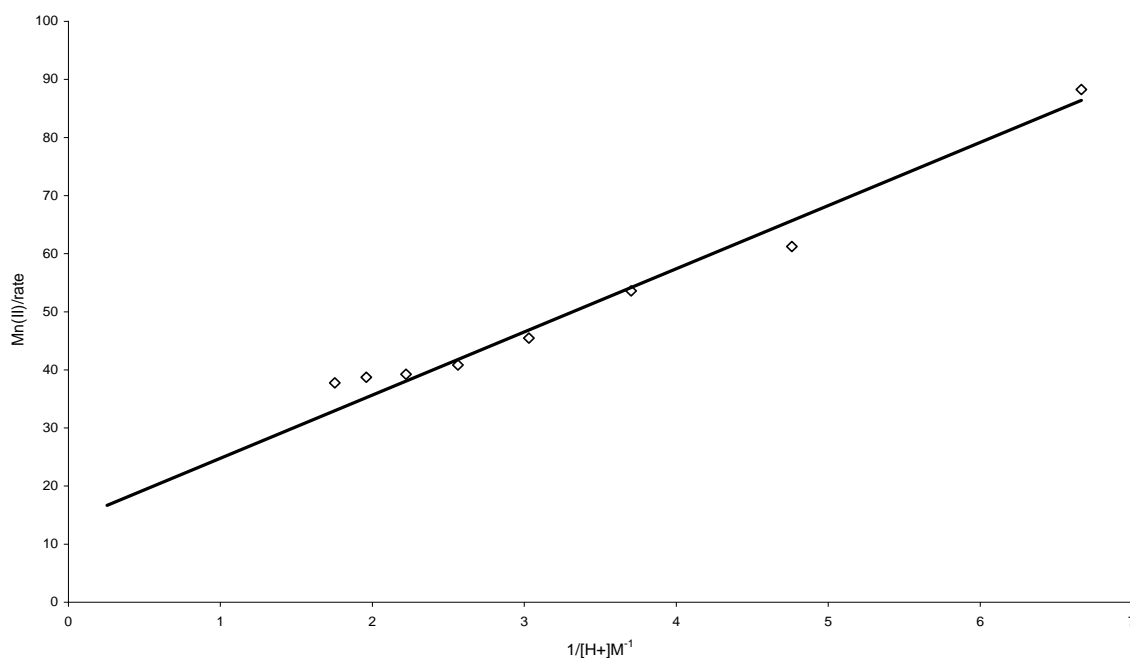
Figure 7. Plots of Mn (II)$_T$/rate against 1/[H$^+$] for arabinose at 40°C. [arabinose] = 0.01 M [V (V)] = 1 × 10^{-3} M, [MnCl$_2$] = 6 × 10^{-4} M; [KCl] = 5 × 10^{-4} M; [NaClO$_4$] = 0.1 M.
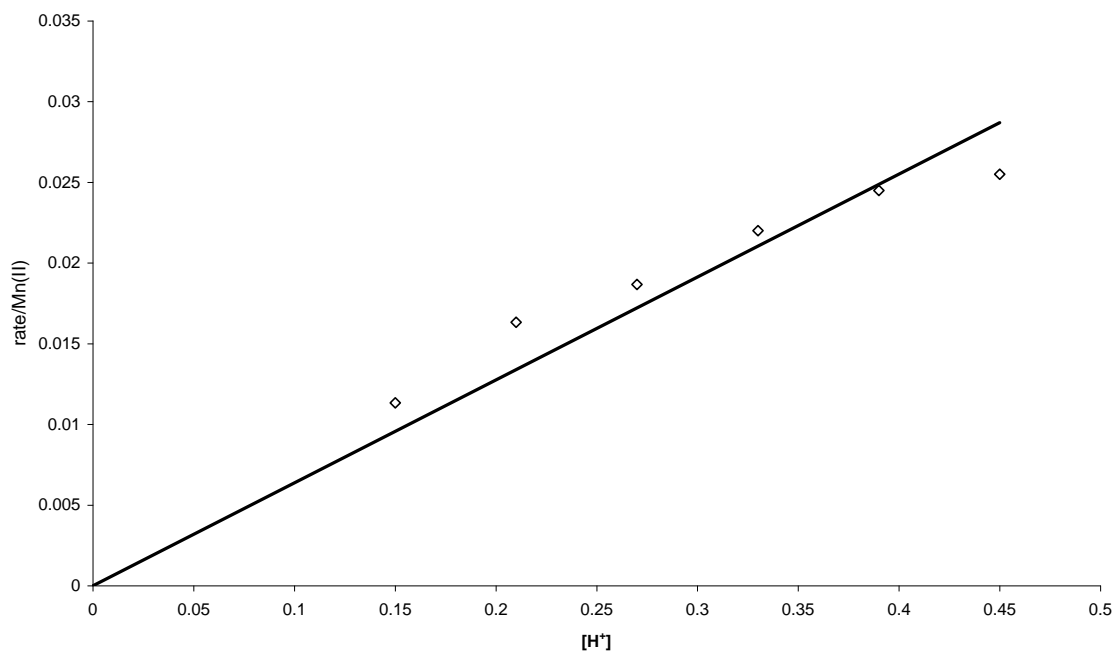
Figure 8: Plots of rate/Mn (II)$_T$ against [H$^+$] for arabinose at 40°C: [arabinose] = 0.01 M, [V (V)] = 1 × 10^{-3} M, [MnCl$_2$] = 6 × 10^{-4} M; [KCl] = 5 × 10^{-4} M; [NaClO$_4$]= 0.1 M.

137

Orbital Elec. J. Chem., Campo Grande, 2(2): 127-139, 2010

A similar plot for arabinose gives the values of (figures 6 and 8) $k_3K_2K_1$ to be 0.342 moldm^{-3}.s and 0.064 moldm^{-3}.s respectively. The table 4a and 4b below gives the value of $k_3K_2K_1$ and k_3 obtained from the various plots above.

Table 4a. Values of $k_3K_2K_1$ obtained from the various plots.

Sugars	Mn (II)/rate vs. 1/[S]	Mn (II)/rate vs. 1/[H$^+$]	Rate/Mn (II) vs.[S]	Rate/Mn (II) vs. [H$^+$]
Xylose	2.123	0.0483	2.045	0.040
Arabinose	0.416	0.092	0.342	0.064

Average linear regression coefficients, r ≥ 0.9, were observed for the parameters.

Table 4b. Values of k_3 were obtained from the plots of Mn (II)/rate versus 1/[S] and Mn (II)/rate.

Sugars	Mn (II)/rate vs. 1/[S]	Mn (II)/rate vs. 1/[H$^+$]
Xylose	0.308	0.033
Arabinose	0.280	0.072

Average linear regression coefficients, r ≥ 0.9, were observed for the parameters.

The plots based on the two equations reveal that the values of $k_3K_2K_1$ and k_3 are in good agreement with one another. These results support the validity of the rate law equation.

$$Mn(II)_T * \frac{1}{Rate} = \frac{1}{k_3K_2K_1[\,S\,]\,[H^+\,]\,[VO_2^+]} + \frac{1}{k_3[\,VO_2^+]}$$

Conclusion

Vanadium, like other transition metals, has catalytic properties due to its participation in the rate determining step (slow step); the vanadium V catalyst works by providing an alternative reaction pathway to the reaction product. The rate of the reaction is increased as this alternative route has lower activation energy than the reaction route not mediated by the catalyst. Our conclusions are based on the spectral information and the observed kinetic data.

i. The observed negative entropy of activation for the oxidation of both sugars supports the fact that a complex is formed between the [sugar], [V (V)] and Mn (II).

ii. The value of activation energy (Ea) of the catalyzed and the uncatalysed paths is consistent with the accepted view that a slow reaction would require a higher energy of activation and also that the reactions are catalysed by Mn (II) under the reaction conditions.

138

Orbital Elec. J. Chem*., Campo Grande,* 2(2): 127-139, 2010

References and Notes

[1]   Odebunmi, E. O.; Iwarere, S. A.; Owalude, S. O. *Int. Journal chem.* **2006**, *16*, 167.

[2]   Odebunmi, E. O.; Marufu, R. *Nigerian Journal of Science*, **1999**, *33*, 133.

[3]   Sen Gupta, K. K; Chatterjee, U. *Carbohydr. Res*. **1984**, *126*, 321.

[4]   Tripathi, R.; Upadhyay S. K. *Int. J. Chem. Kinet.* **2004**, *36*, 441.

[5]   Singh, A. K.; Srivastava, J; Rahmani, S.; Singh, V. *Carbohydr. Res.* **2006**, *341*, 397.

[6]   Singh, A. K.; Chopra, D.; Rahmani, S.; Singh, B. *Carbohydr. Res.* **1998**, *314*, 151.

[7]   Singh, A. K.; Singh, A.; Gupta, R.; Saxena, M.; Singh, B. *Trans. Met. Chem.* **1992**, *17*, 413.

[8]   Singh, A. K.; Chaurasia, N.; Rahmani, S.; Srivastava, J.; Singh, A.K. *J. Chem. Res.* **2005**, 304.

[9]   Khan, Z.; Babu, P. S. S.; Kabir-ud-Din. *Carbohydr. Res.* **2004**, *339*, 133.

[10]   Ogunlaja, A. S.; Odebunmi, E. O; Owalude, S. O. *Pacific Journal of Science and Technology* **2009**, *10*, 451.

[11]   Graham, C. H.; John, S. H. *Chemistry in Context*. 8. ed. UK: Nelson Thornes Ltd., 1995, p. 291.

[12]   Feigl, F. *Spot Tests in Organic Analysis*. New York: Elsevier, 1960, p. 368.

[13]   Mehrotra, R. N. *J. Chem Soc.* **1968**, 642.

[14]   Turney, T. A. *Oxidation Mechanism*, London: Butterworth's, **1965**, p. 35.

[15]   Waters, W. A.; Littler, J. S. *J. Chem. Soc.* **1959**, 3014.

[16]   Huaisheng, W.; Aimei, Z. *Microchemical Journal* **1997**, *57*, 218.

[17]   Zucker, L.; Hammet, L. P. *J. Am. Chem. Soc.* **1939**, *61*, 2791.

[18]   Frost, A. A..; Pearson, R. G. *Kinetics and mechanism*. New York: Wiley & Sons, 1970, p. 123.

[19]   Mulla, R. M.; Hiremath, G. C.; Nandibewoor, S. T. *J. Chem Sci.* **2005**, *117*, 33.

139

Orbital Elec. J. Chem*., Campo Grande*, 2(2): 127-139, 2010

Full Paper

Preparation of Co-Mo catalyst using activated carbon produced from egg shell and SiO$_2$ as support – A hydrogenation study

*Adeniyi S. Ogunlaja[*a], Olalekan S. Alade[b], Funmilola Y. Oladipo[a]*

[a]Department of Chemistry, University of Ilorin, P. M. B. 1515, Ilorin, Nigeria
[b]Department of Biotechnology, Bells University of Technology, PMB 1015, Ota, Ogun state, Nigeria

ABSTRACT: *The preparation of a series of cobalt-molybdenum (Co-Mo) catalysts supported on SiO$_2$ and carbonized egg shells were investigated using standard procedures; the catalysts were further calcined at the 500 ^{o}C temperature to generate the internally consistent set, and the metal atoms content were varied in a regular manner. The ratio 1:4 (Co^{2+}: Mo^{6+}) by weight was employed for the various catalysts prepared. The carbonized egg shells were divided into two parts: the first part was leached with HNO$_3$, as the other one was not leached. Activity tests were run using these catalysts containing leached and unleached carbon for the hydrogenation of methyl orange; the changes in absorbance regarding the unhydrogenated methyl orange at a wavelength of 460 nm were respectively 0.07 and 0.067 when the catalyst containing the leached carbonized egg shell (catalyst A) and the catalyst containing the unleached activated carbon (catalyst B) were used for the hydrogenation reaction. This confirms that catalyst A is more efficient in hydrogenating methyl orange than catalyst B.*

***Keywords**: methyl orange; hydrogenation; cobalt-molybdenum catalyst*

Introduction

The production of active hydrogenation and hydrodesulphurization (HDS) catalysts is one of the most urgent issues in the petroleum industry. Industrial applications of hydrodesulphurization catalysts are generally solid consisting of metals, metal oxides and some salts [1].

These catalysts may be classified in accordance with their customary use.

---

[*] Corresponding author. E-mail: slaja1@yahoo.com

Vigorous catalysts suitable to the hydrogenation of alkyne and alkene linkages, aldehydes and ketones include nickel, cobalt, molybdenum, and tungsten oxides, as well as sulphides. Catalysts working under mild conditions for stepwise hydrogenation include oxides of copper, zinc, chromium, metallic platinum, and palladium. Hydrogen is absorbed on the metal surface [2].

Activated carbon has been used as an efficient sorbent to odor removal, solvent recovery, decolorization, dechlorination, ozone annihilation, H_2S/CS_2 removal, gold recovery, filtration, condensed deviling, fuel gas cleaning, industrial wastewater treatment, drinking water conditioning etc. Activated carbons can be prepared from a variety of materials. The most commonly used raw materials for the preparation of activated carbons in commercial practice are peat, coal, lignite, wood, and agricultural by-products. The production of activated carbon from agricultural by-products serves a double purpose of converting unwanted, surplus agricultural waste into useful, valuable material and provides an efficient adsorbent material for the removal of organic pollutants from waste water.

Activated carbons have a large adsorption capacity for a variety of organic pollutants, but are expensive due to difficult regeneration and higher disposal cost [3–9]. In view of the high cost and tedious procedure for the preparation and regeneration of activated carbon, there is a continued search for the development of adsorbents using cheaper raw materials. Many researchers have studied the feasibility of less expensive activated carbons prepared from spent oil shake [5, 6], bagasse fly ash [4], tamarind nut [8], soybean hulls [7], salvinea molta Mitchell [9], and coconut husk [3] for the removal of phenolic compounds.

Solids such as carbon [10], silica [11] and titania [14] have been reported as active carriers of hydrodesulphurization and hydrogenation catalysts. Co–Mo or Ni–Mo (W)-based catalysts have been extensively used in industry for HDS reactions [19, 20]. The so-called CoMoS model proposed by Topsøe et al. [19, 21, 22] has attracted attention. It is considered that understandings of the active sites of the catalysts are extensively promoted by their selective preparations. It has been found [23-26] that the addition of a chelating agent, such as nitrilotriacetic acid (NTA) in an impregnation solution provides a method to selectively prepare a Co(Ni)MoS phase, excluding the formation of separate Co(Ni) sulfide phases. Numerous studies [27-30] on the catalyst systems, accordingly, have been carried out to investigate the mechanism of synergy generation between Co and Mo, the structure of catalytically active sites, the reaction mechanisms of HDS and hydrogenation, support effects, and so on.

Papadopoulou et al. [31] prepared a series of CoMo/γ-Al$_2$O$_3$ catalysts using various methodologies. One of them was prepared by depositing the Mo species on the support

141

Orbital Elec. J. Chem., Campo Grande, 2(2): 140-150, 2010

via the equilibrium deposition filtration (EDF) technique and then the Co species by dry impregnation. Another catalyst (co-EDF) was prepared by depositing the Co and Mo species simultaneously via EDF. A third catalyst (co-WET) was prepared by depositing Mo and Co species simultaneously using the wet impregnation method. The fourth catalyst (s-DRY) was prepared by depositing the Mo species through wet impregnation and then the Co species by dry impregnation, then the fifth catalyst (WET) was prepared by mounting the Mo species through successive dry impregnations, and then the Co species by dry impregnation. Their catalytic activity for the hydrodesulfurization of thiophene was determined. The trend observed was given as (EDF>co-EDF>co-WET>s-DRY>WET). The EDF and co-EDF catalysts were reported to exhibit relatively low hydrogenating activity.

The catalytic performance of Co–Mo sulfide catalysts depends strongly on preparation variables and additives [19]. The preparation method may modify the edge dispersion and stacking degree of MoS_2 particles and the efficacy of transforming Co into CoMoS.

In this study we prepared Co-Mo/SiO_2-activated carbon catalysts for leached and unleached activated carbons with a varying amount of Co and Mo content. The catalytic activities of the catalysts produced were compared for the hydrogenation of methyl orange.

Material and Methods

Materials and methods used

All reagents and chemicals used in the study were of analytical reagent grade. Ammonium Heptamolybdate (AHM), Colbalt Chloride ($CoCl_2.6H_2O$) and SiO_2. Egg shells, cellulose filter muffle furnace (Uniscope SM9080), UNISPEC SM7504-UV spectrophotometer.

Preparation of activated carbon

The raw material, i.e. egg shells, was collected. The collected egg shells were thoroughly washed with double distilled water to remove any extraneous material and then dried at room temperature. 250 g of the dried egg shell were carbonized for about 4 hours to remove the non-carbonaceous components. The carbonized egg shell was collected, grounded, and sieved with a 90 μm mesh.

Two types of activated carbon were prepared, namely leached and unleached activated carbon.

The leached carbon was prepared by carefully pouring 50 g of carbonized egg shell into a beaker containing 40 mL of concentrated HNO_3. After allowing the mixture to settle for a while, a litmus paper was used to check the level of acidity of the mixture's

142

Orbital Elec. J. Chem., Campo Grande, 2(2): 140-150, 2010

filtrate. Continuous washing of the mixture was carried out with double distilled water until the filtrate was acid free.

The acid free leached carbonized egg shell was dried at 130–150 ^{o}C for 24 hours and then subjected to thermal activation at different temperatures between 600 and 800 ^{o}C for 1 hour in a muffle furnace.

The unleached activated carbon was prepared by subjecting the carbonized egg shell to thermal activation at different temperatures between 600 and 800 ^{o}C for 1 hour in a muffle furnace.

Activation was carried out under closely controlled process parameters to get optimum properties. Finally, the product was adequately cooled before it was exposed to the atmosphere. The temperature and time were optimized by observing the surface properties of the activated products obtained.

Preparation of Co-Mo catalyst and characterization

The technique used for preparing the catalyst below is the impregnation which involves the following procedure:

1.   Evaluation of the porous support.

2.   Contracting the support with a solution containing a soluble salt of the component being added.

3.   Drying the component.

4.   Calcination and activation of the component.

A weighed amount of ammonium heptamolybdate AHM (aqueous mixture) was dispensed into a beaker and impregnated dropwise onto a known weight of leached and unleached activated carbon/SiO_2 in the crucible. The solution was stirred and well soaked. The solution was dried in a muffle at the 120-130 ^{o}C temperature for 6 hours. After this time the temperature of the furnace was adjusted to 500 ^{o}C for calcinations of the MoO_3-activated carbon, which took 4 hours.

 A weighed freshly prepared Cobalt Chloride of weighed amount was impregnated in dropwise into the crucible containing MoO_3/SiO_2-activated carbon. The solution was stirred and well soaked; the other crucibles containing MoO_3-activated carbon were also impregnated with various amounts of $CoCl_2$. Drying and calcination were also carried out at 120 ^{o}C for 6 hours and 500 ^{o}C for 4 hours, respectively. This method was used for both leached and unleached activated carbon.

The ratio of Co^{2+} ($CoCl_2$): Mo^{6+} (MoO_3) used for the various catalysts prepared is 1:4. The equations below were used for preparing the catalyst; tables 1-3 present the

143

Orbital Elec. J. Chem*., Campo Grande,* 2(2): 140-150, 2010

comparison between the expected theoretical weight and the experimental weight observed.

The equations for the reaction were:

Equation 1: $(NH_4)_6Mo_7O_{24} \cdot 4H_2O \xrightarrow{\Delta} 7MoO_{3\ (s)} + 6NH_{3\ (g)} + 7H_2O_{\ (g)}$

Equation 2: $CoCl_2.6H_2O_{(s)} \xrightarrow{\Delta} CoCl_{2(s)} + 6H_2O_{(g)}$
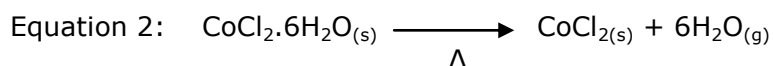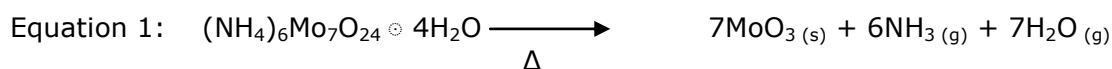
Equation 3:   Weight of the catalyst= $\dfrac{(Weight\ of\ Mo^{6+} + Weight\ of\ Co^{2+}) \times 100}{25}$

Equation 4:   Weight of the support = weight of catalyst – (Weight of Mo^{6+} + Weight of Co^{2+})

Table 1. Theoretical results for both catalysts (leached and unleached).

Sample	Wt. of AHM (g)	Wt. of CC[a] (g)	Wt. of support[b] (g)	Wt. of Mo⁶⁺ (g)	Wt. of Co²⁺ (g)	Wt. of catalyst (g)
1	2.431	0.908	7.437	1.983	0.496	9.916
2	4.650	1.736	14.220	3.792	0.948	18.960
3	6.500	2.427	19.875	5.300	1.325	26.50

[a]CC = calcium chloride. [b]Support = activated carbon/SiO_2.

Table 2. Experimental results for the leached activated carbon (catalyst A).

Sample	Wt. of AHM (g)	Wt. of CC[a] (g)	Wt. of support[b] (g)	Wt. of catalyst (g)
1	2.431	0.908	7.437	8.312
2	4.650	1.736	14.200	17.901
3	6.500	2.427	19.865	25.0

[a]CC = calcium chloride. [b]Support = activated carbon/SiO_2.

Table 3. Experimental results for the unleached activated carbon (catalyst B).

Sample	Wt. of AHM (g)	Wt. of CC[a] (g)	Wt. of support[b] (g)	Wt. of catalyst (g)
1	2.431	0.787	7.434	8.435
2	4.650	1.504	14.210	18.430
3	6.500	2.102	19.843	25.701

[a]CC = calcium chloride. [b]Support = activated carbon/SiO_2.

The tables 1-3 display the weight of the catalyst support and that of the catalyst prepared using the leached and unleached activated carbon. The slight difference in the reported theoretical weight compared to the experimental weight was due to the loss of some extraneous materials, such as impurities, during calcinations and activation of the catalyst and support.

Hydrogenation/reduction of methyl orange

The hydrogenation system setup was composed by a conical flask with an outlet

144

Orbital Elec. J. Chem., Campo Grande, 2(2): 140-150, 2010

connected to another conical flask by a rubber tube and a glass tube. The first conical flask (A) served as the hydrogen generation, as the second flask (B) serves as the hydrogenation flask (Figure 1).
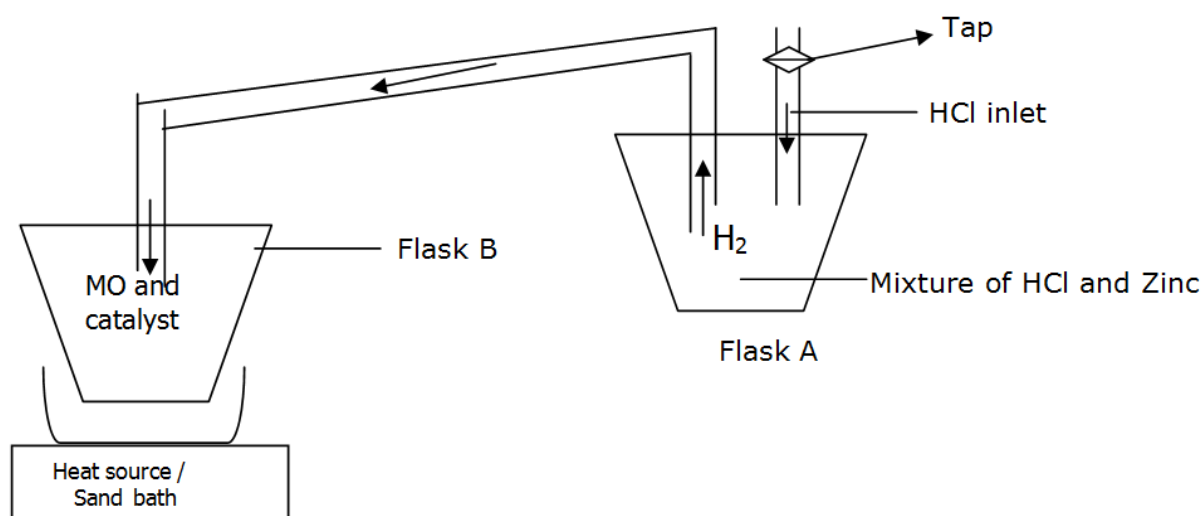
Figure 1. Setup for the hydrogenation of the methyl-orange.

0.5 g of the catalyst was weighed and added into the hydrogenation flask containing a solution of 150 mL methyl orange (0.0199 mM). Hydrogen gas was generated from the first flask (A) through a reaction between zinc dust (22 g) and hydrochloric acid (2 M). The sand bath was used as a source of heat on which the hydrogenation flask was placed. The tap of the burette was opened to purge the system and also to allow the catalyst activation.

The hydrogenation system was maintained at a temperature of about 230 $^\circ$F (110 $^\circ$C) and pressure of 2.64×10^5 Pa for 3 hours. The system was allowed to cool down and then filtered with 0.5 µm cellulose nitrate filter. The reaction product was spectrophotometrically measured using a UNISPEC SM7504UV spectrophotometer (Table 4). The concentration change was calculated from the linear calibration plot of the non-hydrogenated methyl orange at a wavelength of 465 nm.

Table 4. Values of concentration (mol/dm^3) of methyl orange and the corresponding absorbance.

Concentration (mol/dm^3)	Absorbance
0.001	0.144
0.002	0.271
0.003	0.336
0.004	0.451
0.005	0.549
0.006	0.689
0.007	0.824
0.008	1.032
0.009	1.356

Square correlation coefficient (R^2) = 0.9569.

145

Orbital Elec. J. Chem., Campo Grande, 2(2): 140-150, 2010

The calibration plot of absorbance against concentration (mol/dm^3) for methyl orange is shown in Figure 2.
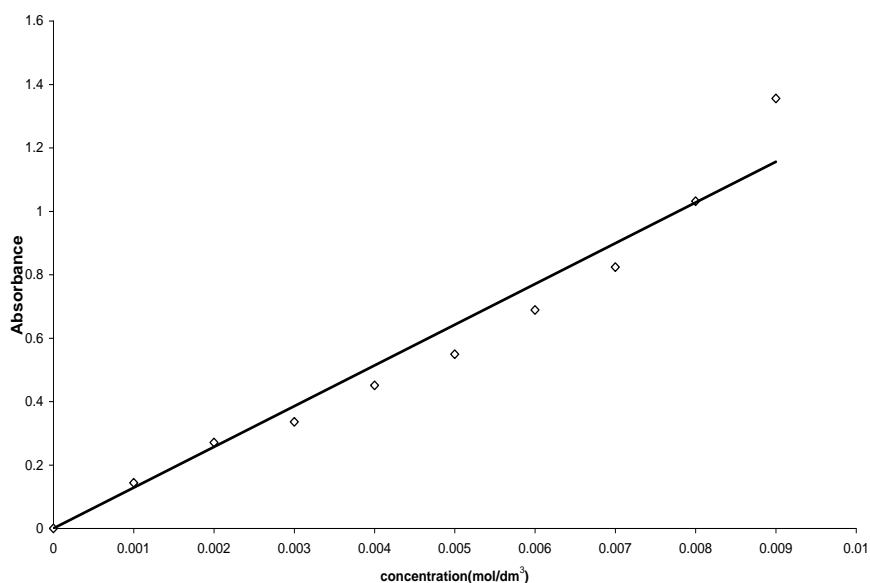
Figure 2. Graphical plot of absorbance against concentration (mol/dm^3).

Results and Discussion

The spectral plot of the various catalyst in distilled water were carried out after subjecting the various catalysts to the same temperature at which the hydrogenation reaction took place (110 ^{o}C) for 3 hours in the absence of methyl orange; this blank experiment was carried out in order to check the influence of filtration and color change produced by the catalyst after the reaction. The spectra graphs of the various catalysts are shown in Figure 3.

From the plots of the two catalysts, it may be reported that the catalyst prepared with leached activated carbon from egg shell (catalyst A) has a maximum absorbance of 0.151 at a wavelength of 500 nm, as the catalyst prepared with unleached activated carbon from egg shell (catalyst B) has an absorbance of 0.142 at the same wavelength, which is about the wavelength of Co (II).

Considering Figure 4, the concentration changes for the hydrogenated methyl orange were calculated at a wavelength of 460 nm [31] with reference to the unhydrogenated methyl orange. Changes in absorbance were observed to be 0.07 and 0.067, respectively, for the leached and unleached activated carbon.

With the catalyst used, it is possible to perform the hydrogenation of methyl orange at lower temperatures (a little above room temperature) and atmospheric pressure. Temperatures and pressures higher than 300 ^{O}C and 10 bars would favor the

146

Orbital Elec. J. Chem*., Campo Grande,* 2(2): 140-150, 2010

hydrogenation of N=N [17, 18].
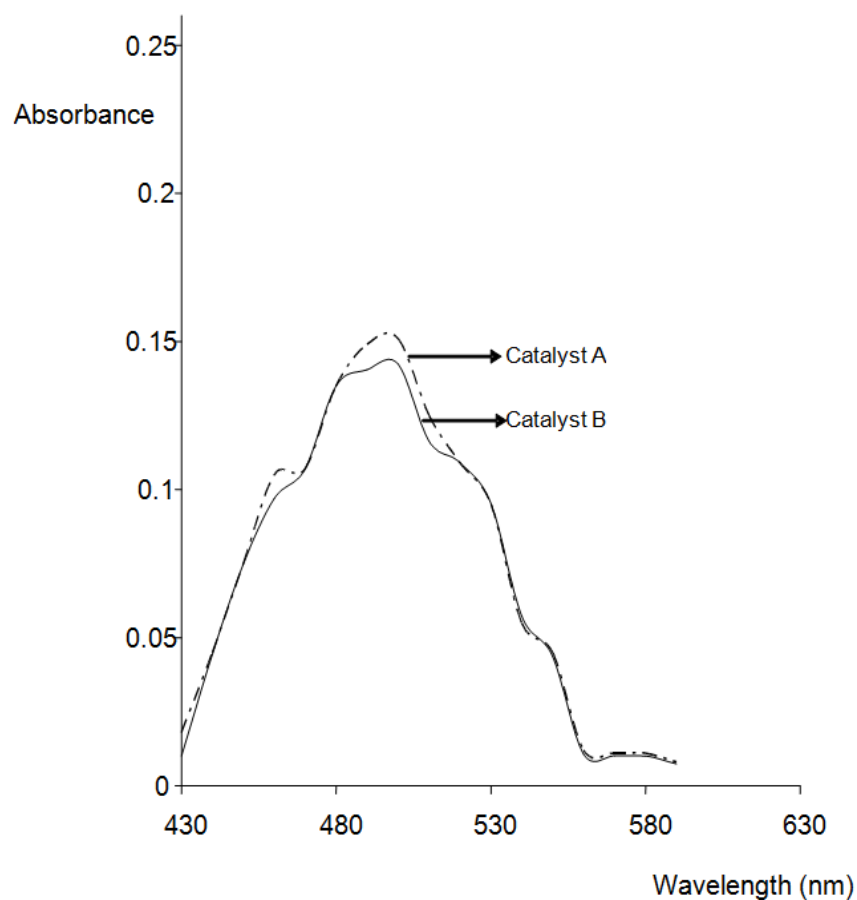
Figure 3. Spectra plot of solution containing catalyst A and B after hydrogenation in the absence of Methyl orange (MO). Catalyst A: Leached activated carbon from egg shell. Catalyst B: Unleached activated carbon from egg shell.
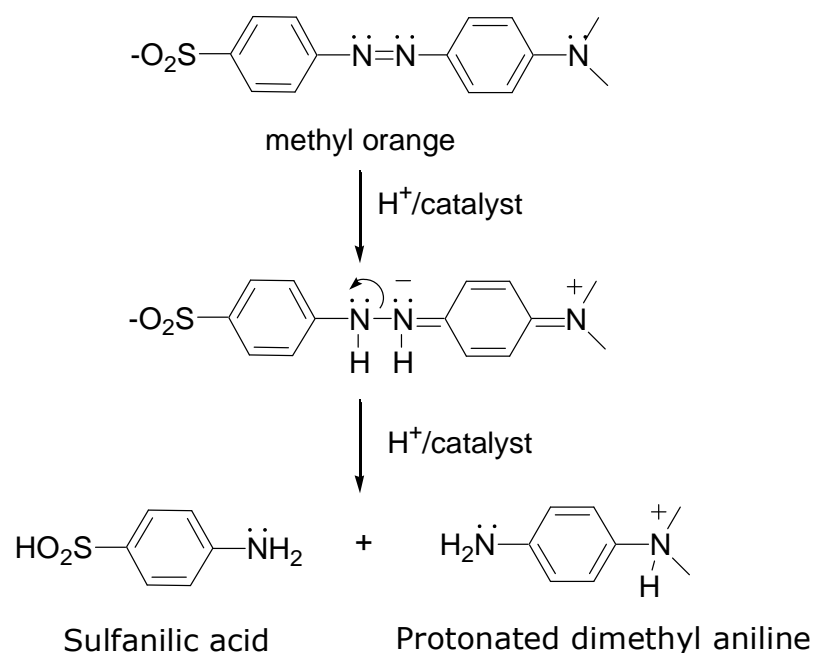
Scheme 1. Hydrogenation of methyl orange.

147

Orbital Elec. J. Chem., Campo Grande, 2(2): 140-150, 2010

The experiment performed with leached activated carbon provided the best result for the hydrogenation process; this was observed through the change in absorbance and the presence of a faint pink-yellowish color.
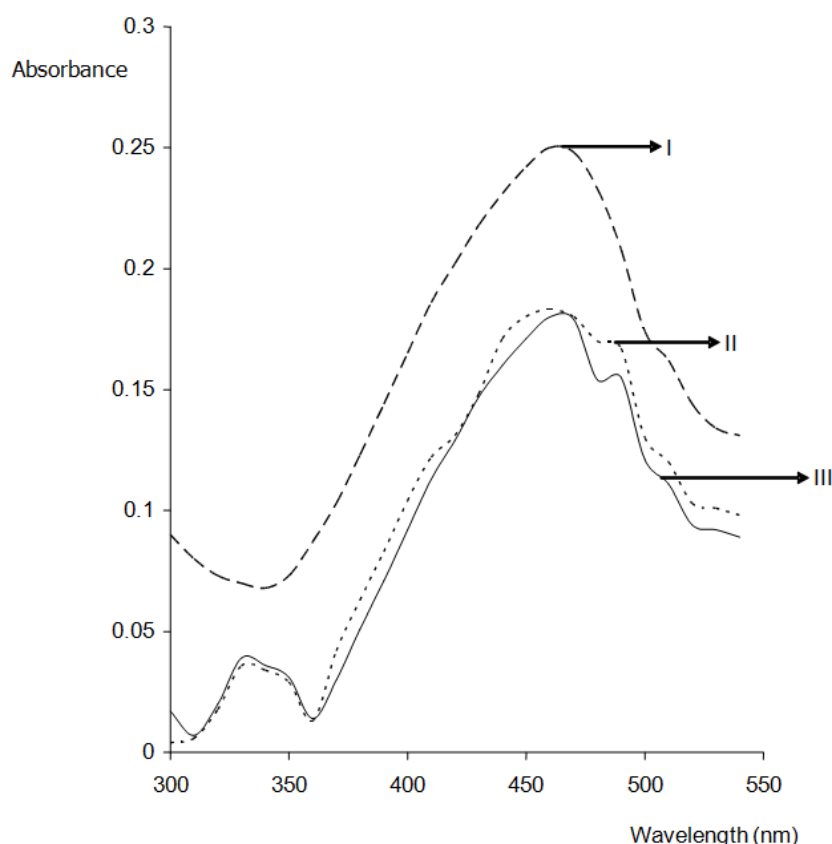
Figure 4. UV-visible spectra of methyl orange (MO) solution (0.0199 mM) and the sample obtained after the hydrogenation reaction experiment. I = UV–visible spectra of methyl orange (MO) solution (0.0199mM). II = UV–visible spectra of hydrogenated ethyl orange (MO) solution (0.0199 mM) using catalyst B. III = UV-visible spectra of hydrogenated methyl orange (MO) solution (0.0199 mM) using catalyst A.

Conclusion

Both the leached and unleached activated carbon has great effects on the hydrogenation process. The hydrogenation reaction was conducted at a low temperature (110°C) in order to prevent a high pressure build-up in the glass system. Due to this low temperature the hydrogenation process could not be very effective [17]. A temperature between 500-1,000 ^{o}C, which imposes a very high pressure into the system, would be more effective.

References and Notes

[1]   Gupta, V. K.; Sharma, S.; Yadav, I. S, Mohan, D. *J. Chem. Technol. Biotechnol*. **1998**, *71*, 180.

[2]   Housecroft, C. E.; Constable, E. C. An Introduction to organic, inorganic and physical chemistry. 2nd ed. New York: Prentice Hall, 2003, p. 867.

148

Orbital Elec. J. Chem., Campo Grande, 2(2): 140-150, 2010

[3]   Vinod, V. P.; Anirudhan, T. S. *J. Sci. Ind. Res*. **2002**, *61*, 128.

[4]   Burleigh, M. C.; Markowitz, M. A.; Spector, M. S.; Gaber, B. P. *Environ. Sci. Technol*. 2002, 36, 2515.

[5]   Darwish, N. A.; Halhouli, K. A.; Al-Dhoon, N. M. *Sep. Sci. Technol*. **1996**, *31*, 705.

[6]   Singh, K. P.; Mohan, D.; Sinha, S.; Tandon, G. S.; Ghosh, D. *Ind. Eng. Chem. Res*. **2003**, *43*, 1965.

[7]   Flock, C.; Bassi, A.; Gijzen, M. *J. Chem. Technol. Biotechnol*. **1999**, *74*, 303.

[8]   Srinivasan, K. R.; Ramadevi, A. *Ind. J. Environ. Hlth*. **1998**, *30*, 303.

[9]   Sankaran, N. B.; Anirudhan, T. S. *Indian J. Eng. Mater. Sci*. **1999**, *6*, 229.

[10]   Topsøe, H.; Clausen, B. S.; Topsøe, N. Y.; Pedersen, E. *Ind. Eng. Chem. Fundam*. **1986**, *25*, 25.

[11]   Muralidhar, G.; Massoth, F. E.; Shabtai, J. *J. Catal*. **1984**, 44.

[12]   Blanchard, P.; Payen, E.; Grimblot, J.; Le Bihan, L.; Poulet, O.; Loutaty, R. *J. Mole. Catal. A-Chem*. **1998**, *135*, 143.

[13]   Singh, K. P.; Mohan, D.; Sinha, S.; Tandon, G. S.; Ghosh, D. *Ind. Eng. Chem. Res*. **2003**, *42*, 1965.

[14]   Ramirez, J.; Fuentes, S.; Diaz, G.; Vrinat, M.; Breysse, M.; Lacroix, M. *Appl. Catal*. **1989**, *52*, 211.

[15]   Radovic, L. R, Moreno-Castilla, C., Rivera-Utrilla, J. In: Radovic, L. R. eds. Carbon materials as adsorbents in aqueous solutions. Chemistry and Physics of Carbon, 27, New York: Marcel Dekker, Chapter 4, p. 227, 2000.

[16]   Urbano, F. J.; Marinas, J. M. *J. Mol. Catal. A-Chem*. **2001**, *173*, 329.

[17]   Talukdar, A. K.; Bhattacharyya, K. G. *Appl. Catal. A-Gen*. **1993**, *96*, 229.

[18]   Zazo, J. A.; Casas, J. A.; Mohedano, A. F.; Gilarranz, M. A.; Rodrıguez, J. *J. Environ. Sci. Technol*. **2005**, *39*, 9295.

[19]   Topsøe, H.; Clausen, B. S.; Massoth, F. E. In: Anderson, J. R.; Boudard, M., eds. Catalysis-science and technology, Berlin: Springer, 11, 1996.

[20]   Kabe, K.; Ishihara, A.; Qian. W. Hydrodesulfurization and hydro-denitrogenation. Tokyo: Kodansha, 1999.

[21]   Topsøe, H.; Clausen, B. S. *Catal. Rev.-Sci. Eng*. **1984**, *26*, 395.

[22]   Candia, R.; Sørensen, O.; Villadsen, J.; Topsøe, N.; Clausen, B. S.;Topsøe, H. *Bull. Soc. Chim. Belg*. **1984**, *93*, 763.

[23]   Van Veen, J. A. R.; Gerkema, E.; Van der Kraan, A. M.; Knoester, A. *J. Chem. Soc. Chem. Commun*. **1987**, 1684.

[24]   Van Veen, J. A. R.; Gerkema, E.; Van der Kraan, A. M.; Hendriks, P. A. J. M.; Beens, H. *J. Catal*. **1992**, *133*, 112.

[25]   Louwen, S. P. A.; Prins, R. *J. Catal*. **1992**, *133*, 94.

[26]   Medici, L.; Prins, R. *J. Catal*. **1996**, *163*, 94.

[27]   Prins, R.; de Beer, V. H. J.; Somorjai, G. A. *Catal. Rev. Sci. Eng*. **1989**, *31*, 1.

[28]   Chianelli, R. R.; Daage, M.; Ledoux, M. J. *Adv. Catal*. **1994**, *40*, 177.

[29]   Whitehurst, D. D.; Isoda, T.; Mochida, I. *Adv. Catal*. **1998**, *42*, 345.

[30]   Breysse, M.; Portefaix, J. L.; Vrinat, M. *Catal. Today*. **1991**, *10*, 489.

[31]   Papadopoulou, Ch.; Vakros, J.; Matralis, H. K.; Kordulis, Ch.; Lycourghiotis, A. *J.*

149

Orbital Elec. J. Chem., Campo Grande, 2(2): 140-150, 2010

Col. and Inter. Sci. **2003**, *261*, 146.

[32] Sadhana, S. R.; Nidhi, D.; Nitin, K. L.; Kagne, S.; Sukumar, D. *Int. J. of Hydrogen Energy*. **2007**, *32*, 2776.

150

Orbital Elec. J. Chem*., Campo Grande,* 2(2): 140-150, 2010

Full Paper

Synthesis and characterization of 12-methyl-7-phenylbenzo[*h*]naphtho[*b*][1,6]naphthyridin-8-one derivatives

Vetrivel Nadaraj[*] and Senniappan Thamarai Selvi

Department of Chemistry (PG & Research), Kongunadu Arts and Science College, G. N. Mills (PO), Coimbatore-641 0299, India

ABSTRACT: *A simple and efficient procedure has been described for the synthesis of 12-methyl-7-phenylbenzo[h]naphtho[b][1,6]naphthyridin-8-ones 3a-g by the multi-component reaction of 4-hydroxy-6-methylquinolin-2(1H)-one 1 with 1-naphthylamine 2 and a variety of aldehydes under microwave irradiation condition. The structures of the newly synthesized compounds were confirmed by analytical and spectral (IR, NMR, and Mass) data.*

Keywords: *condensation; microwave; naphthyridine; naphthylamine; quinoline*

Introduction

Recently there has been an increased interest in the synthesis of naphthyridine and their application in medicinal chemistry as quinoline bioisosteres. The main driving force towards the synthesis of naphthyridine is the search for compounds of therapeutic importance [1, 2]. A large number of derivatives of the naphthyridines and related systems are synthesized for chemotherapeutic and pharmacological evaluation. 1,6-Naphthyridine derivatives represent one of the most active classes of compound possessing a wide spectrum of biological activities such as antibacterial activities [3, 4], antitumor activities [5], antifungal activities [6], muscle relaxant activity [7] and insecticidal activity [8]. Some of the biological active 1,6-naphthyridines compounds are depicted in Figure 1.

Multi-Component Reactions (MCRs) play an increasingly important role in organic

---

[*] Corresponding author. E-mail: vnraj303@yahoo.com

and medicinal chemistry for their high degree of atom economy, convergence, productivity, high selectivity, ease of extraction, excellent yield and broad application in combinatorial chemistry [9-12]. The variation of two or more compounds of the reaction can make available a large number of compound and increase chemical diversity [13, 14]. Recently, microwave induced rate acceleration technology has become a powerful tool in organic synthesis, due to the high heating efficiency giving remarkable rate enhancement and dramatic reduction in reaction time [15-18].

By knowing advantages of multi-component reactions, we wished to synthesize some naphthyridine based nitrogen heterocycles using microwave irradiation coupled with MCR. For this, we have chosen 4-hydroxy-6-methylquinolin-2(1*H*)-one as one of the components.
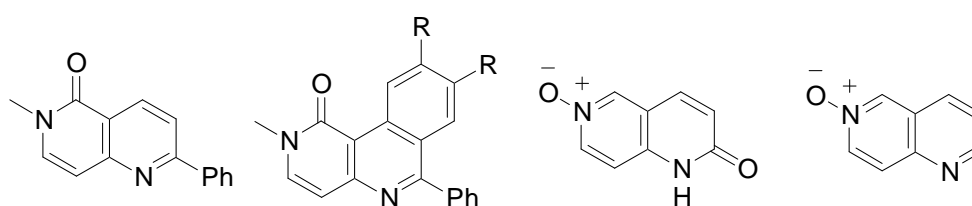
Figure 1. Some 1,6-naphthyridines.

Material and Methods

Melting points (mp) were determined using Boetieus micro-heating table and are uncorrected. IR (KBr, cm^{-1}) spectra were obtained on Shimadzu-8201 spectrophotometer. ^{1}H-NMR spectra were recorded on Bruker AMX-400 spectrometer (400 MHz) using TMS as an internal reference (chemical shifts in δ, ppm). Elemental analyses were performed on Perkin Elmer CHN-analyzer. Mass spectra were recorded on Shimadzu GCMS-QP5050A (70 ev) mass spectrometer. For microwave irradiation a Kenstar (OM-20ESP, 2450 MHz) domestic microwave oven was used.

General Procedure for synthesis of 12-methyl-7-(substituted)phenylbenzo[h] naphtho[b][1,6] naphthyridin-8-ones (3a-g)

A mixture of 1-naphthylamine (0.001 mol), 4-hydroxy-6-methylquinolin-2(1*H*)-ones (1, 0.001 mol), respective aromatic aldehydes (0.001 mol) and 5 drops of TEA was taken in a 100 mL beaker and irradiated in a microwave oven at an output of about 320 W for the specified time (Table 1). The completion of the reaction was tested by TLC, and after completion of the reaction, the mixture was poured in to chilled water. The formed product was filtered, dried and purified by column chromatography using the solvents petroleum ether and ethyl acetate.

12-methyl-7-phenylbenzo[h]naphtho[b][1,6]naphthyridin-8-one (3a)

152

Orbital Elec. J. Chem*., Campo Grande*, 2(2): 151-157, 2010

IR (KBr, cm^{-1}): 1544, 1604 (CN), 1643 (>C=O), 2800-3200 (-NH). ^{1}H NMR (DMSO-d$_6$): δ_H 2.50 (s, 3H, C$_{12}$-CH$_3$), 6.68 (s, 1H, C$_7$-H), 6.71-8.11 (m, 13H, Ar-H), 9.02 (s, 1H, C$_{13}$-H), 11.01 (s, 1H, NH), 11.18 (s, 1H, NH). Ms (*m/z*): 388. Anal. Calculated for C$_{27}$H$_{20}$N$_2$O; C 83.51, H 5.15, N 7.22%, Found C 83.46, H 5.09, N 7.20%.

12-methyl-7-(o-chlorophenyl)benzo[h]naphtho[b][1,6]- naphthyridin-8-one (3b)

IR (KBr, cm^{-1}): 1569, 1604 (CN), 1641 (>C=O), 2800-3260 (-NH). ^{1}H NMR (DMSO-d$_6$): δ_H 2.45 (s, 3H, C$_{12}$-CH$_3$), 6.41 (s, 1H, C$_7$-H), 7.01-8.22 (m, 13H, Ar-H), 13.40 (bs, 2H, 2NH). Ms (*m/z*): 422. Anal. Calculated for C$_{20}$H$_{19}$N$_2$OCl; C 76.78, H 4.50, N 6.64%, Found C 76.75, H 4.47, N 6.60%.

12-methyl-7-(p-chlorophenyl)benzo[h]naphtho [b][1,6]- naphthyridin-8-one (3c)

IR (KBr, cm^{-1}): 1559, 1610 (CN), 1648 (>C=O), 2830-3258 (-NH). ^{1}H NMR (DMSO-d$_6$): δ_H 2.50 (s, 3H, C$_{12}$-CH$_3$), 6.42 (s, 1H, C$_7$-H), 6.92-8.32 (m, 13H, Ar-H), 11.10 (s, 1H, NH), 11.22 (s, 1H, NH). Ms (*m/z*): 422. Anal. Calculated for C$_{20}$H$_{19}$N$_2$OCl; C 76.78, H 4.50, N 6.64%, Found C 76.77, H 4.46, N 6.60%.

12-methyl-7-(m-chlorophenyl)benzo[h]naptho[b][1,6]- naphthyridin-8-one (3d)

IR (KBr, cm^{-1}): 1560, 1618 (CN), 1645 (>C=O), 2860-3280 (-NH). ^{1}H NMR (DMSO-d$_6$): δ_H 2.68 (s, 3H, C$_{12}$-CH$_3$), 6.62 (s, 1H, C$_7$-H), 6.72-8.30 (m, 13H, Ar-H), 11.10 (bs, 2H, 2NH). Ms (*m/z*): 422. Anal. Calculated for C$_{20}$H$_{19}$N$_2$OCl; C 76.78, H 4.50, N 6.64%, Found C 76.78, H 4.48, N 6.62%.

12-methyl-7-(p-hydroxyphenyl)benzo[h]naphtho[b][1,6]- naphthyridin-8-one (3e)

IR (KBr, cm^{-1}): 1564, 1614 (CN), 1643 (>C=O), 2890-3250 (-NH). ^{1}H NMR (DMSO-d$_6$): δ_H 2.43 (s, 3H, C$_{12}$-CH$_3$), 6.48 (s, 1H, C$_7$-H), 6.92-8.10 (m, 13H, Ar-H), 11.10 (s, 2H, 2NH), 11.44 (s, 1H, OH). Ms (*m/z*): 404. Anal. Calculated for C$_{27}$H$_{20}$N$_2$O$_2$; C 80.20, H 4.95, N 6.93%, Found C 80.18, H 4.92, N 6.90%.

12-methyl-7-(o-hydroxyphenyl)benzo[h]naphtho[b][1,6]- naphthyridin-8-one (3f)

IR (KBr, cm^{-1}): 1560, 1604 (CN), 1646 (>C=O), 2800-3300 (-NH). ^{1}H NMR (DMSO-d$_6$): δ_H 2.58 (s, 3H, C$_{12}$-CH$_3$), 6.48 (s, 1H, C$_7$-H), 7.11-8.20 (m, 13H, Ar-H), 11.21 (s, 2H, 2NH), 11.39 (s, 1H, OH). Ms (*m/z*): 404. Anal. Calculated for C$_{27}$H$_{20}$N$_2$O$_2$; C 80.20, H 4.95, N 6.93%, Found C 80.15, H 4.90, N 6.91%.

12-methyl-7-(m-nitrophenyl)benzo[h]naphtho[b][1,6]- naphthyridin-8-one

153

Orbital Elec. J. Chem*., Campo Grande,* 2(2): 151-157, 2010

_(3g)_

IR (KBr, cm^{-1}): 1569, 1618 (CN), 1648 (>C=O), 2890-3380 (-NH).^{1}H NMR (DMSO-d$_6$): δ_H 2.64 (s, 3H, C$_{12}$-CH$_3$), 6.48 (s, 1H, C$_7$-H), 7.08-8.18 (m, 13H, Ar-H), 11.18 (s, 2H, 2NH). Ms (_m/z_): 433. Anal. Calculated for C$_{27}$H$_{19}$N$_3$O$_2$; C 74.83, H 4.39, N 9.70%, Found: C 74.80, H 4.35, N 9.65%.

Results and Discussion

The reaction started with the reactants heterocyclic diketone such as 4-hydroxy-6-methylquinolin-2(1H)-one (**1**). Accordingly, the reaction was carried out by irradiating a mixture of 4-hydroxy-6-methylquinolin-2(1H)-one (**1**), benzaldehyde, 1-naphthylamine (**2**) and five drops of triethylamine (TEA) in a beaker inside the microwave oven at an output of about 320 W for 3 min (TLC check). After the irradiation, the reaction mixture was poured into ice water, which gave a white product, **3a** in 94% yield. The solid obtained was filtered and purified by column chromatography using the solvents petroleum ether and ethyl acetate. The products were characterized on the basis of their IR, ^{1}H NMR, mass spectroscopic and analytic data.

3a
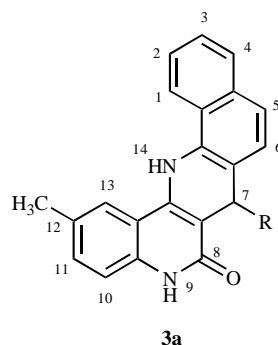
IR spectrum of **3a** showed carbonyl absorption band at 1643 cm^{-1} for carbonyl group, NH absorption appeared broad band in the region 2800-3200 cm^{-1} and other absorptions at 1604, 1544 cm.$^{-1}$ The ^{1}H NMR spectrum of the product **3a** showed three singlets at δ 2.50, 6.68 and 9.02 due to methyl, C$_7$ and C$_{13}$ protons. Other thirteen aromatic protons registered an unresolved multiplet in the region δ 6.71-8.11 and also registered two singlets at δ 11.01 and 11.18 for two NH protons. The mass spectrum showed a molecular ion peak at _m/z_ 388 (M$^{.+}$). The elemental analysis of **3a** corroborated the proposed molecular formula C$_{27}$H$_{20}$N$_2$O; Calcd.: C 83.51, H 5.15, N 7.22%; Found: C 83.46, H 5.09, N 7.20%. From all the above spectral values we confirmed the compound **3a** as 12-methyl-7-phenylbenzo [_h_]naphtho[_b_][1,6] naphthyridin-8-one (Scheme 1). A series of other derivatives (**3b-g**) were also prepared using different aldehydes like _o_-chlorobenzaldehyde, _m_-chlorobenzaldehyde, _p_-chlorobenzaldehyde, _m_-nitrobenzaldehyde, _p_-hydoxybenzaldehyde and _o_-

154

Orbital Elec. J. Chem., Campo Grande, 2(2): 151-157, 2010

hydroxybenzaldehyde (Table 1) (Scheme 1).
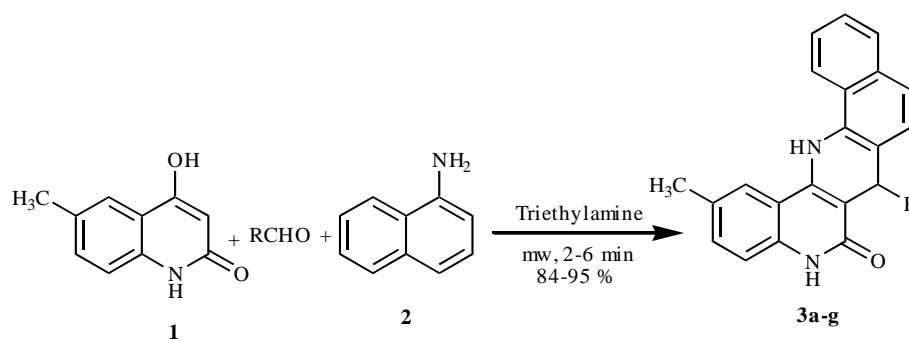
3a: R = C_6H_5, **3b**: R = o-Cl C_6H_5, **3c**: R = p-ClC$_6$H$_5$, **3d**: R = m-ClC$_6$H$_5$,
3e: R = o-OHC$_6$H$_5$, **3f**: R = p-OHC$_6$H$_5$, **3g**: R = m-NO$_2$C$_6$H$_5$,

Scheme 1. Synthetic route of compound **3a-g**.

Table 1. Physical data of Synthesized of Compounds **3a-g**.

Compound	Reaction Time (min)	Yield (%)	mp °C
3a	3.0	94	250-252
3b	4.0	90	190-192
3c	2.0	92	> 300
3d	6.0	82	130-132
3e	2.0	90	> 300
3f	3.0	80	110-112
3g	2.0	89	260-264

The plausible mechanism (Scheme 2) proposed for the above reaction involves three steps. In the first step, condensation takes place between 4-hydroxy-6-methylquinolin-2(1*H*)-one (**1**) and 1-naphthylamine (**2**) to form intermediate enamine **A**. In the second step, the enamine **A** attack to aromatic aldehydes (addition reaction) to give intermediates **B**, which further undergoes dehydration reaction to give 1,6-naphthyridine **3** (Step 3).

Conclusion

In conclusion, we have developed an efficient and high yield protocol for synthesis of new 12-methyl-7-phenylbenzo[*h*]naphtho[*b*]naphthyridin-8-ones 3a-g by multi-component reaction of 4-hydroxy-6-methylquinolin-2(1*H*)-one, aldehydes and 1-naphthylamine in triethylamine by using microwave irradiation. These methods offer tremendous reduction in reaction time, operational simplicity, cleaner reaction, easier work-up and better yields and are environmentally co-friendly compared to conventional methods.

155

Orbital Elec. J. Chem., Campo Grande, 2(2): 151-157, 2010
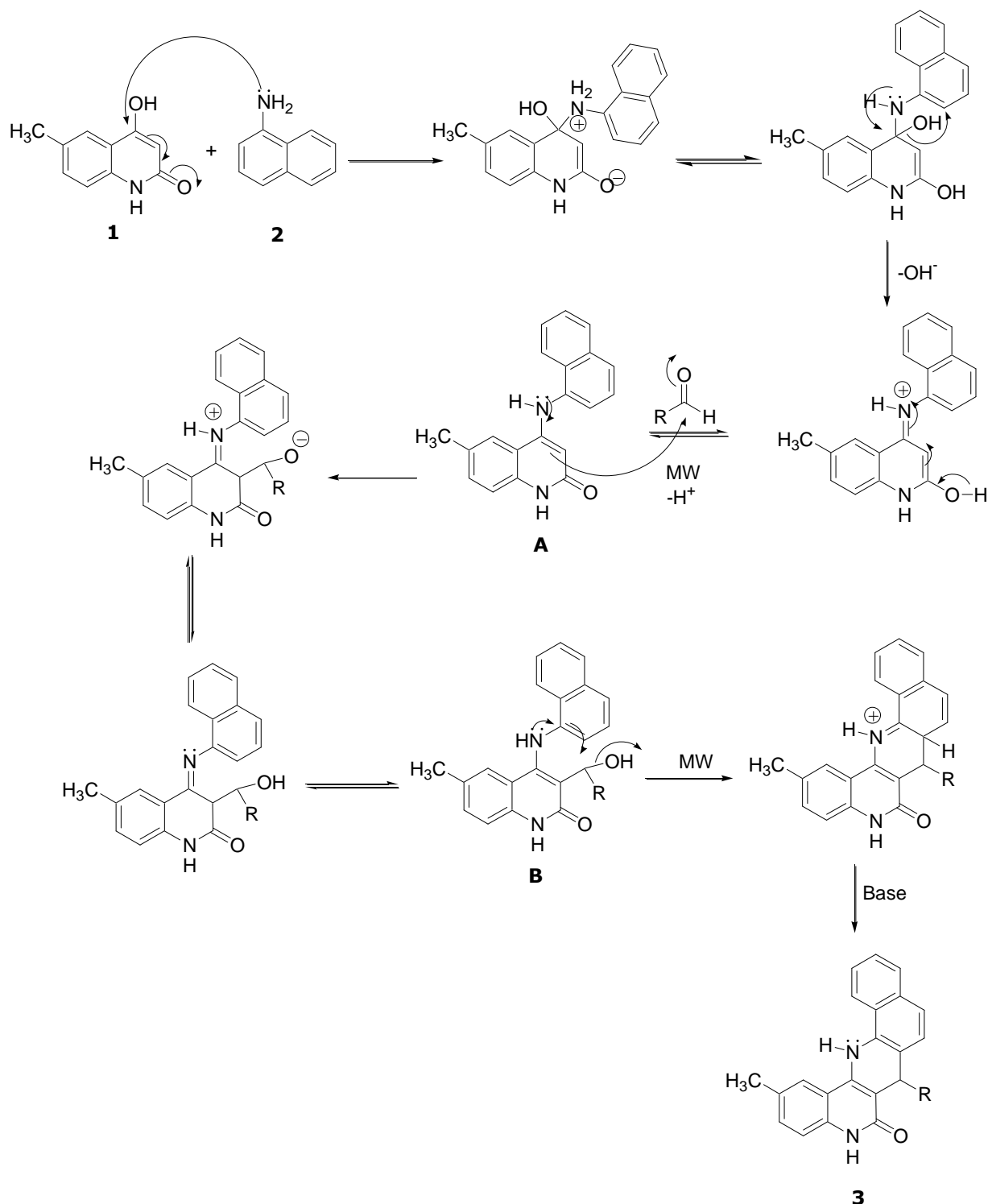
Scheme 2. Proposed mechanism of synthesized Compound 3.

References and Notes

156

Orbital Elec. J. Chem., Campo Grande, 2(2): 151-157, 2010

[1]   Egawa, H.; Miyamota, T.; Minamida, A.; Nishimura, Y.; Okada, H.; Uno, H.; Motosumota. *J. Med. Chem*. **1984**, *27*, 153.

[2]   Cooper, C. S.; Klock, P. L.; Chu, D. T. W.; Hardy, D. J.; Swanson, R. N.; Plattner, J. *J. Med. Chem.* **1992**, *35*, 1392.

[3]   Gupta, K. G.; Kessar S. V.; Singh, B. *Appl. Microbiol*. **1970**, *19*, 1017.

[4]   Takahashi, T.; Hamada, Y.; Takeuchi, I.; Uchiyumu, H. *Yatugaku Zasshi*. **1969**, *89*, 1260.

[5]   Buui-Hoi, N. P.; Jacquignon, I. P.; Thany, D. C.; Bartnik, T. *J. Chem. Soc., Perkin Trans-I* **1972**, 263.

[6]   Fathy, N. M.; Aly, A. S.; Abd.-El.; Mohi F.; Abdel-Megeid F. M. E. *Egypt. J. Chem.* **1987**, *29*, 609.

[7]   Takeuchi, I.; Hamada, Y. *Chem. Pharm. Bull*. **1976**, *24*, 1813.

[8]   Shiozawa, A.; Ishikawa, Y.; Jchikawa, M.; Miyazaki, H; Yamakana, H. *Fr. Pat*. **1982**, *2*, 492; *Chem. Abstr*. **1983**, *98*, 72076.

[9]   Dömling, A. *Chem. Rev.* **2006**, *106*, 17.

[10] Ramón, D. J.; Yus, M. *Angew. Chem., Int. Edn*. **2005**, *44*, 1602.

[11] Ulaczyk-Lesanko, A.; Hall, D. G. *Curr. Opin. Chem. Biol.* **2005**, *9*, 266.

[12] Li, C. J. *Chem. Rev*. **2005**, *105,* 3095.

[13] Ellman, J. A. *Acc. Chem. Res.* **1996**, *29*, 232.

[14] Hudlicky T. *Chem. Rev.* **1996**, *96*, 3.

[15] Thamarai Selvi, S.; Nadaraj, V.; Mohan, S.; Sasi, R.; Hema, M. *Bioorg. Med. Chem*. **2006**, *14*, 3896.

[16] Nadaraj, V.; Thamarai Selvi, S.; Sasi, R. *Arkivoc* **2006**, 82.

[17] Thamarai Selvi, S.; Nadaraj, V.; Mohan, S. *Eur. J. Med. Chem*. **2008**, *44*, 976.

[18] Nadaraj V.; Thamarai Selvi S. *Oriental J. Chem.* **2009**, *25*, 549.

157

Orbital Elec. J. Chem., Campo Grande, 2(2): 151-157, 2010

Full Paper

Synthesis and anticancer activity of some novel 3-(1,3,4-thiadiazol-2-yl)-quinazolin-4-(*3H*)-ones

Alex Joseph[*a]*, *Aravinda Pai*[a]*, *K. K. Srinivasan*[a]*, *Tukaram Kedar*[b]*, *Angel Treasa Thomas*[b]*,
Jessy E. M.[a]*, *Rajeev K. Singla*[a]

[a]Department of Pharmaceutical Chemistry, Manipal College of Pharmaceutical Science, Manipal University, Manipal-576104, Karnataka, India
[b]Department of Pharmaceutical Biotechnology, Manipal of College of Pharmaceutical Sciences, Manipal University, Manipal-576104, Karnataka, India

ABSTRACT: *Quinazolinone is a versatile lead molecule for designing potential bioactive agents. The compounds that have quinazolin-4-ones moiety are associated with interesting biological activities such as antifungal, antibacterial, antiviral, antitubercular and anticancer. In view of this we have undertaken synthesis of various thiadiazol substituted quinazolin-4-(*3H*)-ones. Novel 3-(1,3,4-thiadiazol-2-yl)-quinazolin-4-(*3H*)-ones (5a-5h) were synthesized by reaction of 5-alkyl/aryl substituted 1,3,4-thiadiazoles with 2-methyl/phenyl-4H-1,3-benzooxazin-4-ones in the presence of pyridine. All the synthesized compounds were characterized by spectral and physical data. In vitro anticancer activity of all the synthesized compounds was determined by MTT assay on HeLa (Human cervical cancer cell) cells. Most active compounds found in vitro studies were further evaluated for their in vivo activity on Liquid tumor (Ehrlich's Ascites Carcinoma; EAC) induced mice. The anticancer activity of compound 5f was found to be comparable to that of cisplatin against HeLa cells and was also effective in preventing the growth of tumor in mice as indicated by decrease in progressive gain in body weight as well as increase in life span when compared to animals of control group.*

Keywords: *quinazolin-4-one; MTT; hela; liquid tumor; Ehrlich's ascites carcinoma*

Introduction

Cancer is a disease of striking significance in the world today. It represents the second leading cause of human mortality after cardiovascular diseases. In order to develop more effective and reliable anticancer agents, a large number of compounds possessing fused nitrogen-containing heterocyclic skeletons, such as 4-anilinoquinazol-

---

* Corresponding author. E-mail: alex.j.manu@gmail.com

-ines, quinazolinones, pyrazolopyrimidines, triazolopyrimidines, pyrrolopyrimidines, pyrazolopyridazines and imidazopyrazines, have been synthesized and many of them exhibited excellent anticancer activity [1, 2].

Recently, quinazolin-4(*3H*)-ones have aroused increasing attentions since they were proved to be the promising anticancer agents with an interactive mechanism with tubulin [3]. It is also reported that some 2-substituted quinazolin-4(*3H*)-ones analogs bearing halogen groups at 6 and 8 positions were reported for significant anticancer activity [4]. Owing to our interest in the anticancer profile of quinazolin-4(*3H*)-ones, we report herein the synthesis and *in vitro* and *in vivo* anticancer studies of novel 3-(1,3,4-thiadiazol-2-yl)-quinazolin-4-(*3H*)-ones with the hope to develop some promising anticancer agents.

Material and Methods

Chemistry

All melting points were determined in open capillary tubes in Toshniwal Melting point apparatus and are presented without any corrections. Using TLC, we assessed the reactions and the purity of the products using Merck Precoated silica gel GF aluminium plates and Toluene: Methanol (9:1) as solvent system. The infrared (IR) spectra were recorded on a FTIR-8310 Shimadzu spectrometer using potassium bromide pellets. The proton nuclear magnetic resonance (^{1}H-NMR) spectra were recorded on Bruker AMX 400 NMR spectrometer, using tetramethylsilane (TMS) as the internal standard and DMSO-d as solvent. The chemical shifts are expressed in part per million (ppm) downfield from the internal standard; the coupling constants are in Hz, and signals are quoted as *s* (singlet), *d* (doublet), *t* (triplet), *q* (quartet), or *m* (multiplet). The Mass spectral was recorded as EI spectra on Shimadzu GCMS QP 5050.

Synthesis of 2-methyl/phenyl-4H-1,3-benzooxazin-4-ones (2a-2c)

2-phenyl-4H-1,3-benzoxazin-4-ones (2a): To a stirred solution of anthranillic acid (0.01 M) (1) in pyridine (60 mL), benzoyl chloride (0.01 M) was added dropwise, maintaining the temperature near 8 °C for 1 h. Reaction mixture was stirred for another 1 h at room temperature and neutralized with 10 % w/v sodium bicarbonate solution . A pale yellow solid as crude product was precipitated out, which was filtered, washed with distilled water, and recrystallised from ethanol to give pure product 2a in a yield of 94% [5].

2-methyl-4H-1,3-benzoxazin-4-ones (2b/2c): A mixture of anthranilic acid or 3, 5 dibromo anthranilic acid (0.01 M) and acetic anhydride (0.02 M) were added to acetic acid (0.01 M). The reaction mixture was refluxed for 4 h. Acetic acid together with acetic anhydride was distilled off under reduced pressure and the solid separated was filtered and recrystallized from ethanol to offer pure product 2b in a yield of 89% [6].

159

Orbital Elec. J. Chem., Campo Grande, 2(2): 158-167, 2010

Synthesis of 2-amino-5-aryl substituted-1,3,4-thiadiazoles (4a-4f)

Step 1. Aromatic aldehyde (0.2 M) in warm alcohol (300 mL) was added to a solution of thiosemicarbazide (0.2 M) in hot water (300 mL). The reaction mixture was stirred for a period of 1 h. After cooling down, the crude product was precipitated out, which was filtered and recrystallised from 50% aqueous ethanol.

Step 2. Thiosemicarbazone (0.005 M) obtained above was suspended in 300 mL distilled water in a 100 mL beaker. Ferric chloride (0.15 M) in 300 mL distilled water was added to it. After the reaction mixture was stirring for one hour at temperature of 80-90 °C, it was filtered while hot. A mixture of citric acid (0.11 M) and sodium citrate (0.05 M) was added to the filtrate and continue stirring for 15 minutes. After cooling the whole solution, it was taken in a bigger vessel (to account for the increase in volume) and neutralized with 10% aqueous ammonia. The precipitate which separated out was filtered and recrystallised from 25% aqueous ethanol to give pure product in the yield ranging from 72-84% [7].

Synthesis of 2-amino-5-ethyl-1,3,4-thiadiazoles (4g)

Propionic acid (0.15 M), concentrated sulfuric acid (25 mL) and thiosemicarbazide (0.125 M) were slowly heated to 80-90 °C on a thermostatically controlled water bath for 7 h. After cooling down, the reaction mixture was poured on to crushed ice and neutralized with 10% ammonia solution. The precipitate as crude product was filtered, washed several times with distilled water, and dried. It was recrystallised from hot water to offer pure product 4g in a yield of 76 %.

Synthesis of title compounds: 3-(1,3,4-Thiadiazol-2-yl)-quinazolin-4(3H) ones (5a-5h)

To a solution of 2-methyl/phenylsubstituted-4*H*-1,3-benzoxazin-4-ones (0.005 M) in 15 mL of dry pyridine, added 2-amino-5-alkyl/aryl substituted-1,3,4-thiadiazoles (0.005 M) in portions with constant stirring for 10 minutes. The reaction mixture was refluxed for 9 h. The hot solution was added to a beaker containing 100 g of crushed ice and 5 mL of concentrated HCl. The solid separated was filtered, dried and recrystallised from methanol to give pure product [8].

6,8-dibromo-3-(5-ethyl-1,3,4-thiadiazol-2-yl)-2-methylquinazolin-4(3H)-one (5a): Prepared from 6, 8-dibromo-2-methyl-4*H*-1,3-benzooxazin-4-one (2c) and 5-ethyl-1,3,4-thiadiazol-2-amine (4g)**.** Yield 70%, M.P. 154-156 ^{o}C, IR (KBr) (cm^{-1}): 1444 (C-H def.), 1606 (C=N str.), 1750 (C=O str.), 1321 (C-N str.), 686 (C-S str.). ^{1}H-NMR (DMSO) δ ppm: 2.3 (s, 3H, 2nd position C$\underline{H}_3$), 3.2 (q, 2H, thiadiazole -C$\underline{H}_2$-CH$_3$), 1.4 (t, 3H, thiadiazole - CH$_2$-C$\underline{H}_3$), 7.8 (d, 1H, J = 2.12, Ar-H$_5$), 8.1 (d, 1H, J = 2.09, Ar-H$_7$). EIMS m/z: [M+2]$^{+}$ 430 (C$_{13}$H$_{10}$Br$_2$N$_4$OS).

160

Orbital Elec. J. Chem*., Campo Grande,* 2(2): 158-167, 2010

3-(5-ethyl-1,3,4-thiadiazol-2-yl)-2-phenylquinazolin-4(3H)-one (5b): Prepared from 2-phenyl-4*H*-1,3-benzooxazin-4-one (2a) and 5-ethyl-1,3,4-thiadiazol-2-amine (4g)**.** Yield 72%, M.P. 165-170 $^{\circ}$C, IR (KBr) (cm^{-1}): 1410 (C-H def.), 1604(C=N str.), 1690(C=O str.), 1328 (C-N str.), 681 (C-S str.). ^{1}H-NMR (DMSO) δ ppm: 2.3 (s, 3H, 2nd position CH$_3$), 3.31 (q, 2H, thiadiazole -CH$_2$-CH$_3$), 1.5 (t, 3H, thiadiazole - CH$_2$-CH$_3$), 7.6-8.4 (m, 9H, Ar-H). EIMS m/z: [M]$^{+}$ 334 (C$_{18}$H$_{14}$N$_4$OS).

2-methyl-3-(5-phenyl-1,3,4-thiadiazol-2-yl)quinazolin-4(3H)-one (5c): Prepared from 2-methyl-4*H*-1,3-benzooxazin-4-one (**2b**) and 5-phenyl-1,3,4-thiadiazol-2-amine**.** Yield 69%, M.P. 147-150 $^{\circ}$C, IR (KBr) (cm^{-1}): 1420 (C-H def.), 1610 (C=N str.), 1734 (C=O str.), 685(C-S str.). ^{1}H-NMR (DMSO) δ ppm: 2.4 (s, 3H, 2nd position CH$_3$), 7.2-8.7 (m 9H, Ar-H). EIMS m/z: [M]$^{+}$ 320 (C$_{17}$H$_{12}$N$_4$OS).

6, 8-dibromo-2-methyl-3-(5-phenyl-1, 3, 4-thiadiazol-2-yl) quinazolin-4(3H)-one (5d): Prepared from 6,8-dibromo-2-methyl-4*H*-1,3- benzooxazin-4-one (2c) and 5-phenyl-1,3,4-thiadiazol-2-amine**.** Yield 74%, M.P. 170-174 $^{\circ}$C, IR (KBr) (cm^{-1}): 1607 (C=N str.), 1732 (C=O str.), 675 (C-S str.). ^{1}H-NMR (DMSO) δ ppm: 2.7 (s, 3H, 2nd position CH$_3$), 7.6-8.7 (m 7H , Ar-H). EIMS m/z: [M+2]$^{+}$ 480 (C$_{17}$H$_{10}$Br$_2$N$_4$OS),

6,8-dibromo-3-(5-(3-chlorophenyl)-1,3,4-thiadiazol-2-yl)-2-methylquinazolin-4(3H)-one 5e): Prepared from 6,8-dibromo-2-methyl-4*H*-1,3-benzooxazin-4-one (2b) and 5-(3-chlorophenyl)-1,3,4-thiadiazol-2-amine. Yield 70%, M.P. 160-162 $^{\circ}$C, IR (KBr) (cm^{-1}): 1604 (C=N str.), 1728 (C=O str.), 683 (C-S str.). ^{1}H-NMR (DMSO) δ ppm: 2.65 (s, 3H, 2nd position CH$_3$), 7.5-8.5 (m 6H , Ar-H). EIMS m/z: [M+2]$^{+}$ 514 (C$_{17}$H$_9$Br$_2$ClN$_4$OS).

3-(5-(3-chlorophenyl)-1,3,4-thiadiazol-2-yl)-2-phenylquinazolin-4(3H)-one   (5f): Prepared from 2-phenyl-4*H*-1,3-benzooxazin-4-one (2a) and 5-(3-chlorophenyl)-1,3,4-thiadiazol-2-amine. Yield 75%, M.P. 154-158 $^{\circ}$C, IR (KBr) (cm^{-1}): 1615 (C=N str.), 1735 (C=O str.), 685 (C-S str.). ^{1}H-NMR (DMSO) δ ppm: 7.2-8.5 (m 13H, Ar-H). EIMS m/z: [M+2]$^{+}$ 416 (C$_{22}$H$_{13}$ClN$_4$OS).

3-(5-(4-chlorophenyl)-1,3,4-thiadiazol-2-yl)-2-methylquinazolin-4(3H)-one   (5g): Prepared from 2-methyl-4*H*-1,3-benzooxazin-4-one (2b) and 5-(4-chlorophenyl)-1,3,4-thiadiazol-2-amine. Yield 69%, M.P. 190-195 $^{\circ}$C, IR (KBr) (cm^{-1}): 1610 (C=N str.), 1740 (C=O str.), 692 (C-S str.). ^{1}H-NMR (DMSO) δ ppm: 2.60 (s, 3H, 2nd position CH$_3$), 7.4-8.5 (m 8H , Ar-H). EIMS m/z: [M+1]$^{+}$ 355 (C$_{17}$H$_{11}$ClN$_4$OS).

3-(5-(4-methoxyphenyl)-1,3,4-thiadiazol-2-yl)-2-phenylquinazolin-4(3H)-one   (5h): Prepared from 2-phenyl-4*H*-1,3-benzoxazin-4-one (2a) and 5-(4-methoxyphenyl)-1,3,4-thiadiazol-2-amine. Yield 71%, M. P. 180-184 $^{\circ}$C, IR (KBr) (cm^{-1}): 1608 (C=N str.), 1725 (C=O str.), 1100 (C-O str.), 685 (C-S str.). ^{1}H-NMR (DMSO) δ ppm: 3.89 (s, 3H, -OCH$_3$), 7.3-8.4 (m, 13H, Ar-H). EIMS m/z: [M+2]$^{+}$ 412 (C$_{23}$H$_{16}$N$_4$O$_2$S).

161

Orbital Elec. J. Chem., Campo Grande, 2(2): 158-167, 2010

Biological Activity

Chemicals and cell culture

MTT (3-(4,5-dimethylthiazol-2-yl)-2,5-diphenyl tetrazolium bromide) was obtained from Sigma, USA, DMEM (Dulbecco's modified Eagles medium), fetal bovine serum (FBS) and antibiotic solution (containing penicillin and streptomycin) were obtained from Himedia, India, and dimethyl sulfoxide (DMSO) was obtained from Merck, India. Human cancer cell line HeLa (Human Cervical Cancer) cell line was provided by NCCS, Pune, India. Cells were grown in DMEM, containing L-glutamine and 25mM HEPES and supplemented with 10% fetal bovine serum, penicillin (100 units/mL), streptomycin (100 mcg/mL), and amphotericin B (0.25 mg/mL) at 37 ^{0}C, 5% CO_2, 100% humidity.

In-vitro cytotoxicity assay

Cells (1.5×10^4) were incubated with the compounds (5a–5h) dissolved in DMSO (final DMSO conc <0.1%) in triplicate wells to obtain drug concentration of 1–100 µg/mL. Cytotoxicity was measured after 72 h using MTT assay as described by Mosmann [9]. Each experiment was repeated thrice and mean IC_{50} values (half inhibitory concentration) have been reported.

In-vivo anticancer activity against EAC Cells by Liquid Tumor Model

The most active two compounds found in *in vitro* studies were selected for *in vivo* anticancer studies. Ehrlich ascites carcinoma (EAC) was used to develop the liquid tumor model. EAC was obtained from Cancer Research Institute, Mumbai and was propagated by serial transplantation in swiss albino mice in Central Animal Research Facility, Manipal University, India.

Acute Toxicity Studies

Acute toxicity studies were conducted to determine the safe dose as per OECD guidelines. Drugs were administered intraperitonially. After administration, the animals were observed continuously for 1 h, frequently for the next 4 h and then after 24 h [10].

The ascitic carcinoma bearing mice (donor) was taken 15 days after tumor transplantation. The ascitic fluid is drawn using a 22 gauge needle into sterile syringe. A small amount tested for microbial contamination. Tumor viability was determined by Trypan blue exclusion test and cells were counted using Haemocytometer. The Ascitic fluid was suitably diluted in phosphate buffer saline to get a concentration of 10^6 cells/mL of tumor cell suspension. This was injected intraperitonially to obtain ascitic tumor. The mice were weighed on the day of tumor inoculation and then for three subsequent days. Treatment was started 24 h after tumor inoculation. Cisplatin was used as positive

162

Orbital Elec. J. Chem., Campo Grande, 2(2): 158-167, 2010

control and injected on two alternate days (3.5 mg/kg/bw) i.e. the 1st and 3rd day. Test compounds were administered at the selected two doses till 9th day intraperitonially. Tumor response was assessed on the basis of mean survival time (MST) and % increase in life span (% ILS) [11]. One way ANOVA followed by post Hoc Tukey test in SPSS 11.5 computer package was used for statistical analysis.

Results and Discussion

Chemistry

Literature review revealed that some 3-(alkyl/aryl substituted 1,3,4-thiadiazol-2-yl)-quinazolin-4(*3H*) ones have been earlier reported for their CNS depressant, anticonvulsant [6], MAO inhibitory , anticholinergics [12], antibacterial and antifungal activity [13]. Although some 2-substituted quinazolin-4(*3H*)-ones analogs has been reported for their anticancer activity, no reports are there on the anticancer activity of 3-(alkyl/aryl substituted 1,3,4-thiadiazol-2-yl)-quinazolin-4(*3H*) ones. Thus it was thought worthwhile to synthesize various 3-(alkyl/aryl substituted 1,3,4-thiadiazol-2-yl)-quinazolin-4(*3H*) ones and to evaluate them for anticancer activity.

Scheme 1
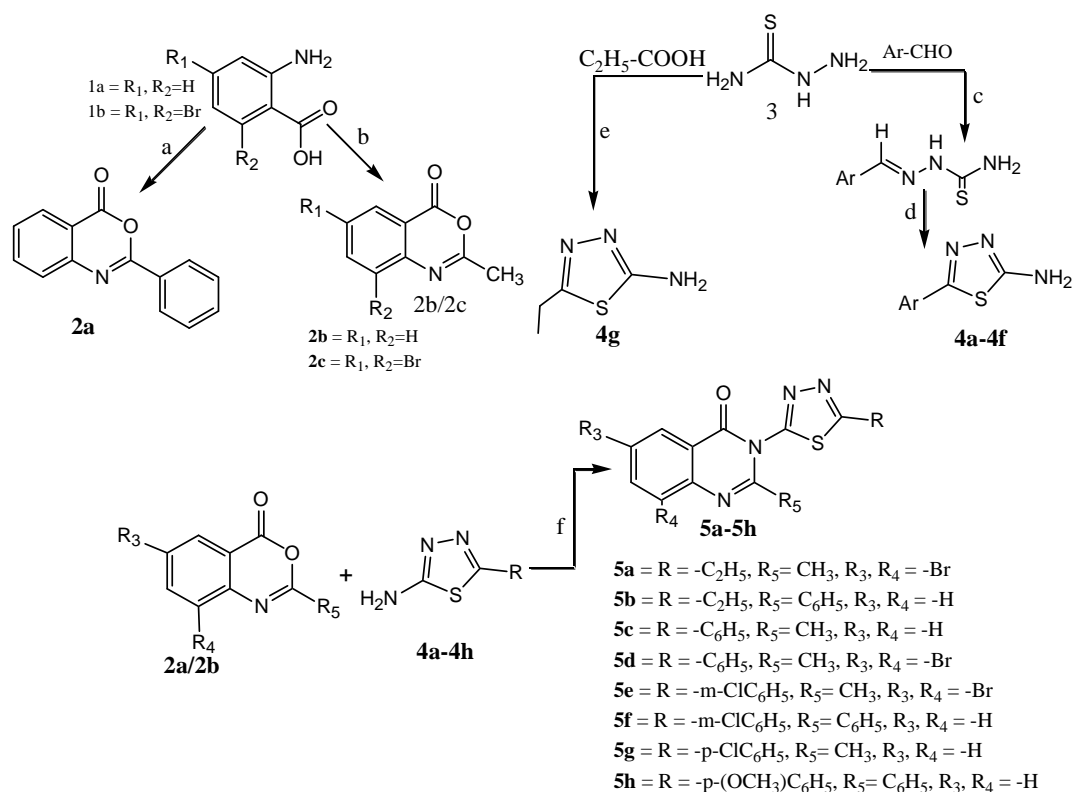
Reagents and conditions : a) C_6H_5-COCl/ Pyridine, Strried at room temperature for 1h b) $(CH_3CO)_2O$/ Re for 4 h c) Ar-CHO/C_2H_5-OH, Strried at room temperature for 1h d) $FeCl_3$, Strried at room temperature for 1h e) Propionic acid/Con H_2SO_4 / Strried at 80-90 ^{0}C for 7 h f) Pryridine reflux for 9 h

The title compounds 3-(alkyl/aryl substituted 1,3,4-thiadiazol-2-yl)-quinazolin-

163

Orbital Elec. J. Chem., Campo Grande, 2(2): 158-167, 2010

4(*3H*) ones (5a-5h) were synthesized by the reaction of alkyl/aryl substituted 1,3,4-thiadiazoles (4a-4g) with 2-methyl/phenyl-4*H*-1,3-benzooxazin-4-ones (2a-2c) in the presence of pyridine. 2-methyl/phenyl-4*H*-1,3-benzooxazin-4-ones (2a-2c) were obtained by cyclocondensation of antranilic acid with acetic anhydride/benzoyl chloride. While 2-Amino-5-aryl/alkyl substituted-1,3,4-thiadiazole (4a-4g) were synthesized from aromatic aldehyde or aliphatic acid via thiosemicarbazone intermediate (Scheme 1). The structure of the all the synthesized compounds (5a-5h) were confirmed by ^{1}H-NMR, EIMS, IR spectroscopic and physicochemical data.

Biological Activity

In-vitro cytotoxicity assay

The effect of all the synthesized compounds on the viability of cancer cells was determined by MTT (3-[4, 5-dimethylthiazol-2-yl]-2, 5-diphenyltetrazolium bromide) assay on HeLa cells. The results are expressed in terms of IC_{50}, as mean±SEM (Table 1).

Table 1. Cytotoxicity of 3-(1, 3, 4-thiadiazol-2-yl)-quinazolin-4-(*3H*)-ones by MTT method on HeLa cells.

Compound code	$IC_{50}±SEM^{a}$ µg/mL
5a	84.35±3.26
5b	24.19±1.57
5c	> 100[b]
5d	7.32±2.24
5e	26.39±1.75
5f	9.43±1.08
5g	18.28±2.16
5h	16.74±1.84
Cisplatin	6.58±0.81

[a]Average of three determinations
[b]Concentration above 100 µg/mL not done

Most of the synthesized 3-(alkyl/aryl substituted 1, 3, 4-thiadiazol-2-yl)-quinazolin-4(*3H*) ones showed a cytotoxicity with IC_{50} less than 30 µg/mL. Among the synthesized title compounds 6,8-dibromo-2-methyl-3-(5-phenyl-1,3,4-thiadiazol-2-yl) quinazolin-4(*3H*)-one (5d) and 3-(5-(3-chlorophenyl)-1,3,4-thiadiazol-2-yl)-2-phenylquinazolin-4(*3H*)-one (5f) registered maximum cytotoxicity with IC_{50} of 7.32 and 9.43 µg/mL, respectively on HeLa cells. The standard drug cisplatin showed an IC_{50} of 6.58 µg/mL on HeLa cells. The cytotoxicity of 5d and 5f were comparable with that of cisplatin. Based on these results compounds 5d and 5f were selected for *in vivo* anticancer studies.

In-vivo anticancer activity against EAC Cells by liquid tumor model

In vivo anticancer activities of selected compounds were studied on swiss albino mice by liquid tumour model. Acute toxicity studies revealed that maximum tolerated safe dose for all the selected compounds were at 1000 mg/kg. Therefore the compounds were

164

Orbital Elec. J. Chem*., Campo Grande,* 2(2): 158-167, 2010

studied at two dose levels, 50 and 100 mg/kg bw and were administered by i.p. route. Parameters such as percentage increase in body weight, mean survival time and percentage increase in life span were studied and the results are summarized in tables 2 and 3.

In the *in vivo* cancer model of Ehrlich Ascites Carcinoma (EAC), the compounds selected for the study (5d and 5f) significantly reversed the tumor induced changes in the parameters monitored such as percentage increase in body weight and percentage increase in life span.

Weight change: Control animals showed a progressive gain in body weight after the tumor inoculation. By day 13, they gained a maximum average weight of 43.9%. Among the compounds selected for the study 6, 8-dibromo-2-methyl-3-(5-phenyl-1, 3, 4-thiadiazol-2-yl) quinazolin-4(*3H*)-one (5d) and 3-(5-(3-chlorophenyl)-1, 3, 4-thiadiazol-2-yl)-2-phenylquinazolin-4(*3H*)-one (5f) significantly (P<0.001) reduced the tumor induced gain in weight as compared to the control at a both dose level studied. The percentage average weights gained by animals treated with these compounds were 13.1 and 8.8%, respectively for 5d and 5f at dose of 100 mg/kg. Cisplatin significantly (P<0.001) reduced the tumor induced gain in weight as compared to the respective control. The percentage average weight gained by animals treated with cisplatin at a dose of 3.5 mg/kg was 2.1%.

Mean survival time: MST for control group of animals was 17.0 days. MST of cisplatin treated group (32.0 days) was significantly (p<0.01) prolonged compared to that of control. The percentage increase in life span (%ILS) was 88.23. Among the compounds selected for the study, 3-(5-(3-chlorophenyl)-1, 3, 4-thiadiazol-2-yl)-2-phenylquinazolin-4(*3H*)-one (5f) was the most active compound showing an increase in life span of 51.76% at the dose level of 100 mg/kg as compared to the control group.

Table 2. Effect of compounds on the survival time in tumor induced mice.

Group	*Dose* *(mg/kg)*	*Mean Survival Time (Days)* *(Mean ± SEM)*	*% ILS*
Control	-	17±0.707	-
Cisplatin	3.5	32±3.06[b]	88.23
5d	50	18.2±1.59	7.05
5d	100	19.2±1.01[a]	12.9
5f	50	22±0.4[b]	29.41
5f	100	25.8±1.52[b]	51.76

One way ANOVA followed by Post hoc Dunnett's test
a = p<0.05, b = p<0.01 Vs Control group

165

Orbital Elec. J. Chem*., Campo Grande,* 2(2): 158-167, 2010

Table 3. Effect of selected compounds on percentage increase in body weight in tumor induced mice.

Compound code	Percentage change in body weight as compared to day- 0 weight (MEAN±S.E.M)					
	3rd day	5th day	7th day	9th day	11th day	13th day
Control	11.2±1.02	18.2±2.56	24.5±1.45	28.5±2.27	36.7±5.3[b]	43.9±4.8[b]
Cisplatin	0.001±001[a]	0.53±0.017[b]	0.55±0.0[b]	0.56±0.2[b]	1.66±.01[a]	2.1±.01[a]
5d (50mg/kg)	1.4±1.5[b]	3.9±2.59[b]	10.5±2.0[b]	11.5±2.1[b]	14.4±2.9[a]	17.6±3.05[a]
5d (100mg/kg)	7.48±2.4[b]	2.1±1.55[b]	7.04±1.3[b]	3.41±2.7[b]	8±5[b]	13.1±5.8[b]
5f (50mg/kg)	3.14±2.17	5.28±2.1[a]	5.35±2.2[b]	6.99±2.1[b]	10.1±1.1[b]	8.8±3.8[a]
5f (100mg/kg)	0.88±3.59[a]	11.2±3.14	4.11±3.0[b]	3.9±4.6[b]	1.9±8.47	9.9±11.1

One way ANOVA followed by Post hoc Tukey test
a = $p < 0.05$, b = $p < 0.001$ Vs Control group

Conclusion

A series of 3-(1, 3, 4-thiadiazol-2-yl)-quinazolin-4-(*3H*)-ones (5a-5h) were synthesized and evaluated for *in vitro* and *in vivo* anticancer studies. The *in vitro* cytotoxicity of compounds 5d and 5f were found to be comparable with that of cisplatin. The *in vivo* anticancer activity of compound 5f was notable on liquid tumor (Ehrlich's Ascites Carcinoma; EAC) induced mice as indicated by decrease in progressive gain in body weight as well as increase in life span when compared to control group animals.

Acknowledgements

References and Notes

[1]   Abdel-Rahman, T. M. *Boll. Chim Farm*. **1998**, *137*, 47.

[2]   El-Bayouki, K, A. M.; Aly, M. M.; Mohamed, Y. A.; Basyouni, W. M.; Abbas, S. Y. *World J. Chemistry* **2009**, *4*, 170.

[3]   Jack, B.; Jiang, D. P.; Hesson, B. A.; Dusak, D. L.; Dexter, G. J.; Kang, E. H. *J. Med. Chem*. **1990***, 33*, 1728.

[4]   Murugan, V.; Caroline, C. T.; Ramasarma, G. V. S.; Kumar, E. P.; Suresh, B. *Indian J. Pharm. Sciences* **2003**, *65*, 386.

[5]   Jatav, V.; Kashaw, S.; Mishra, P. *Med. Chem. Res*. **2008**, *17*, 169.

[6]   Selvam, P. *Indian J. Pharm. Sciences* **2004**, **66**, 82.

166

Orbital Elec. J. Chem*., Campo Grande,* 2(2): 158-167, 2010

[7]   Jatav, V.; Mishra, P.; Kashaw, S.; Stables, J. P. *Eur. J. Med. Chem*. **2008**, *43*, 141.

[8]   Satsangi, R. K. *J. Indian Chem. Soc*. **1978**, *55*, 478.

[9]   Mosmann, T. *J. Immunol Methods* **1983**, *65*, 55.

[10] OECD   Guidelines   for   acute   toxicity   studies. http://www.epa.gov/scipoly/sap/meeting/2001/december/12/up   and   down.pdf Access October, 2008.

[11] Echardt, A. E.; Malone, B. N.; Goldstein, I. *Cancer Res*. **1982**, *42*, 2977.

[12] Jatav, V.; Mishra, P.; Kashaw, S.; Stables, J. P. *Eur. J. Med. Chem*. **2008**, *43*, 1954.

[13] Satsangi, R. K. *Indian Drugs* **1979**, *17*, 81.

167

Orbital Elec. J. Chem*., Campo Grande*, 2(2): 158-167, 2010

Full Paper

Allowed energetic pathways for the three-body recombination reaction of nitrogen monoxide with the hydroxyl radical and their potential atmospheric implications

Luca D'Ottone[a] [*] and Adeel Jamal[a]

[a]Miami Dade College Wolfson Campus, 200 NE 2nd Street, Room 2103, Miami, Fl, 33132

ABSTRACT: *The OH initiated oxidation of nitric oxide (NO) is an important atmospheric reaction being, during the day time, the main channel that leads to the formation of HONO a reservoir species for both OH and odd nitrogen. This work reports ab initio study of the Potential Energy Surface (PES) of NO + OH using density functional theory calculations conducted at the B3LYP level of theory with a 6-311g (d,p) basis set. We confirmed experimental observations pointing out that the main channel for this reaction is the formation the HONO. From the addition of OH to NO both cis and trans isomers of HONO were found to be the formed as stable intermediate, both having a negative enthalpy of formation relative to the reactants, the cis isomer being more stable than the trans one. The ab initio calculations were extended to include the hydrogen extraction mechanism with its respective transition state to investigate the potential existence of a reaction channel leading to the formation of NO_2 + H, that was found not to be of significant interest.*

Keywords: ab initio calculations; HONO; nitric oxide; hydroxyl radical

Introduction

Nitrous Acid HONO is an atmospheric constituent important in urban contexts being a reservoir species both for OH and odd nitrogen [1-5]. During the day HONO is formed in the OH initiated oxidation of Nitrogen Monoxide, but it quickly decomposes back into reactants via a photolytic process. At nighttime, in absence of a light source, HONO is produced via different dark reactions and accumulates both in gaseous and liquid phases effectively creating a reservoir for both OH and NO. In the early morning

---

hours the sun comes up again over the horizon photolyzing progressively, as it rises toward the zenith, HONO. It has been estimated that OH early morning production due to HONO photolysis may account to up to 60% of the overall tropospheric OH budget kick-starting in turn the tropospheric chemistry of the daytime [6-8]. Another reason to look into the allowed pathways for the title reaction is HONO has been used as precursor for the hydroxyl radical in laboratory studies [9-11].

One of the main accepted mechanisms for the formation of HONO is the three body recombination reaction of the hydroxyl radical with nitric oxide [12]:

$$OH + NO + (M) \rightarrow HONO + (M^*) \qquad (1)$$
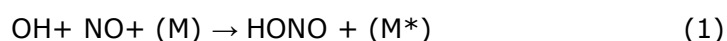
Reaction (1) it is not a simple mechanism but occurs via a three steps process that can be broken down as:

$$OH + NO \rightarrow HONO^* \qquad (2a)$$

$$HONO^* \rightarrow OH + NO \qquad (2b)$$

$$HONO^* + (M) \rightarrow HONO + (M^*) \qquad (3)$$
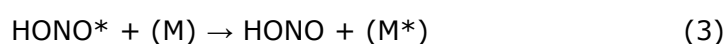
Reaction (2a) is the reversible addition of OH to the NO radical with the formation of an energized adduct indicated as HONO*. The adduct so formed can either re-decompose back into the reactants (2b) due to its lack of ability to store the excess energy or can be stabilized by the transfer of said excess energy to a third body M, dissipating in this way at least part of the energized adduct.

Recent field studies [6-8] have focused their attention on evaluating the impact of nitrous acid (HNO_2 or HONO) photolysis on the overall OH tropospheric budget. The interpretation of the field measurements seems to point out that under certain conditions mainly related to the polluted and urban environment the relative importance of nitrous acid as precursor of the hydroxyl radical are much larger as a percentage than what previously estimated [13-14].

The kinetic community has shown significant interest in reaction (1) [14-29]. As shown in Fig. 1 an accurate determination for the rate of recombination for the OH initiated oxidation of nitrogen monoxide has been recently determined by Pulsed Laser Photofragmentation-Laser Induced Fluorescence (PLP-LIF) [12] in the range of pressure and temperature characteristic of the troposphere, notwithstanding a lack of information on the geometry and the structure of the reaction product. It has been hypothesized that the yield in HONO for the title reaction is 0.8 [25], but little work has been done in investigating the potential reaction pathways allowed for this reaction. These observations have renewed our interest for the title reaction. Our main goal in this study was to check for possible allowed reaction pathways for the recombination of OH with NO

169

Orbital Elec. J. Chem., Campo Grande, 2(2): 168-179, 2010

and clarify the structure of what was thought to be the main product: HONO.

Material and Methods

The present study reports *ab initio* calculation on the formation of HONO from gas phase reaction between the hydroxyl radical and nitric oxide. The goal of this study is to clarify the nature of the products for the title reaction and predict verifiable vibrational frequencies that can be scrubbed against literature data or in separate laboratory work to validate our conclusions. The Density Functional Theory employed in this study is at the B3LYP level of theory with a 6-311g (d,p) basis set. Density Functional Theory is a computational method that solves the electronic (time-independent) Schrödinger equation, with atomic structure (internal coordinates) as variables. In this method, molecular geometry is proportional to Energy, with varying functions of bond distance, bond angles, and dihedral angles, resulting in a gradient of Energy with specific coordinates. That Energy is minimized, resulting in an equilibrium situation reflecting optimized coordinates. A consequence of this equilibrium coordinate calculation is the determination of vibrational frequencies, which is also reported in this study and can be measured experimentally. B3LYP is a type of Density Functional Theory, which accounts for relativistic effects from other electrons in sub shells. B3LYP is widely accepted in the theoretical chemistry community as an accurate (within 1-2 kcal/mol) *ab initio* PES method. 6-311g (d,p) is a basis set to the functional employed in Density Functional Theory [30-32] .

All optimized cartesian geometries, relative energies, zero-point energy, rotational constants, moments of inertia, and harmonic frequencies were performed at the B3LYP/6-311G(d,p) level of theory using Gaussian 98 *ab initio* software [33]. In order to perform a constrained optimization of the PES for the present reaction path forming algorithm the energy is expressed as the Taylor expansion:

$$E=E'+gT * \Delta x + 0.5 \Delta x * H * \Delta x + \ldots \qquad (4)$$

Where E' is the energy at a point x' on a sphere of radius 0.5 s centered at x, g is the gradient and H is the Hessian operator. Gaussian algorithm provides for self consistent field values for the Energy values including the TS energy by starting with the analytical Hessian equation for the transition state:

$$H'=H''+(\Delta g' * \Delta g'^t)/(\Delta g'^{\ t} * \Delta x') - (H'' * \Delta x') * (\Delta x'^T * H'')/(\Delta x'^{\ T} * H * \Delta x') \qquad (5)$$

where $\Delta g'=g'-g''$, $\Delta x'=x'-x''$ and the superscripts ' and " refer respectively to the current and previous points. The algorithms provided are iterated over and over according to the self consistent field theory to minimize the differences between the valued for the energies at the current and previous point *via* an iterative process. Detailed explanation

of the Gaussian 98 algorithm is found in Gonzalez and Schlegel [36-37].
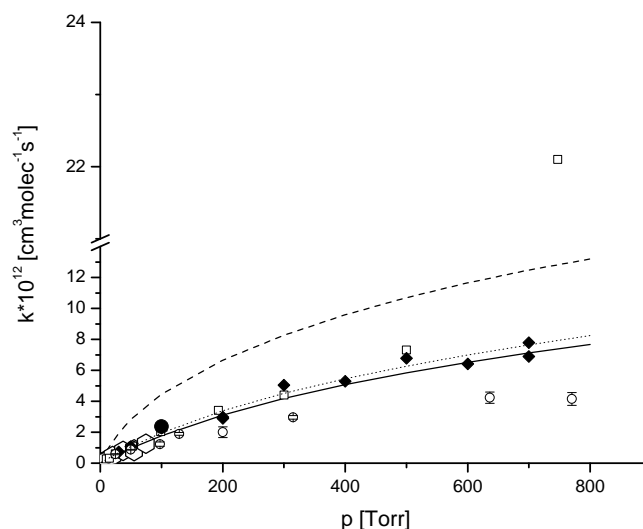
Figure 1. Absolute rate coefficient for the gas phase recombination of OH with NO in Nitrogen, (♦) [12]; (□) [29]; (○) [24] ; (□) [38] (Δ) [18].; The solid line represents the curve produced using the NASA-JPL, 2003 parametrization; the dashed line is the IUPAC, 1997; and the dotted line is the IUPAC 2003.

At the B3LYP/6-311g(d,p) level, TS HONO has only one imaginary vibrational frequency, whose vibrational vector corresponds to the H translational motion leading to *cis*-HONO and *trans*-HONO. IRC calculations at this level of theory were carried out on TS HONO, confirming that this transition state is the saddle point that connects to *cis*-HONO to *trans*-HONO on its surface [34-35].

Results and Discussion

In this study, the Energies of NO and OH, both radical species with an unpaired electron, were determined. The combined Energy of NO and OH were set to zero, to create an arbitrary scale for the PES. All intermediates, transition states, and products Energy's was mapped relative (Erel) to this zero energy of the reactants. Table 1 shows the Erel of all species studied. The intermediates examined are NOOH, *cis*-HONO, *trans*-HONO, and HNOO. The only thermodynamically favorable intermediate that resulted were *cis*-HONO (-46.2 kcal/mol) and *trans*-HONO (-45.9 kcal/mol). These results are generally in agreement with previous literature data [38,39] but place in evidence that the role of the *cis* isomer may be more important than what previously assumed. Intuitively one would expect the *trans* isomer to be more stable because of sterical reason, but according to our calculation for this particular molecule the *cis* isomer seems to´ have a slightly deeper (ΔE approx. -0.3 kcal/mol) well. Either way such small difference only points out that the main product for the title reaction is in fact a mix of *cis*

171

Orbital Elec. J. Chem*., Campo Grande, 2(2): 168-179, 2010

and *trans* HONO rapidly interconverting one into each other with a slight prevalence of the *cis* one.

The stability of these two intermediates is based on the fact that both of them are stable species with no unpaired electrons. All of the other intermediates are radicals, and as such, a higher energy would be expected. Hence according to our *ab initio* study the net equation then is:

$$NO + OH \rightarrow HONO \qquad (1)$$

A transition state between *cis*-HONO and trans-HONO was located (labeled as TS HONO). The geometry of its terminal H lies in the plane of O-N on the HONO surface, serving as a "half-way point" between the *cis*-HONO and *trans*-HONO isomers. The Erel of TS HONO is at -34.3 kcal/mol, suggesting the *cis*-HONO and *trans*-HONO readily go isomerization to one another, relative to the reactants thermodynamic conditions. No other transition states were located since all intermediates. Also, this and all transition states contain an imaginary frequency. Intrinsic Reaction Coordinates (IRC) were not performed since the TS involved are H shifts. For the purpose of this study it was sufficient to find the TS as a half-way point in terms of geometry between two intermediates. It is understood that the H geometry of the TS followed geometrically to those intermediates, and serves as barriers.

Table 1. Energy and Erel of all species considered in the *ab initio* calculations reported in the present paper. (*)calculated using b3lyp/6-311g(d,p)

	NO	*OH*	*NO+OH*	*NOOH*	*HONO*	*HNOO*
E*	-129.92217	-75.74609	-205.66826	-205.66522	-205.74190	-205.62061
ΔE			0.00000	0.00304	-0.07364	0.04765
E [cal/mol]			0.00000	1.90512	-46.20792	29.90209
E*	**HNOO** (linear)	**HONO** (t)	**ONO**	**H**	**ts**	**HNO**
ΔE	-205.406946	-205.741469	-205.626059	-0.502156	-205.697004	-130.38739
E [cal/mol]	0.26131	-0.07321	0.04220	205.16610	-0.02874	75.28087
E*	163.97641	-45.93998	26.48090	128743.69718	-18.03776	47239.46599

A possible product that can develop from the NO + OH reaction is the ONO species, this channel may be relevant and it has been included in our calculations due the high energetic stability of the NO_2 molecule. H + ONO is the result after a proton extraction of HONO. If the channel leading to the formation of hydrogen atom and nitrogen dioxide would be energetically allowed then on of the possible reaction's channel would be the following:

$$NO + OH \rightarrow H + ONO \qquad (3)$$

The pathway to ONO would be from the HONO route, so the overall reaction

172

Orbital Elec. J. Chem*., Campo Grande, 2(2): 168-179, 2010*

scheme is:

$$NO + OH \leftrightarrow HONO \rightarrow H + ONO \qquad (6)$$
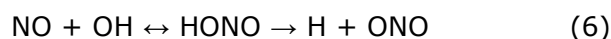
This route is examined to verify whether HONO is the prevailing product or if the channel leading to the dissociation of the product into H + ONO is rather an energetically comparable alternative. The proton extraction that leads to ONO formation comes from a H-ONO transition state (labeled TS ONO). According to the results of our calculations as reported in Table 2 together with the molecular geometries, reaction coordinates, and vibrational , the NO_2 formation is an energetically prohibited channel for this reaction. The H-ONO transition can form from either *cis*-HONO or *trans*-HONO, at -18.0 kcal/mol but the proton extraction proceeds the H-ONO transition formation, resulting in ONO as a product (at 26.5 kcal/mol). Having a H + ONO product with an energy barrier relative to the reactants suggests that H + ONO does not develop, and indeed the net general reaction scheme remain:

$$NO + OH \rightarrow HONO \qquad (1)$$

The decomposition of the *trans* isomer back into the reactants has also been object of a recent theoretical study by Bauerfeldt and its group [40]. Despite considering only the decomposition of the *trans* isomer in the (X^1A') state into the reagents for reaction (1) at a higher level of theory, their conclusions seems to be in general agreement with the calculations reported in the present paper confirming the general validity of our conclusion.

A careful comparison between this work and other *ab initio* studies including ref. [35] can be made by looking at the vibrational frequencies predicted by the different sets of calculations for the *trans*-HONO and the experimental values currently accepted in the literature [38-40]. Said comparison is shown in Table 3 and serves as stronghold for that part of the work that cannot be otherwise verified because of the lack of data in the current literature. The experimental data in general seems to be the less precise, for different reasons. First for the internal discrepancies among the three studies quoted, and with the more recent study by Guilmot [46]. In addition to that ref. [41-43] are very old and substantial improvements could be made with more modern techniques.

Finally the results of our *ab initio* calculation can be plotted in an energy diagram for reaction (1) including the bonding and non bonding channels as shown in Fig. 2. As expected the two structural isomers having an atomic sequence HONO are more stable than the other possible tetra atomic combinations such as HOON or OONH that are far more unstable than the isomer having a central nitrogen atom. The complete details of the calculated bond length and bond angles of all species considered in this study and

that constitute the basis for Fig. 2 are shown in Table 4.
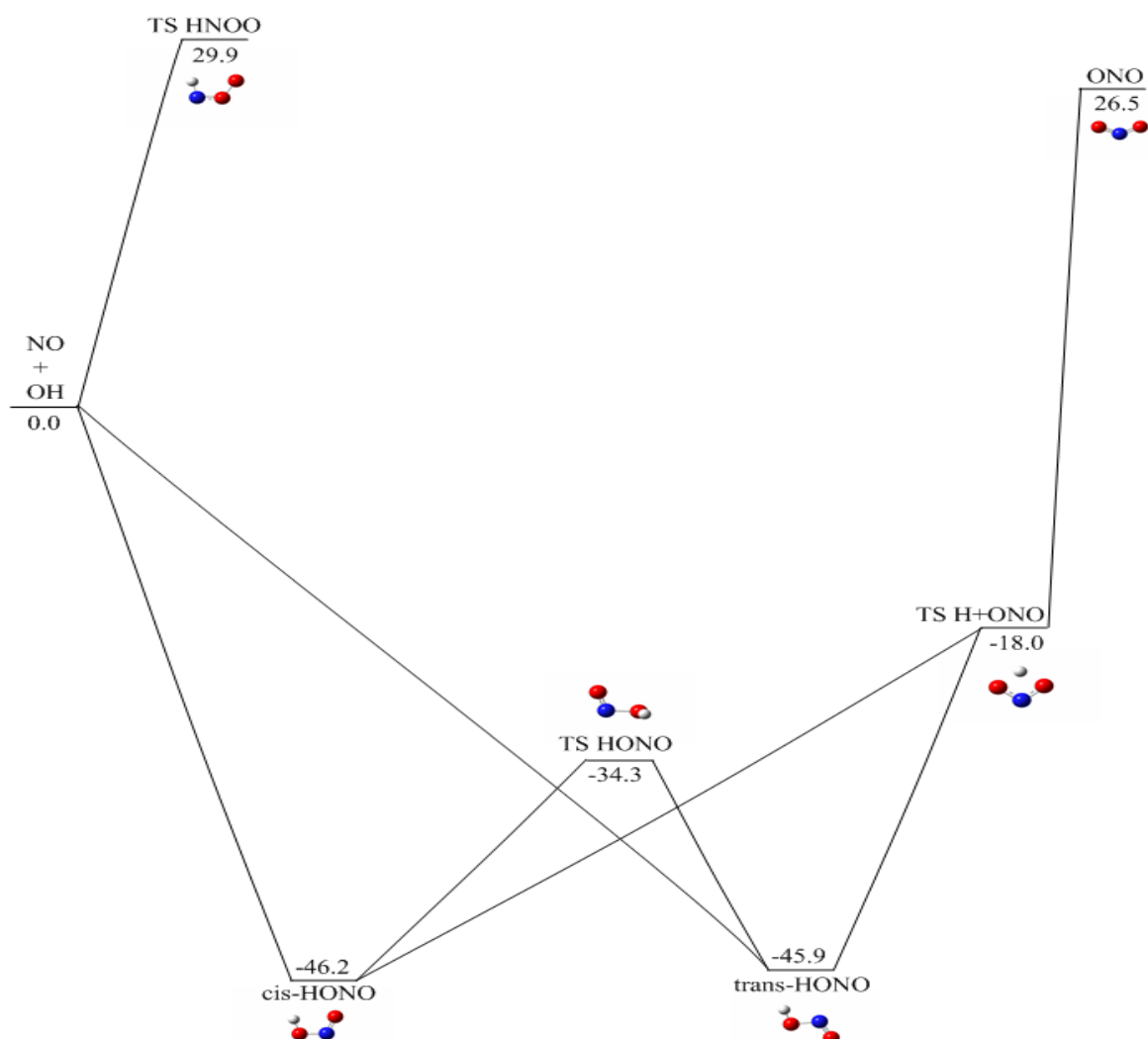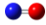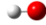
Figure 2. The Energy diagram of the Potential Energy Surface of the NO + OH reaction scheme calculated with GAUSSIAN and plotted with CHEMDRAW [47] based on the output of the GAUSSIAN calculation.

Remarkably, according to our calculations the *cis* isomer seems to be slightly more stable than the *trans* one, probably because of some hydrogen bond like interaction between the hydrogen atom and the opposing oxygen. According to the preliminary calculations of this study the hydrogen is not shared between the two oxygen atoms though since such "sharing" configuration would require a higher energetic content. On the other hand the low energy barrier between the *cis* and the *trans* isomer seem to indicate a fast interconversion between these two structural isomers. Details on the calculated geometry of the reaction's products have not yet been fully explored and more theoretical work is needed to present a conclusive possible reaction's pathway for this reaction.

174

Orbital Elec. J. Chem., Campo Grande, 2(2): 168-179, 2010

Table 2. In the following page B3LYP (with zero-point energy corrections (ZPE)) energies at 0 K, B3LYP/6-311G** optimized Cartesian coordinates, unscaled vibrational frequencies (v_i), moments of inertia (I_i), and rotational constants (B_i) of all species involved in the NO+OH reaction mechanism.   Molecular structures were drawn with CHEM 3 D [48] based on the output of Gaussian.

Species, (point group)	Energies, a.u.	i	I_i, a.u.	B_i GHz		Cartesian coordinates, angstroms			v_i, cm^{-1}
					Atom	X	Y	Z	
H	**E(B3LYP+ZPE) - 0.502155930011**								
NO **(C$_{\infty v}$)**	**E(B3LYP+ZPE)- 129.922172**	A	0.00000	0.0000000	N	0.0	0.0	-0.612	1989
		B	35.15744	51.3331257	O	0.0	0.0	0.536	
		C	35.15744	51.3331257					
HO **(C$_{\infty v}$)**	**E(B3LYP+ZPE) -75.746087**	A	0.00000	0.0000000	O	0.0	0.0	0.108	3705
		B	3.21989	560.4975584	H	0.0	0.0	-0.867	
		C	3.21989	560.4975584					
NO + OH	**E(B3LYP+ZPE) -205.66826 Erel = 0.0**								
HNOO **(C$_s$)**	**E(B3LYP+ZPE) -205.620607** Erel = 29.90209	A	20.26613	89.05211	N	1.123	-0.102	0.0	662, 943, 1081, 1311, 1532, 3234
		B	134.77669	13.39060	H	0.907	-1.119	0.0	
		C	155.04282	11.64028	O	0.0	0.466	0.0	
					O	-1.096	-0.237	0.0	
cis-HONO **(C$_s$)**	**E(B3LYP+ZPE) -205.74190** Erel = -46.20792	A	21.27843	84.81552	N	0.0	0.547	0.0	638, 718, 892, 1338, 1720, 3585
		B	136.01953	13.26825	O	1.084	0.081	0.0	
		C	157.29796	11.47339	O	-1.014	-0.401	0.0	
					H	-0.565	-1.272	0.0	
trans-HONO **(C$_s$)**	**E(B3LYP+ZPE) -205.741469**	A	19.18850	94.05329	N	0.0	0.519	0.0	591, 619, 834, 1298, 1793, 3776
		B	143.83744	12.54709	O	-1.112	0.169	0.0	
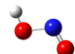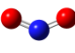
	Erel = -45.93998	C	163.02594	11.07027	O	0.892	-0.602	0.0	
					H	1.760	-0.174	0.0	
TS HONO **(C₁)**	**E(B3LYP+ZPE)** **-205.72286** Erel = -34.26265	A B C	21.70686 150.32025 166.21717	83.14150 12.00597 10.85773	N O O H	0.236 1.08 -1.116 -1.365	0.509 -0.280 -0.119 -0.377	0.042 0.0118 -0.122 0.778	671i, 558, 802, 1059, 1805, 3758
TS H+ONO **(Cₛ)**	**E(B3LYP+ZPE)** **-205.697004** Erel = -18.03776	A B C	24.26982 114.35836 138.62818	74.36155 15.78145 13.01857	N O O H	0.0 -1.000 1.000 -0.001	0.575 -0.187 -0.187 -1.027	0.0 0.0 0.0 0.0	1921i, 1029, 1243, 1302, 1400, 2097
ONO **(Cₛ)**	**E(B3LYP+ZPE)** **-205.626059** Erel = 26.48090	A B C	7.50385 138.35432 145.85817	240.50866 13.04434 12.37326	N O O	0.0 1.100 -1.100	0.323 -0.141 -0.141	0.0 0.0 0.0	767, 1399, 1705

Table 3. Comparison between the calculated vibrational frequencies [cm^{-1}] reported in this work, [38], and [39] and the experimental data available for this system.

	This work	*[38]*	*[39]*	*Exp. [41-43]*
n_1	519.0	596.0	600.9	540
n_2	619.0	631.1	-	593
n_3	834.0	862.2	796.0	791
n_4	1298.0	1305.9	1267.6	1265
n_5	1793.0	1791.8	1690.0	1699
n_6	3776.0	3756.8	3591.0	3588

Table 4. Bond length [Å] and bond angle [degrees] calculated in this study

Species	Bond	Length [Å]	Bond	Angle [degree]
OH	OH	0.98		
NO	NO	1.15		
HNOO	HO	1.04	NOO	120.5
	NO	1.26	HNO	104.8
	OO	1.3		
cis-**HONO**	HO	0.98	ONO	113.7
	ON	1.18	HON	105.8
	NO	1.39		
trans-**HONO**	HO	0.97	ONO	111
	ON	1.17	HON	102.3
	NO	1.43		
TS HONO	HO	0.97	ONO	111.6
	ON	1.16	HON	109.5
	NO	1.5		
TS H+ONO	NO	1.26	ONO	105.4
	NO	1.26	HNO	7.3
	HO	1.31		
ONO	NO	1.19	ONO	134.2
	NO	1.19		

In addition to that while this study bring some light in uncovering the energetic pathway for the formation of HONO from the reaction of the hydroxyl radical and nitric oxide in gas phase more work is needed in terms of experimental product yield determination to confirm the conclusion of this study and to eventually infer possible atmospheric implications.

Conclusion

The kinetic of formation of nitrous acid (HONO) has been previously investigated, and literature indicates a general agreement on the overall rate of reaction under atmospheric conditions [12] the kinetic constant four reaction (1) being in the range of $k=6*10^{-12}$ [cm^3 molecule^{-1} s^{-1}] under tropospheric pressure at room temperature. Complementing ref. [12] the present work presents a detailed *ab intio* study focused on the allowed reaction's pathways for the HONO formation from OH and NO and of the geometry of the resulting products confirming that the main product for this reaction is HONO. From the theoretical point of view the most recent studies published so far on the HONO system are the ones by Richter, et al. [41-42], and the ones by Bauerfeldt and its group [40] but, for the purpose of this work, they lack of focus in terms of analyzing possible atmospheric implication for the title reaction although they serve to support indirectly the conclusions of the present work.

References and Notes

[1]   Monks, P. S. *Chem. Soc. Rev.* **2005**, *34*, 376.

[2]   Pitts-Jr, J. N.; Biermann, H. W.; Winer, A. M.; Tuazon, E. C. *Atmos. Environ.* 1984,

177

Orbital Elec. J. Chem*., Campo Grande, 2(2): 168-179, 2010*

18, 847.

[3] Finlayson-Pitts, B. J.; Saliba, N. A.; Wingen, L. M.; Barney, W. S.; Mochida, M.; Yang, H. The formation of gaseous nitrous acid (HONO): a key determinant of tropospheric ozone and fine particles, Final Report for Contract No. 91-311, prepared for the California Air Resources Board and the California Environmental Protection Agency, 166, 2001.

[4] Harris, G. W.; Carter, W. P. L.; Winter, A. M.; Pitts-Jr, J. N.; Platt, U. Perner, D. *Environ. Sci. Technol.* **1996**, *35*, 3207.

[5] Harrison, R. M.; Peak, J. D.; Collins, G. M. *J. Geophys. Res.* **2001***, 101*, 14429.

[6] Roher, F.; Bhon, B.; Brauers, T.; Brüning, D.; Johen, F. J.; Wahner, A.; Kleffmann, J. *Atmos. Chem. Phys.* **2005**, *5*, 2189.

[7] Alicke, B.; Platt, U.; Stuz, J. *J. Geophys. Res.* **2003***, 108*, 8247.

[8] Alicke, B.; Geyer, A.; Hofzumnahaus, A.; Holland, F.; Konrad, S.; Pätz, H. W.; Shäfer, J.; Stuz, J.; Voltz-Thomas, A.; Platt, U. *J. Geophys. Res.* **2003***, 108*, 8247.

[9] Cox, R. A.; Derwent, R. G.; Holt, P. M. *J. Chem. Soc. Faraday Trans*. I, **1976**, *72*, 2031.

[10] Jenkin, M. E.; Cox, R. E. *Chem. Phys. Lett.* **1987***, 137*, 548.

[11] Wahner, A.; Ravishankara, A. R. *J. Geophys. Res.* **1987***, 92*, 2189.

[12] Di Loreto, G.; D'Ottone, L. *Annali di Chimica* **2004**, *94*, 899.

[13] Kleffman, J. *Chem. Phys. Chem.* **2007**, *8*, 1137.

[14] Lammel, G.; Cape, J. N. *Chem. Soc. Rev.* **1996***, 10*, 361.

[15] Anderson, J. G.; Kaufman, F. *Chem. Phys. Lett*. **1972**, *16*, 375.

[16] Anderson, J. G.; Magitan, J. J.; Kaufman, F. *J. Chem. Phys.* **1974**, *60*, 3310.

[17] Burrows, J. P.; Wallington, T. I.; Wayne, R. P. *J. Chem Soc. Farad. Trans.* **1983**, *79*, 111.

[18] Donahue, N. M.; Dubey, M. K.; Mohrschladt, R.; Demerjian, K. L.; Anderson, J. G. *J. Geophys. Res.* **1997**, *102*, 6159.

[19] Forster, R,; Frost, M.; Fulle, D.; Hamann, H. F.; Hippler, H.; Schiepegrell, A.; Troe, J. *J. of Chem. Phys. 1995*, *103*, 8.

[20] Fulle, D.; Hamann, H. F.; Hippler, H.; Troe, J. *J. Chem. Phys*. **1998**, *108*, 13.

[21] Harris, G. W.; Wayne, R. P. *J. Chem. Soc. Faraday Trans*. **1975**, *71*, 610.

[22] Howard, C. J.; Evenson, K. M. *J. Chem. Phys.* **1974***, 61*, 1943.

[23] Morley, C.; Smith, I. W. M. *J. Chem. Soc., Faraday Trans. II* **1976**, *68*, 1016.

[24] Overrend, R.; Paraskevopoulos, G.; Black, C. *J. Phys. Chem*. **1976**, *64*, 4149.

[25] Pagsberg, P.; Bjergbakke, E.; Ratajczak, E.; Sillesen, A. *Chem. Phys. Lett.* **1997**, *272*, 383.

[26] Smith, I. W. M.; Williams, M. D. *J. Chem. Soc., Faraday Trans*. **1985**, *91*, 1849.

[27] Stuhl, F.; Niki, H. *J. Chem Phys.* **1972**, *57*, 3677.

[28] Westemberg, A. A. de Haas, N. *J. Chem. Phys.* **1972**, *12*, 5375.

[29] Zabranick, C. *Chem. Phys*. **1993**, *171*, 265.

[30] Becke, D. *J. Chem. Phys.* 1993, *98*, 5648.

[31] Lee, C.; Yang, W.; Parr, R. G. *Phys. Rev. B* **1988**, *37*, 785.

178

Orbital Elec. J. Chem*., Campo Grande*, 2(2): 168-179, 2010

32] Zhang, F.; Kim, S.; Kaiser, R. I.; Jamal, A.; Mebel, A. M. *J. Chem. Phys.* **2009***, 130*, 234308.

[33] Gaussian 98 (Revision **A.7**) Frisch M J, Trucks G W, Schlegel H B, Scuseria G E, Robb M A, Cheeseman J R, Zakrzewski V G, Montgomery J A, Stratmann R E, Burant J C, Dapprich S, Millam J M, Daniels A D, Kudin K N, Strain M C, Farkas O, Tomasi J, Barone V, Cossi M, Cammi R, Mennucci B, Pomelli C, Adamo C, Clifford S, Ochterski J, Petersson J A, Ayala P Y, Cui Q, Morokuma K, Malick D K, Rabuck A D, Raghavachari K, Foresman J B, Cioslowski J, Ortiz J V, Stefanov B B, Liu G, Liashenko A, Piskorz P, Komaromi I, Gomperts R, Martin R L, Fox D J, Keith T, Al-Laham M A, Peng C Y, Nanayakkara A, Gonzalez C, Challacombe M, Gill P M W, Johnson B J, Chen W, Wong M W, Andres J L, Head-Gordon M, Replogle E S, Pople J A, Gaussian, Inc. , Pittsburgh, PA, 1998.

[36] Gonzalez, C.; Schlegel, H. B. *J. Chem. Phys.* **1989***, 90,* 2154.

[37] Gonzalez, C.; Schlegel, H. B. *J. Phys. Chem.* **1990**, *94*, 5523.

[38] Sharkey, P.; Sims, I. R.; Smith, I. W. M.; Bocherel, P.; Rowe, B. R. *J. Chem. Soc. Faraday Trans.* **1994**, *90*, 3609.

[39] Nguyen, M. T.; Sumathi, R.; Sengupta, D.; Peeters, D. *J. Chem. Phys*. **1998**, *230*, 1.

[40] Bauerfeldt, G, F.; Arbilla, G. Da Silva, E. C. *J. Braz. Chem. Soc*. **2005**, *16*, 2.

[41] Ricther, F.; Gatti, F.; Leonard, C. Le que're', F.; Meyer, H. D. *J. Chem. Phys*. **2007**, *127*, 164315.

[42] Richter, F.; Hochlaf, M.; Rosmus, P.; Gatti, F.; Meyer, H. D. *J. Chem. Phys.* **2004**, *120*, 130.

[43] Cox, A. P.; Brittain, A. H.; Finnigan, D. J. *Trans. Faraday Soc.* **1971**, 67, 2179.

[44] Hezberg, G. Molecular Spectra and Molecular Structure. III: Electronic Spectra and Electronic Structure of Polyatomic Molecules, Krieger: Florida, 1991.

[45] Deeley, C. M.; Mills, I. M. *Mol. Phys.* **1985**, *54*, 23.

[46] Guilmot, J. M.; Mélen, F.; Herman, M. *J. Mol. Spectrosc.* **1993**, *160,* 401.

[47] Cambridgesoft, London, UK CHEMDRAW.

[48] Chempute Software, Pretoria South Africa CHEM 3D.

179

Orbital Elec. J. Chem., Campo Grande, 2(2): 168-179, 2010

Full Paper

Spectrophotometric methods for simultaneous estimation of pantoprazole and itopride hydrochloride in capsules

Krishna R. Gupta*, Rajesh B. Chawla and Sudhir G. Wadodkar

Department of Pharmaceutical Chemistry, S. K. B. College of Pharmacy, New Kamptee 441002, Nagpur (MS) India

ABSTRACT: *Three simple, accurate and economical methods for simultaneous estimation of pantoprazole and itopride hydrochloride in two component solid dosage forms have been developed. The proposed methods employ the application of simultaneous equation method (Method A), absorbance ratio method (Method B) and multicomponent mode of analysis method (Method C). All these methods utilize distilled water as a solvent. In distilled water pantoprazole shows maximum absorbance at a wavelength of 289.0 nm while itopride hydrochloride shows maximum absorbance at a wavelength of 258.0 nm also the drugs show an isoabsorptive point at a wavelength of 270.0 nm. For multicomponent method, sampling wavelengths 289.0 nm, 270.0 nm and 239.5 nm were selected. All these methods showed linearity in the range from 4-20 μg/mL and 15-75 μg/mL for pantoprazole and itopride hydrochloride respectively. The results of analysis have been validated statistically and by recovery studies.*

Keywords: pantoprazole; itopride hydrochloride; distilled water; simultaneous equation; absorbance ratio; multi-component mode of analysis

Introduction

Pantoprazole (PAN) is chemically 5-(Difluoromethoxy)-2-[[(3,4-dimethoxy-2-pyridinyl)methyl]sulfinyl]-1H-benzimidazole. It is a substituted benzimidazole proton pump inhibitors and used as anti ulcerative. It is official in The Merck Index [1] and Martindale, The Extra Pharmacopoeia [2]. PAN is very soluble in water and methanol. Itopride Hydrochloride (ITH) chemically is, N-{p-[2-(Dimethylamino) ethoxy]benzyl} veratramide hydrochloride. It is a dopamine antagonist and used as prokinetic and

---

antiemetic. It is not official in any of the Pharmacopoeias and is listed in Martindale, The Extra Pharmacopoeia [3]. ITH is very soluble in water and freely soluble in alcohol. An extensive literature survey revealed HPLC [4] and UV spectrophotometric [5] methods for the analysis of PAN alone, whereas ITH has been determined by UV spectrophotometric [6], RP-HPLC [7] and HPTLC [8] alone in formulation. So far no spectrophotometric method has been reported for the simultaneous estimation of both these component in a combined dosage form. Spectrophotometric methods are reported for estimation of these drugs alone and would require tedious procedure for analysis if the reported methods are applied for their estimation in combined pharmaceutical formulation, difference spectroscopic method of analysis [5] of PAN in two different media (acidic and basic). The same cannot be applied to ITH. If present in same formulation the methodology has to be modified, or will create interference in the analysis. Similarly involves the formation of a colored chloroform extractable complex of drug (ITH) with bromocresol green in acidic media [6]. However the same complex formation may not be possible with PAN under same specified conditions. Hence both the above methods cannot be applied for the simultaneous estimation of the drugs in combined dose formulations.

Therefore, it was thought to develop a precise, accurate and simple method for estimation of these drugs in combined dosage formulation that would not require any prior separation of the drugs from each other and can be analyzed simultaneously.

Material and Methods

A Shimadzu UV-1700 UV/Vis spectrophotometer with 1 cm matched quartz cell was used for all absorbance measurements. Double distilled water was used as a solvent. PAN and ITH were purchased from Zim Labs. Ltd., Nagpur and Relief Labs., Nagpur.

Preparation of standard stock solution

PAN standard stock solution.

An accurately weighed quantity of pantoprazole sodium sesquihydrate (~25 mg PAN) was transferred in 50.0 mL volumetric flask, dissolved in sufficient quantity of distilled water and volume was made up to the mark with distilled water (concentration: 500 µg/mL).

ITH standard stock solution

An accurately weighed quantity of ITH (~25 mg) was transferred in 50.0 mL volumetric flask, dissolved in sufficient quantity of distilled water and volume was made up to the mark with distilled water (concentration: 500 µg/mL).

Selection of wavelength

These stock solutions were appropriately diluted with distilled water to obtain the

181

Orbital Elec. J. Chem*., Campo Grande,* 2(2): 181-188, 2010

concentration of 10 µg/mL and were scanned in the UV range (200-400 nm) in 1 cm cell against solvent blank. The overlain spectra of both drugs are depicted below in Figure 1.
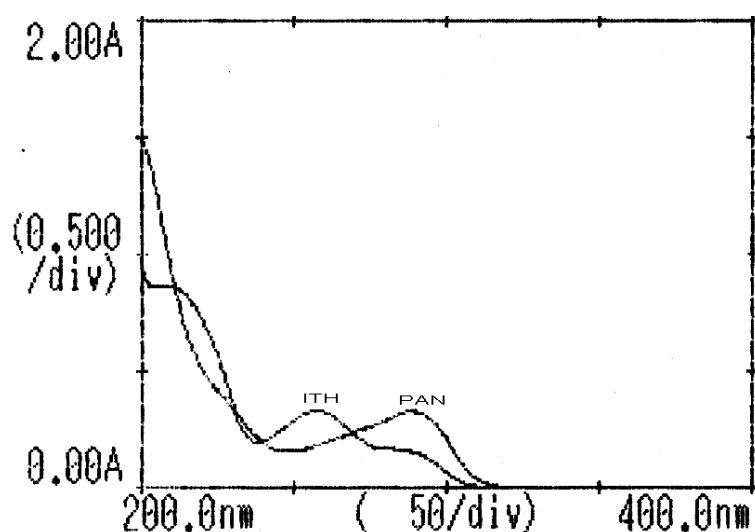
Figure 1. Overlain spectra of pantoprazole (PAN) and itopride hydrochloride (ITH).

PAN shows a well-defined λ_{max} at 289.0 nm and ITH shows a well-defined λ_{max} at 258.0 nm, these two wavelengths were selected for development of simultaneous equation method. Also overlain spectra, shows an isoabsorptive wavelength where both the drugs shows same absorbance at 270.0 nm and 239.5 nm. The wavelengths 289.0 nm and 270.0 nm were considered for estimation of drugs by absorbance ratio method.

The stock solutions of PAN and ITH were further diluted with distilled water in the series from 4-20 µg/mL for PAN and 15-75 µg/mL for ITH respectively. From the overlain spectra depicted in Figure 1, sampling wavelengths 289.0 nm, 270.0 nm, 239.5 nm were selected such that both the drugs have sufficient absorbance. The concentrations of individual drugs were fed to the multicomponent mode of the instrument; all five mixed standards of drug solutions were scanned over a range of 230 nm to 300 nm against solvent blank. The spectrums so recorded of five different mixed standards are depicted below in Figure 2.

Calibration curves were plotted as concentration *versus* absorbance. The optical characteristics such as absorption maxima, Beer's law limit, $A^{1\%}_{1cm,}$ correlation coefficient and limit of detection of both methods were recorded in Table 1.

Application of the proposed methods for determination of PAN and ITH in Capsules:

An accurately weighed quantity of capsule content equivalent to 20.0 mg of PAN (~ 75.0 mg of ITH) was transferred to 100.0 mL volumetric flask, dissolved by shaking for 30 min. with sufficient quantity of distilled water and volume was made up to mark

182

Orbital Elec. J. Chem., Campo Grande, 2(2): 181-188, 2010

with distilled water. The contents was filtered through Whatmann filter paper (no.41) and a 5.0 mL portion of the filtrate was further diluted to 100.0 mL with distilled water to get final concentration of about (10.0 µg/mL PAN, 37.5 µg/mL ITH, on label claim basis). The absorbance of the resulting solution was measured at 289.0, 270.0 and 258.0 nm in 1.0 cm cell using solvent blank. The contents of PAN and ITH were calculated by substituting values in the formulae given below for method A, B and C.
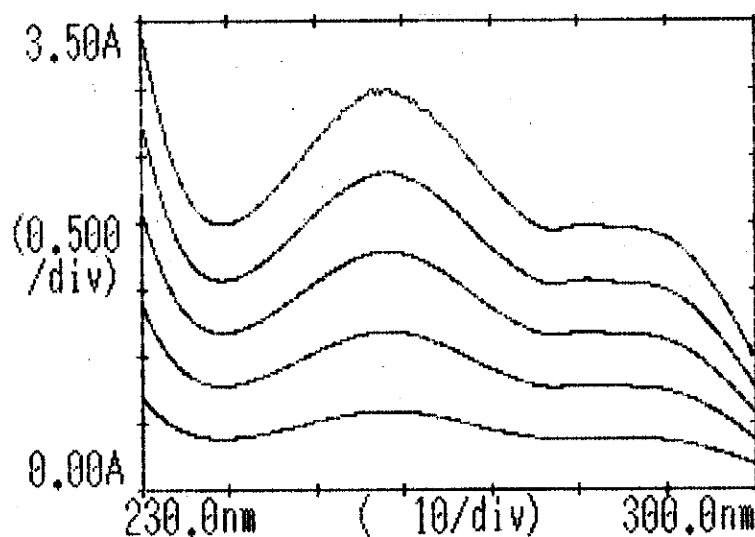
Figure 2. Overlain spectra of five mixed standards.

Table 1. Optical characteristics.

Parameters	PAN	ITH
λ_{max} **and Isobestic**	289.0 nm and 270.0 nm	258.0 nm and 270.0 nm
Beer's law limit	4-20 µg/ml	15-75 µg/ml
$A^{1\%}_{1cm}$	379.56 and 278.0	335.90 and 231.0
Correlation coefficient	0.9993 and 0.9997	0.9991 and 0.9997
Limit of detection	67 ng /mL	250 ng /mL

Simultaneous equation method (Method A) [9]

For estimation of PAN   For estimation of ITH

$$c_y = \frac{A_1 ax_2 - A_2 ax_1}{ax_2 ay_1 - ax_1 ay_2} \quad c_x = \frac{A_2 ay_1 - A_1 ay_2}{ax_2 ay_1 - ax_1 ay_2}$$

Where: A_1 and A_2 are absorbance of diluted mixture at 289.0 nm and 258.0 nm respectively; Cx and Cy are the concentrations of PAN and ITH respectively (g/100 mL); ax_1, ax_2 are absorptivities of PAN and ay_1, ay_2 for ITH at 289.0 nm and 258.0 nm

183

Orbital Elec. J. Chem*., Campo Grande,* 2(2): 181-188, 2010

respectively.

Absorbance ratio method (Method B) [9]

Amount of each drug in sample was determined using following formulas:

For estimation of PAN

$$Cx = \frac{Qm - Qy}{Qx - Qy} \times \frac{A}{ax}$$

For estimation of ITH

$$Cy = \frac{Qm - Qx}{Qy - Qx} \times \frac{A}{ay}$$

Where: x= PAN and y= ITH

Cx = Concentration of PAN in g/100 mL; Cy = Concentration of ITH in g/100 mL

Qm = Ratio of absorbance of laboratory mixture at 289.0 nm and 270.0 nm; Qx = Ratio of absorptivity of PAN at 289.0 nm and 270.0 nm; Qy = Ratio of absorptivity of ITH at 289.0 nm and 270.0 nm; ax = Absorptivity of PAN at 289.0 nm; ay = Absorptivity of ITH at 270.0 nm; A = Absorbance of mixture at isoabsorptive point.

From the amount of each drug estimated by above methods, percent estimation for each drug was calculated.

Multi-component mode method (Method C) [9]

Sample solution prepared for above two methods were scanned over the range of 230 nm to 300 nm in multi-component mode against solvent blank and concentration of each drug component was obtained by the analysis of spectral data of sample solution with reference to that of five-mixed standard in terms of concentration in μg/mL

Amt of Drug (mg) = Concentration of drug (mg) X Dilution factor

Results of estimation in marketed formulation are shown in Table 2.

Table 2. Summary of result of estimation in marketed formulation

Sample		% Label claim estimated*					
		Simultaneous Equation Method		Absorbance Ratio Method		Multicomponent Mode	
Itop 1	**Mean ±SD CV**	**PAN**	**ITH**	**PAN**	**ITH**	**PAN**	**ITH**
		100.05	100.68	99.40	100.96	100.75	100.94
		0.56	1.02	0.10	0.65	0.26	0.33
		0.56	1.02	0.10	0.65	0.26	0.33
Itop 2	**Mean**	99.77	100.12	99.49	100.31	100.62	100.63
	± SD	0.61	0.90	0.36	0.89	0.30	0.53
	CV	0.62	0.89	0.36	0.89	0.30	0.53
	SE	0.27	0.40	0.16	0.40	0.13	0.23

*Mean of five observations ± Standard Deviation. Itop 1 and 2: are Marketed formulations used in analysis.

184

Orbital Elec. J. Chem*., Campo Grande, 2(2): 181-188, 2010*

The recovery studies were performed by standard addition method. To a known amount of previously analyzed capsule powder, pure drugs were added at four different levels and the samples were analyzed by proposed methods. The results of recovery studies are recorded in Table 3.

Table 3. Summary of result of estimation in recovery study.

Sample		Simultaneous Equation Method		Absorbance Ratio Method		Multicomponent Mode	
		PAN	ITH	PAN	ITH	PAN	ITH
Itop 1	Mean ± SD CV	99.29	99.70	99.90	99.73	100.51	99.17
		0.11	0.70	1.20	1.35	0.93	0.67
		0.11	0.70	1.20	1.35	0.92	0.67

* Mean of four observations, Itop 1: is Marketed formulation used in analysis.

Validation of proposed methods [10]

Validation of proposed method was carried out as per ICH guidelines.

Accuracy

Accuracy of the proposed methods was ascertained on the basis of recovery study performed by standard addition method and results are recorded in Table 3 indicate the accuracy of the proposed methods.

Precision

The precision of the method was ascertained by replicate analysis and SD values were found to be within limits. Results are shown in Table 2.

Intermediate Precision

Inter-day precision

It was done by analyzing the solutions by same analyst on alternate days till 7th day. The % RSD (CV) is shown in Table 4.

Intra-day precision

It was done by analyzing the solutions by same analyst within a day. The % RSD (CV) is shown in Table 4.

Specificity studies

An accurately weighed quantities of capsule powder equivalent to 20 mg were transferred to series of 100 mL volumetric flask and kept under following stress conditions viz. 0.5 N NaOH, 0.5 N HCl reflux for 3 h; 6% H_2O_2 24 h at 50 ^{0}C; heat (60 ^{0}C), humidity (75%) and UV exposure for 24 h; direct sun light (photochemical exposure)

185

Orbital Elec. J. Chem*., Campo Grande,* 2(2): 181-188, 2010

for 6 h. After the specified time period volumes were made up to mark with distilled water, filtered and procedure described under marketed formulation was followed. Results of specificity studies are recorded in Table 5.

Table 4. Summary of result of Precision (Intermediate) and Ruggedness.

Time	% Label Claim					
	Simultaneous Equation Method		Absorbance Ratio Method		Multicomponent Mode	
	PAN	ITH	PAN	ITH	PAN	ITH
0 Hrs	99.25	100.83	99.51	100.65	100.92	100.36
3 Hrs	99.25	100.97	99.70	100.70	101.10	100.82
6 Hrs	99.40	100.72	99.20	100.89	100.54	100.30
Mean	**99.30**	**100.84**	**99.47**	**100.74**	**100.85**	**100.49**
Day	**% Label Claim**					
	Simultaneous Equation Method		Absorbance Ratio Method		Multicomponent Mode	
	PAN	ITH	PAN	ITH	PAN	ITH
Day 1	99.25	100.83	99.51	100.65	100.92	100.36
Day 4	93.32	99.97	93.12	100.14	93.96	95.93
Day 7	88.00	99.99	88.25	99.81	90.29	92.51
Mean	**93.52**	**100.26**	**93.62**	**100.20**	**95.05**	**96.27**
Analyst	**% Label Claim**					
	Simultaneous Equation Method		Absorbance Ratio Method		Multicomponent Mode	
	PAN	ITH	PAN	ITH	PAN	ITH
Analyst 1	100.22	100.22	99.62	100.02	100.82	100.69
Analyst 2	99.18	99.14	98.79	99.49	99.68	99.66
Analyst 3	100.58	100.24	99.29	99.90	100.27	100.18
Mean	**99.99**	**99.86**	**99.23**	**99.80**	**100.25**	**100.18**

Table 5. Summary of results of Specificity study.

Sample (Treated)	%Label claim					
	Simultaneous Equation Method		Absorbance Ratio Method		Multicomponent Mode	
	PAN	ITH	PAN	ITH	PAN	ITH
0.5 N NaOH reflux for 3 h	76.18	103.29	75.89	102.69	71.53	99.22
0.5 N HCl reflux for 3 h	115.22	99.37	117.69	99.18	114.52	102.18
6% H_2O_2 for 24 h at 50 ^{0}C	51.49	93.53	50.13	92.89	45.89	76.54
60 °C for 24 h	79.35	99.23	79.13	99.06	82.19	96.79
Humidity (75% RH)	96.78	97.12	96.44	97.03	96.89	97.43
UV-exposure (254.0 nm)	95.64	99.13	95.43	99.47	95.13	100.04
Photochemical	86.78	100.86	86.92	100.09	81.57	95.84

Linearity and Range

An accurately weighed quantity of capsule powder equivalent to 80-120% of label claim was transferred and procedure as described under marketed formulation was followed, graphs were plotted as percentage label claim vs. absorbance for Method A and

186

Orbital Elec. J. Chem*., Campo Grande,* 2(2): 181-188, 2010

B and percentage label claim vs. amount estimated for Method C.

Ruggedness

It was done by analyzing the samples solutions by three different analysts. The % RSD (CV) by proposed methods is shown in Table 4.

Results and Discussion

The well-defined λ_{max} for PAN is at 289.0 nm while ITH shows at 258.0 nm. The drugs show the isobestic point at 270.0 nm, as shown in Figure 1. The absorptivity values of PAN and ITH were found to be 379.56 and 156.57 at 289.0 nm; 212.99 and 335.90 at 258.0 nm; 278.0 and 231.0 at 270.0 nm, respectively. All the proposed methods were found to be rapid, economical and precise for the determination of PAN and ITH in its combined dosage form. The percent label claim was found to be from 99.40-100.75 for PAN and 100.68-100.75 in formulation (Itop 1) while 99.77-100.62 for PAN and 100.12-100.63 for ITH in formulation (Itop 2) using the three proposed methods. The percent recovery was found to be nearly 100%. Specificity study shows degradation of drug under different stressed conditions. Interference studies revealed that the common excipients and other additives usually present in the dosage form did not interfere in all the proposed methods. The values of standard deviation were satisfactory and percentage recovery was close to 100%, indicating the reproducibility and accuracy of the methods. Linearity study showed that all the proposed methods were found to be linear. The Coefficient of correlation at 289.0, 270.0 and 258.0 were found to be 0.9993, 0.9997 and 0.9991, respectively for Method A and B and 0.9996 and 0.9998 for PAN and ITH in Method C.

Our proposed methods do not involve complex formation whose stability is dependent on pH or interference from other drugs/excipients as compared with reported methods for analysis of the either drugs in single formulation. Also no reported methods give little idea about the stability of the drugs under different stress conditions which we have tried to explain to some extent.

Conclusion

All proposed methods can be easily applied to analysis of the said drugs in combined formulation containing PAN and ITH in its dosage forms as they produce comparable results and can be used for precise and accurate analysis of PAN and ITH in its capsule dosage form.

Acknowledgements

187

Orbital Elec. J. Chem*., Campo Grande,* 2(2): 181-188, 2010

Labs., Nagpur for providing us the gift sample of pure drug and to the Principal, S. K. Bhoyar College of Pharmacy, Kamptee for providing research facilities.

References and Notes

[1] The Merck Index*: An Encyclopedia of Chemicals, Drugs, and Biologicals,*, 13th ed., monograph no. 7084. O'Neal, M. J., ed. New Jersey: Merck Research lab, Whitehouse Station, 2001.

[2] Reynolds, J. F.; Martindale, The Extra Pharmacopoeia, 35t[h] ed. London: Pharmaceutical   Press, p. 1217.

[3] Reynolds, J. F.; Martindale, The Extra Pharmacopoeia, 35th ed. London: Pharmaceutical   Press, p. 1229.

[4] Mansour, A. M.; Sorour, O. M. *Chromatographia* **2001**, *53*, 468.

[5] Mashru, R. C.; Patel, P. M. *Indian Drugs* **2003**, *40*, 300.

[6] Smitha, G.; Areefulla, H. S.; Swamy, P. V.; Appala, R. S. *Asian J. Chem.* **2007**, *19*, 3445.

[7] Dighe, V. V.; Sane, R. T.; Menon, S. N.; Tambe, H.; Inamdar, S.; Pillai, S. *Indian Drugs* **2006**, *43*, 282.

[8] Suganthi, A.; Karthikeyan, R.; Ravi, T. K. *Indian Drugs* **2006**, *43*, 827

[9] Beckett, A. H.; Stenlake, J. B. Practical Pharmaceutical Chemistry, 4th ed., Part II. New Delhi: CBS Publisher and Distributors, 1997, p. 276.

[10] International Conference on Hormonisation: ICH Harmonised Tripartite Guidelines - Validation of Analytical Procedures, Federal Register 62, 1997, 27463.

188

Orbital Elec. J. Chem*., Campo Grande*, 2(2): 181-188, 2010

Full Paper

An alternative process for hydrogenation of sunflower oil

Rosana de C. de Souza Schneider[a]*, Luciano R. Silva Lara[a], Marcia Martinelli[b]

[a]Departamento de Química e Física - Universidade de Santa Cruz do Sul- UNISC – Av. Independência, 2293, Santa Cruz do Sul, CEP 96815-900, RS, Brazil
[b]Instituto de Química, Universidade Federal do Rio Grande do Sul – UFRGS – Av. Bento Gonçalves 9500, Porto Alegre, CEP 91501-970, RS, Brazil

ABSTRACT: *Classic methodologies for hydrogenation of vegetable oils have traditionally been carried out by nickel catalysts under high pressure of H_2 and high temperature. An alternative method for hydrogenation of sunflower oil using limonene and palladium-on-carbon was investigated in this study. The use of limonene as a hydrogen donor solvent was proposed in order to avoid high temperature and high-pressure conditions. The catalytic transfer of hydrogenation was studied by using 0.5 to 2% of Pd as a catalyst, a limonene:oil ratio of 3:1, and reaction times from 0.5 to 2 hours. Under these conditions, high selectivities for oleic acid and low concentrations of stearic acid were obtained.*

Keywords: *sunflower oil; CTH; hydrogenation; limonene; palladium catalyst*

Introduction

Vegetable oils have received much attention as natural and renewable resources of starting materials for several industries. Vegetable oils and their derivatives present biodegradable properties that make them good alternatives to petrochemical products. In Brazil, crops such as soybean, corn, rice, and cotton are well established in the agro-alimentary and vegetable oil industry. Recently, sunflower has gained some interest as an alternative crop because of its high polyunsaturated fatty acid content (C18:2 and C18:3) and productivity.

In the vegetable oil chemical industry, hydrogenation is one of the most important processes. Hydrogenated products are starting materials used in the cosmetic,

---

* Corresponding author. E-mail: rosana@unisc.br

pharmaceutical, food and chemical industries [1-4]. Hydrogenation processes using copper-chromite catalysis are commercially employed for the selective hydrogenation of soybean oil due to their selectivity for hydrogenating the linolenic acid contents.

In the vegetable oil chemical industry, hydrogenation is one of the most important processes. Hydrogenated products are starting materials used in the cosmetic, pharmaceutical, food and chemical industries [1-4]. Hydrogenation processes using copper-chromite catalysis are commercially employed for the selective hydrogenation of soybean oil due to their selectivity for hydrogenating the linolenic acid contents. However, copper-chromite catalysts require high temperature and high-pressure conditions because of their poor activity at low hydrogen pressures [5]. Other processes using nickel-based catalysts are also commercially available and are most commonly used for conventional hydrogenation [6-8]. Nickel-based catalysts promote high activity, linolenic acid selectivity, low cost and easy removal from oils by filtration. Catalyst activity is usually independent of the nature of the support, and differences in catalyst selectivity have been ascribed to differences in the morphology of the support [9]. However, a drawback of nickel-based catalysts is that they isomerize the natural *cis* double bond to *trans* olefin. The hydrogenation performance of commercial Ni catalysts in sunflower oil has being recently discussed [10]. Noble metal catalysts (such as Pd, Pt and Ru), supported on silica, have been used for hydrogenation of the ethyl ester of sunflower oil.

Palladium on different supports is efficiently used in the reduction of double bonds in oils [2, 11–12]. Another important factor in the choice of the catalyst system is the temperature of reaction. Generally, the catalysts require reaction temperatures above 150 °C and high hydrogen pressure.

In heterogeneous catalysis, catalyst systems containing noble metals (Pd, Pt, Ru) supported over silica allow one to work under gentle conditions: for example, hydrogenations at 40 °C under 10 bar of hydrogen. In this situation and others, the major catalyst is Pd [2, 11, 13].

An alternative method for vegetable oil hydrogenation is the use of catalytic transfer hydrogenation (CTH), which can utilize organic molecules as hydrogen donors at ambient pressure.

In CTH, the reaction requires only moderate temperatures and agitation. The hydrogen donor is used as solvent along with a selected catalyst, negating the need for special reactors.

The CTH process (with Pd/C and different donor hydrogen solvents) has already been studied for oils such as soy [2, 14]**,** safflower [15], castor [16], canola [17], and

190

Orbital Elec. J. Chem*., Campo Grande,* 2(2): 189-200, 2010

others [11].

The donor hydrogen molecules commonly used are, among others, hydrazine, alcohols, aromatic hydrocarbons, limonene, cyclohexene, formic acid, formiates, phophinates and phosphinic acid. Limonene is the most widely used terpene in catalytic transfer reductions.

Limonene, compared to the ciclohexene, has advantages. Namely, it demands shorter reaction times and exclusively reduces the olefin linkage in the presence of certain functional groups [18].

This donor has already been monitored by gas chromatography equipped with mass spectroscopy and it was discovered that disproportionation occurs when the system begins to boil. In this moment, limonene (substance A) starts to disappear and substances C, D and E appear (Scheme 1). There is a possibility that substance D is the effective hydrogen donor for the acceptor of interest. The isopropyl group linked to the olefin of substance C impedes the interaction with the catalyst more than the methyl group of olefin D [11, 19].

The results with limonene in hydrogenation of castor oil were promising, as it presented a high conversion in saturated products (72%) and major selectivity for ceto-stearic production.

Therefore, it is desirable to apply this hydrogen donor to the hydrogenation of other oils. The scope of the present investigation is to evaluate sunflower oil CTH using a citrus industry sub product, limonene, as the hydrogen donor and Pd on carbon as the metal catalyst.
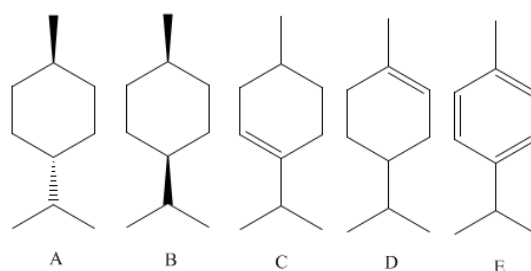
Scheme 1. Limonene disproportionation products: A) limonene, B) *p*-menthane, C e D) *p*-menthenes and E) *p*-cymene.

In this work, the use of limonene as a solvent hydrogen donor was investigated for the hydrogenation of the sunflower oil. The hydrogenation products were then characterized.

Material and Methods

191

Orbital Elec. J. Chem*., Campo Grande*, 2(2): 189-200, 2010

Oil extraction

Sunflower seeds grown in the Santa Cruz do Sul region were used in this work. An oil extraction procedure was done on 100 g of seeds with a hydraulic press at a 10 ton pressure. After extraction, degaming and purification processes were carried out in order to characterize the oil prior to its use (see Table 1). The oil was characterized according to American Oil Chemist's Society (AOCS) official methods [20].

Table 1. Sunflower oil specification.

Parameters	Values
Specific gravity (AOCS Cc 10 a -25 (95))	0.915
Peroxide Value (Cd 8b-90(03))	0.43
Iodine Value (Cd 1 d - 92 (97))	131
Acid Value (Cd 3d-63(03))	0.20
Refraction Index (Cc 7-25 (05))	1.4682
Saponification Value (Cd 3-25 (03))	189

Chemicals

Palladium on carbon (Pd/C, 10% w/w) and boron trifluoride–methanol (BF$_3$.MeOH, 14% wt/vol) were purchased from Across Organics (Fairlawn, NJ). Deuterated chloroform (99.8%), heptane, methanol, and anhydrous sodium sulfate were from Merck (Hohenbrunn, Germany). Other materials such as hexane, sodium chloride and sodium hydroxide were purchased from Synth (Diadema, SP). Limonene ([*R*]-4-isopropenyl-1-methyl-1-cyclohexene; [*R*]-*p*-mentha-1,8-diene) was donated by Dierberger Óleos Essenciais (São Paulo, Brazil). All reagents were used as received. The methyl ester standards (all above 99% purity) for gas chromatography (GC) were palmitic acid (hexadecanoic acid), stearic acid (octadecanoic acid), oleic acid (*cis*-9-octadecenoic acid), elaidic acid (*trans*-9-octadecenoic acid) and linoleic acid (*cis*-9,*cis*-12-octadecadienoic acid) (Supelco, Bellefonte, PA)

Standard hydrogenation procedure

The hydrogenation reaction was performed in a 50 mL, two-necked, round-bottomed flask connected to a thermometer and a reflux condenser under vigorous stirring. The reaction was done with 1 g of sunflower oil (5.634 mmol), 2.28 g of limonene (16.902 mmol) (1:3) and 24 mg of Pd/C 10% (corresponding to 2% molar Pd in relation to the double bonds of the sunflower oil). The reaction was carried out for 1-4 hours at 178 °C. After that, the suspension was immediately centrifuged and filtered. The products were dried under vacuum and derivatized for further analysis. The Pd/C was washed with solvent, dried and stored.

Derivatization

Sunflower oil and its hydrogenated products were converted to their methyl esters by reaction with BF$_3$·MeOH and methanol [21], extracted with heptane and dried over

192

Orbital Elec. J. Chem., Campo Grande, 2(2): 189-200, 2010

anhydrous sulfate sodium. The products were stored for chromatography analysis.

Gas Chromatography

The fatty acid methyl esters were characterized by gas chromatography with Varian model 3300 fitted with a flame ionization detector (FID). The column was a DB-wax polyethylene glycol fused silica column (30 m long x 0.53 mm i.d. x 0.43 μm film thickness). The temperature gradient consisted of an initial temperature of 80 °C that was held for 0.2 min, followed by increasing steps of 5 °C min^{-1} up to 140 °C (maintained for 2 min), then increasing steps of 8 °C min^{-1} up to 215 °C (maintained for 15 min). The sample volume was 0.4 μL and nitrogen was used as the carrier gas. The chromatographic analysis also was carried out by gas chromatography (GC model QP2010 plus; Shimadzu, Kyoto, Japan) fitted with a mass spectrometer detector (MSD) operating in the EI ionization mode at 70 eV. The capillary columns used were DB-5ms - polydimethyl siloxane fused silica open tubular column with 5% phenyl groups (30 m long x 0.25 mm i.d. x 0.25 μm film thickness). The temperature gradient for these columns consisted of an initial temperature of 180 °C, followed by increasing steps of 1.3 °C min^{-1} up to 210 °C, then steps of 5 °C min^{-1} up to 250 °C (this temperature was maintained for 2 min).

NMR analysis

^{1}H NMR spectra were recorded using a Varian Inova 300 MHz instrument (Varian, Palo Alto, CA) at room temperature with CDCl$_3$ as the solvent. All chemical shifts are relative to tetramethylsilane (TMS) using the positive downfield convention. Quantitative analysis was done using methodology that has been described previously [22-24].

IR Spectroscopy

Data were collected on a Nicolet Magma 550 spectrometer (local) equipped with accessories for horizontal attenuated total reflectance (HATR) using the surface of a ZnSe crystal. The spectra were recorded in the region of 650 to 4000 cm^{-1} with 32 scans, and these scans were compared with those in the literature [25]. The observed infrared bands are shown in Table 2.

Table 2- Characteristic IR-Absorption bands of sunflower oil.

Assignment	Observed band (cm^{-1})
ν =C-H	3007 weak
ν as CH$_2$	2921 strong
ν sim CH$_2$	2852 strong
ν C=O	1743 strong
δ CH$_2$	1459 medium
ν C-O as (ester)	1159 medium
ν C-O sim (ester)	1117 medium
δ CH$_2$	721 medium

193

Orbital Elec. J. Chem., Campo Grande, 2(2): 189-200, 2010

Results and Discussion

CTH of sunflower oil

The sunflower oil CTH reactions were followed by determination of the iodine index and IR spectroscopy. Characterization of the products was accomplished by ^{1}H NMR and GC with flame ionization and mass detectors.

Via gas chromatography, it was possible to determine the fatty acid composition of the sunflower oil: palmitic (C16:0) 5%, stearic (C18:0) 5%, oleic (C18:1) 25%, linoleic (C18:2) 61% and linolenic (C18:3) 4%.

Comparison of the IR spectra of the oil before and after hydrogenation was used to confirm that the reaction products were more saturated that the raw material.

The presence of specific bands from C=C bonds in the spectra of the oil allows the qualitative evaluation of the transformations promoted in the chemical structure of triacylglicerols during the hydrogenation reaction.

It is observed that in the spectrum of the hydrogenated oil, the band indicating oil double bonds at 3007 cm^{-1} disappears, and in some samples a weak band (related to the presence of the *trans* isomer) appears at 966 cm^{-1}. This is advantageous due to the consumer desire for low *trans*-fat hydrogenated oils for cooking. The band shift observed in this study shows that the *trans*-isomer production was insignificant, and it indicates that *cis–trans* isomerization could be reduced using the CTH system.

With regard to iodine index, it was possible to evaluate the best set of conditions to obtain less unsaturated material. Determining the composition of the final products, however, required gas chromatography. The presence of saturated and unsaturated fatty acids in the triacylglicerols of the sunflower oil were determined in this manner; we were able to quantify by GC the following fatty acids: estearic, oleic, linoleic and linolenic. In the products of the more saturated hydrogenation, polyunsaturated fatty acids were not observed, suggesting that this reaction was selective.

In the GC-FID chromatograms, the products were identified and quantified but the isomers of oleic acid were not separated; the oleic acid isomers were separated by GC-MS. The more abundant components that were quantified and identified in the reaction products were palmitic, stearic, and oleic acid.

Considering that the isomers of oleic acid present the same detector response, it was verified that the total isomers did not exceed 5% of the total *cis*-9-octadecenoic acid. The interpretation of the mass spectra suggests that a significant constituent of the C18:1 isomers are from double bonds or geometry (Fig. 1).
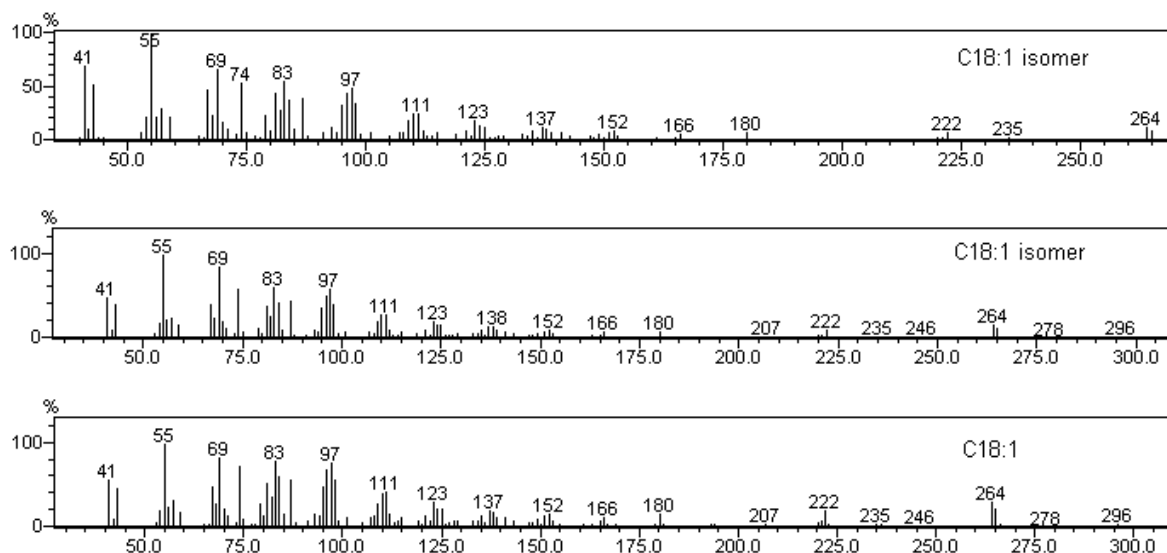
Figure 1 - Mass spectra of C18:1 isomers obtained in CTH reaction, at 178^0 C, 1h , 1:3 oil-limonene and 1% of the Pd/C.

In general, the hydrogenation of vegetable oils is a complex network of chemical reactions involving several reactant species and their isomers. The various fatty acids and isomers compete with each other for the catalyst active sites. Thus, the hydrogenation reaction produces consecutive saturation of *cis* C18:2 to C18:1 in *cis* configuration, and *cis* C18:1 to C18:0 as well as the parallel, reversible isomerization of *cis* C18:2 to *trans* C18:2 isomers and *cis* C18:1 to *trans* C18:1 isomers [26]. The results with CTH of sunflower oil do not exhibit evidence of *cis-trans* C18:2 isomerization since experiments after 1 h do not present polyunsaturated products.

Preliminary experiments demonstrated that C18:2 isomerization occurred during the shorter reactions.

Better results were found with a longer reaction time (1 to 3 h), similar to the hydrogenation of the castor oil [10] where the amount of catalyst and the reaction time were the main factors that contributed to reaction selectivity.

Conversion

The CTH reactions utilizing 0.5% Pd/C demonstrated the conversion of C18:2 to C18:1; CTH reactions also demonstrated the conversion of C18:1 to C18:0 and the reduction of C18:1 levels in the final product if the percentage of catalyst was increased. For the 0.5% Pd/C, the conversion of double bonds were high; with 1.0% Pd/C, increased C18:0 was found in the products, as shown by Fig. 2, and C18:2 was not observed after 1 hour. Also it was important to observe that the C18:3 present in sunflower oil was quickly consumed to form the other, less unsaturated fatty acids such as C18:2, C18:1 and their isomers.

195

Orbital Elec. J. Chem*., Campo Grande,* 2(2): 189-200, 2010

The reduction of unsaturated sunflower oil probably converted more unsaturated into less unsaturated fatty acids.

The reaction products obtained were found to be triacylglicerols of estearic and palmitic acids in small quantities and oleic acids in large quantities; approximately 90% hydrogenation was achieved using 0.5% Pd/C, which is more than was obtained using classical methods of hydrogenation.

Reaction selectivity was favored the formation of oleates. Concerning the selectivity of the reaction in relation to the percentage of the Pd/C, it was observed in all experiments that selectivity for oleate formation increased with decreasing percentages of Pd/C.

The concentration of catalyst and the reaction time can be selected according to the desired final product. If the final product was still polyunsaturated, the reaction could be run with a shorter reaction time and less catalyst. Or, if the products had to be rich in monounsaturated fatty acids, 2% Pd/C and a 30 min to 1 h reaction time would be appropriate conditions (Fig. 3).
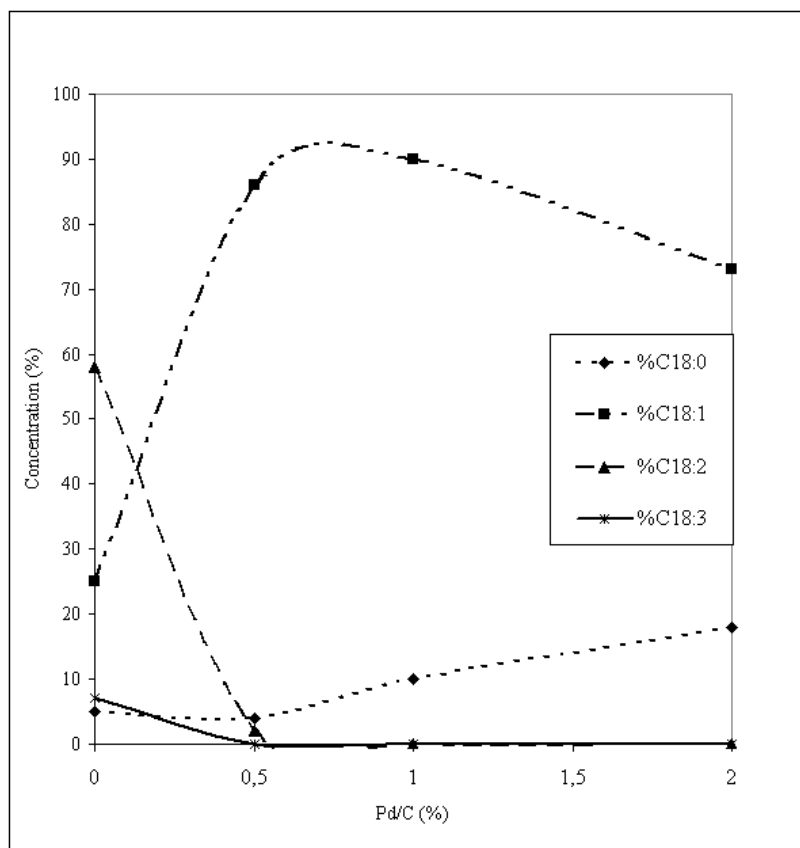

Figure 2. Fatty acids of the triacylglicerols of sunflower oil conversion in relation at quantities of Pd/C, at 178^0C, 1 h and 1:3 oil-limonene.

Some experiments have been conducted at reaction times of 3 and 4 hours (at 1

196

Orbital Elec. J. Chem*., Campo Grande,* 2(2): 189-200, 2010

or 2% Pd/C, with an oil-limonene ratio of 1:3) until C18:0 comprised 10% of the final product. With 1 hour of reaction (at 1% Pd/C), C18:1 was formed and varied from 25% in the initial oil to 90% of the final product. The conversion of the C18:2 was rapid, with 87.7% converted to C18:1 in the first hour of the reaction. After the second hour, the products contained more C18:0, however, the reaction was proceeding more slowly. The conversion of C18:2 to C18:1, C18:1 to C18:0 or C18:2 to C18:0 depends on the interactions of oil-catalytic sites and limonene-catalytic sites. This varies with quantities of limonene and Pd/C, stirring velocity, temperature and reaction time.
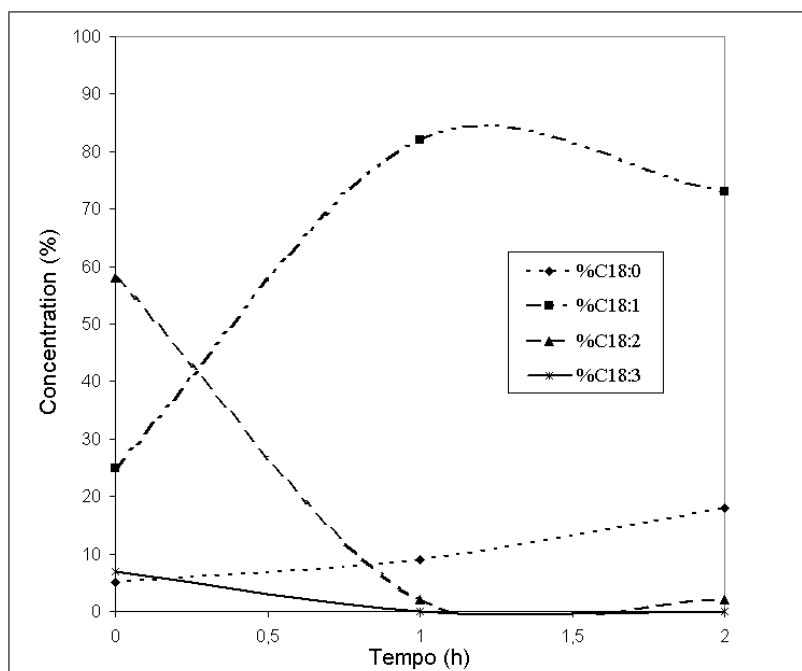

Figure 3. Fatty acids of the triacylglicerols of sunflower oil conversion in function of the reaction time, at 178^0C, 2% of Pd/C and 1:3 oil-limonene.

The proposed reaction mechanism was developed for a hydrogen solvent donor and a triacyglicerol on a catalytic surface. In this reaction mechanism [27], both hydrogen from the solvent donor and olefin from the oil were adsorbed onto the catalyst surface. The hydrides on the surface were used to reduce the carbon−carbon double bonds on fatty acids of the triacylglicerols (TG), giving partially or fully saturated products as well as compounds obtained by the disproportionation of limonene (see Fig. 4).

This result was unexpected because studies of hydrogenation of polymeric systems [27, 28] and other oils have shown that in such systems, CTH proceeds in the same way as classic hydrogenation. Our results suggest the formation of palladium hydride (Pd-H) via hydrogen transfer from the hydrogen donor to the palladium catalyst; this results in the hydride donating a hydrogen to the double bond of the sunflower oil

197

Orbital Elec. J. Chem*., Campo Grande,* 2(2): 189-200, 2010

and generates a semi-hydrogenated intermediate that is converted into the saturated product by the transfer of another hydrogen from the hydride. For the reaction to proceed, it is important to promote close contact between the double bond of the sunflower oil and the Pd/C catalyst prior to the addition of limonene [10].

The temperature of the reaction appeared to be an important parameter in the CTH of vegetable oil using Pd/C as the catalyst when limonene was the hydrogen donor. In the temperature where the reaction proceeded, disproportionation of the limonene occurred along with hydride production and reduction of the double bonds. Subsequently, double bonds of the fatty acid chain were reduced. In conditions with high concentrations of the Pd-hydride, the hydrogenation of the double bonds of the fatty oil was concomitant.
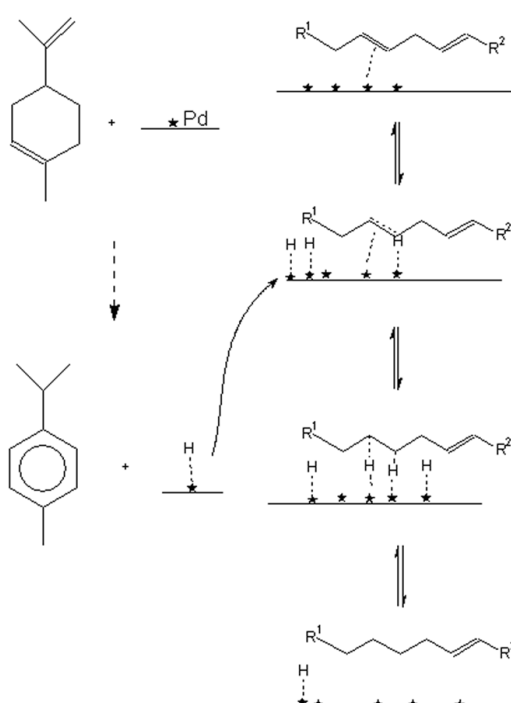
Figure 4. Proposed mechanism for the hydrogenation of sunflower oil using the catalytic transfer hydrogenation system Pd/C and limonene. R^1 = carbon chain bonded to the TG and R^2 = terminal carbon chain.

The principal reduction was obtained for C18:2 for C18:1 and although after 1 hour, C18:0 increased, there was no total reduction of unsaturation because more solvent or catalyst was needed to generate additional hydride.

On the other hand, the high limonene concentrations could interfere with the availability of catalytic sites and the limonene can be adsorbed more easily in active sites. The highly adsorbed limonene can allow the generated hydrogen to be used in the

reduction of previously formed molecules of menthenes and menthadienes to form menthane. This product (menthane) does not donate more hydrogen, according to Schneider [19], who monitored this using solid phase microextraction (SPME) during the CTH of castor oil. In this case, double bond hydrogenation is barely observed, which is similar to that observed in a preliminary study with 1:7 and 1:10 oil-limonene.

Conclusion

In conclusion, this study investigated the selective hydrogenation of sunflower oil on palladium catalysts and shows that it is difficult, but possible, to avoid the secondary reaction of *cis–trans* isomerization of the required compound (C18:1). All the results obtained in this work show that control of the selectivity could be obtained by reaction time and concentration of the Pd/C utilized in CTH.

The CTH of sunflower oil using limonene as hydrogen solvent donor was efficient for the production of oleates. For the production of more oleates with low of *trans* isomer content, optimal experimental conditions consisted of 0.5 to 1% Pd/C for 1 h using a 1:3 oil-limonene ratio.

A combination of limonene and Pd/C in CTH of sunflower oil was enough to make hydrogenation selective and rapid in comparison with classic methods.

In this study, it was determined that hydrogenated oil can be produced with cleaner technology; the solvent comes from the residue of juice industries, and limonene was extracted from the peel of citrus fruits. For that reason, CTH does not require press control and, with the use of limonene, does not create toxic residues. The sub products of the limonene disproportionation could be purified.

Some evidence on oleate isomerization was obtained, but the influence of the catalyst and hydrogen donor solvent on isomerization will be a subject for future work.

Acknowledgements

References and Notes

[1]   Nohair, B.; Especel, C.; Marécot, P.; Montassier, C.; Hoang, L. C.; Barbier, J. *C. R. Acad. Sci. II C* **2004**, *7*, 113.

[2]   Nohair, B.; Especel, C.; Lafaye, G.; Marécot, P.; Hoang, L. C.; Barbier, J. *J. Mol. Catal. A: Chem.* **2005**, *229*, 117.

[3]   Farmani, J.; Hamedi, M. ; Safari, M. ; Madadlou, A. *Food Chem*. **2007**, *102*, 827.

199

Orbital Elec. J. Chem., Campo Grande, 2(2): 189-200, 2010

[4] Ribeiro, A. P. B. ; Grimaldi, R. ; Gioielli, L. A. ; Gonçalves, L. A. G. *Food Res. Int.* **2009**, *42*, 401.

[5] Tike, M. A.; Mahajani, V. V. *Chem. Eng. J.* **2006**, *123*, 31.

[6] Jang E. S.; Jung, M. Y.; Min, D. B. *Compre. Rev. Food Sci. Food Saf*. **2005**, *1*, 22.

[7] Jovanovic, D.; Radovic, R.; Mares, L.; Stankovic, M.; Markovic, B. *Catal. Today* **1998**, *43*, 21.

[8] Gabrovska, M.; Krstic, J.; Edreva-Kardjieva, R.; Stankovic, M.; Jovanovic, D. *Appl. Catal. A: Gen.* **2006**, *299*, 73.

[9] Rodrigo, M. T.; Daza L.; Mendioroz, S. *Appl. Catal. A: Gen. 1992*, *88*, 101.

[10] Fernández, M. B.; Tonetto, G. M.; Crapiste, G. H.; Damiani, D. E. *J. Food Eng.* **2007**, *82*, 199.

[11] Fernández, M. B.; Sánchez, J. F.; Tonetto, G. M.; Damiani, D. E. *Chem. Eng. J.* **2009**, *155*, 941.

[12] Fritsch, D.; Bengtson, G. *Catal. Today* **2006**, *118*, 121.

[13] Coenen, J. W. E. *J. Am. Oil Chem. Soc*. **1976**, *53*, 382.

[14] Smidovnik, A.; Stimac, A.; Kobe, J. *J. Am. Oil Chem. Soc.* **1992**, *69*, 405.

[15] Devi, B. L. A. P.; Karuna, M. S. L.; Rao, K. N.; Saiprasad, P. S.; Prasad, R. B. N. *J. Am. Oil Chem. Soc*. **2003**, *80*, 1003.

[16] Martinelli, M.; Schneider, R. C. S.; Baldissarelli, V. Z.; Von Holleben, M. L.; Caramão, E. B. *J. Am. Oil Chem. Soc*. **2005**, *82*, 279.

[17] Mondal, K.; Lalvani, S. B. *J. Am. Oil Chem. Soc*. **2000**, *77*, 1.

[18] Zini, C. A. Utilization of Limonene as a Hydrogen Donor in the Catalytic Transfer Hydrogenation of some Unsaturated Alicyclic a , b – Ketones. [Master Dissertation.] Porto Alegre, Brazil: Universidade Federal do Rio Grande do Sul, 1990.

[19] Schneider, R. C. S.; Baldissarelli, V. Z.; Martinelli, M.; Von Holleben, M. L. A.; Caramão, E. B. *J. Chromatogr. A* **2003**, *985*, 313.

[20] Official Methods and Recommended Practices of the AOCS, 2006. 5th Edition, 2nd Printing.

[21] Christie, W. W. Gas chromatography and lipids**:** a practical guide. Ayr: The Oily Press, 1992.

[22] Miyake, Y.; Yokomizo, K.; Matsuzaki, N. *J. Am. Oil Chem. Soc*. **1998**, *75*, 15.

[23] Schneider, R. C. S. Extraction, Characterization and Transformation of castor oil. [Ph.D. Dissertation.] Porto Alegre, Brazil: Universidade Federal do Rio Grande do Sul, 2003.

[24] Gerbase A. E.; Brasil, M.; Gregório, J. R.; Mendes, A. N. F.; Von Holleben, M. L. A.; Martinelli, M. *Grasas Aceites* **2002**, *53*, 175.

[25] Pretch, E.; Clerc, T.; Seibl, J.; Simon, W. Tables of spectral data for structure determination of organic compounds, 2nd, New York: Springer-Verlag, 1989.

[26] Belkacemia, K.; Boulmerkab, A.; Arulb, J.; Hamoudi, S. *Top. Catal.* **2006**, *37*, 2.

[27] Von Holleben, M. L. A.; Zucolotto, M.; Zini, C. A.; Oliveira, E. R. A. *Tetrahedron* **1994**, *50*, 973.

[28] Von Holleben, M. L. A.; Calcagno, C. I. W.; Mauler, R. S. *Quim. Nova* **1999**, *22,* 218.

200

Orbital Elec. J. Chem*., Campo Grande,* 2(2): 189-200, 2010

Full Paper

Cobalt (II), nickel (II), copper (II) and zinc (II) complexes of 1-(phenyl(phenylamino) methyl)pyrrolidine-2,5-dione and 2-((phenylamino)methyl) isoindoline-1,3-dione and their biological activity

D. Tamil Vendan[a], S. Rajeswari[a], S. Ilavenil[b] and G. Venkatesa Prabhu[a]*

[a]Department of Chemistry, National Institute of Technology, Tiruchirappalli, Tamil Nadu-620 015. India
[b]Department of Biotechnology, PRIST University, Thanjavur, Tamil Nadu - 613 403, India

ABSTRACT: *The new Mannich bases 1-(phenyl(phenylamino)methyl)pyrrolidine-2,5-dione (SBA) was synthesized from the condensation of succinimide, benzaldehyde and aniline. 2-((phenylamino)methyl)isoindoline-1,3-dione (PFA) was derived from pthalimide, formaldehyde and aniline. The general formula of the Co(II), Ni(II), Cu(II) and Zn(II) chloro complexes, ML_2X_2 are reported. The ligands and the complexes have been characterized by various physical-chemical techniques such as elemental analysis, molar conductance, magnetic susceptibility measurements, infrared and electronic spectra. The spectral analysis to ascertain mode of bonding and overall geometry of the complexes revealed octahedral geometries.*

Keywords: Mannich bases; metal complexes; octahedral geometries

Introduction

The synthesis, characterization and spectral study of metal complexes containing biologically important ligands assume importance because certain metal ions are active in many biological processes [1-3]. The fact that transition metals are essential metallic elements and exhibit great biological activity when associated with certain metal–protein complexes, participating in oxygen transport, electronic transfer reactions or the storage of ions [4], has created attention in the study of systems containing these metals. There

---

* Corresponding author. E-mail: venkates@nitt.edu

has been considerable interest directed towards the isolation of new complexes of these ligands and their spectral and magnetic characterization [5, 6]. Mannich type reactions are among the most important carbon-carbon bond forming reactions in organic synthesis [7]. They provide amino methylated/benzylated compounds which are important synthetic intermediates for various pharmaceuticals and natural products [8]. The increasing popularity of the Mannich reaction has been fueled by the ubiquitous nature of nitrogen containing compounds in drugs and natural products [9]. Metal complexes of succinimide and phthalimide are of interest due to their unique structural features and potential pharmacological applications [10-11]. In view of these findings, Mannich bases of succinimide and phthalimide and their metal complexes have been synthesized, characterized and screened them for their biological activity.

Material and Methods

The chemicals used in the synthesis were obtained from Aldrich Chemical Company and were used without further purification. The solvents used were of spectroscopic grade. Infrared spectra were recorded on a Perkin-Elmer FTIR spectrophotometer in KBr. ^{1}H NMR spectra were recorded on a Bruker Advance DPX 300 MHz Ultra-Shield FTNMR Spectrophotometer in DMSO-d_6 and CDCl$_3$ with TMS as internal reference. Chemical shifts are expressed in δ units (ppm). Ultraviolet-visible (UV-Vis) absorption spectra were recorded on Perkin-Elmer Spectrophotometer (EZ 301) at the wavelength of maximum absorption ($λ_{max}$) in dimethylsulfoxide (DMSO)/*N,N*-dimethylformamide (DMF). All melting points were taken in open capillary tubes in ^{o}C by using Elico instrument and mass spectra on a LUNA instrument. The micro-elemental results were obtained on a Vario-EL instrument. The human pathogenic bacterial species (*Pseudomonas aeuroginosa, Escherichia coli, Salmonella typhi, bacillus cereus, and klebsilla pneumonia*) were used for the anti microbial studies.

Microbial inoculums preparation

The young microbial inoculums/culture was prepared and used in the entire research period. The nutrient broth (NB) for bacteria and potato dextrose broth (PDB) for fungi were prepared and poured into tubes and sterilized. The pure microbial cultures collected were inoculated in the tubes using inoculation needles and loops. Then these tubes were incubated at different temperatures and time duration (at 37 °C and 24-48 hours for bacteria and at 27 °C and 48-72 hours for fungi). 20 mg of synthesized organic compounds dissolved in 2 mL of DMSO were used as a stock solution. From the stock solution, various concentrated discs (60 μg) were prepared.

Synthesis

Synthesis of 1-(phenyl(phenylamino)methyl)pyrrolidine-2,5-dione (SBA)

202

Orbital Elec. J. Chem*., Campo Grande,* 2(2): 201-208, 2010

Aniline (10 mL, 0.1M) was added slowly to a solution of succinimide (9.09 g, 0.1M) in water, taken in a beaker. Benzaldehyde (10 mL, 0.1M) was added in drops with stirring of the solution. The mixture first become oily and then after 10 days it slowly turned into a white crystalline mass which was separated by suction filtration and washed several times with water. The product was dried at 60 ^{o}C and recrystallized using toluene by slow evaporation method.

Molecular formula: $C_{17}H_{16}N_2O_2$, Yield: 76%, MP: 73-74 ^{o}C, Mol. wt: 280.32. FT- IR KBr in cm^{-1}: 3440, 3333 (NH), 3111, 3059 (CH aromatic), 1691, 1625 (C=O), 1182 (C-N-C), 785, 747 (mono substituted benzenoid ring). ^{1}H NMR (300 MHz, CDCl$_3$) δ 2.74 (s, 4H), 8.20 (s, NH), 6.14 (d, 2H), 6.52-6.58 (m, 5H phenyl ring), 7.51-7.27 (m, 5H aniline). ^{13}C NMR (300 MHz, CDCl$_3$) δ 29.57 (s, 2C, (CH$_2$)$_2$), 64.18 (s, 1C, CH), 108.53 (s, C), 114.46-160.48 (m, 5C, benzyl ring), 177.71 (s, 2C, C=O). FABMS m/z: 280.32 ($C_{17}H_{16}N_2O_2$), base peak m/z 182.24 ($C_{13}H_{12}N^{+\cdot}$); 203.21 ($C_{11}H_{11}N_2O_2^{+\cdot}$); 104.98 ($C_7H_7N^{+\cdot}$); 77.10 ($C_6H_5^{+\cdot}$). Calculated: C 72.84 %, H 5.75 %, and N 9.99 %, O 11.42%. Found: C 72.89 %, H 5.71 %, and N 9.96 %, O 11.44 %.

succinimide benzaldehyde aniline 1-(phenyl(phenylamino)methyl)pyrrolidine-2,5-dione
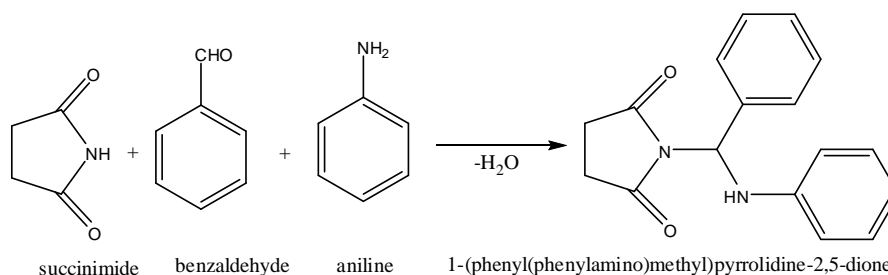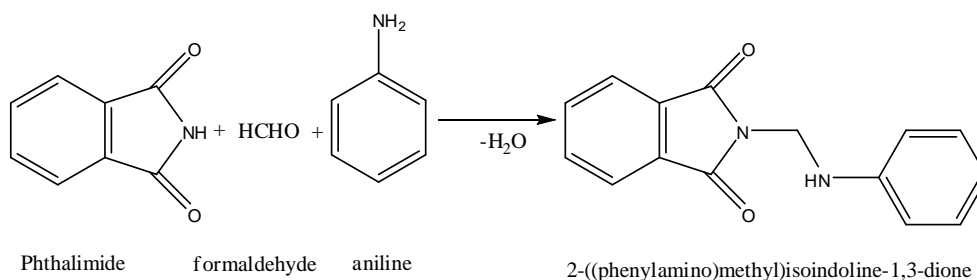
Scheme1

Synthesis of 2-((phenylamino)methyl)isoindoline-1,3-dione (PFA)

9.5 g (0.1mol) of phthalimide and 10 mL (0.1mol) of formaldehyde were dissolved in minimum amount of ethanol and the contents were mixed well at room temperature until a clear solution was obtained. 10 mL (0.1mol) of aniline was added to this mixture. After 10 days a yellow solid was obtained and it was washed with ethanol several times and dried in the air oven at 60 ^{o}C and recrystallized from ethanol.

Molecular formula: $C_{15}H_{12}N_2O_2$, Yield: 87, MP: 132-133 ^{o}C, Mol. wt: 252.26. FT IR KBr in cm^{-1}: 3447, 3384 (-NH), 3050, 2957 (CH aromatic), 1765, 1708 (C=O stretching), 1602 (C=C, C=N stretching), 1510 (NH bending), 1407 (C-N stretching), 1166 (C-N-C stretching), 722 (benzene CH out of plane bending). ^{1}H NMR (300 MHZ, CDCl$_3$) δ 2.47 (s, 4H), 3.32 (s, NH), 4.75 (d, 2H), 6.76-7.09 (m, 5H, phenyl ring). ^{13}C NMR (300 MHZ, CDCl$_3$) δ 28.21 (s, 2C, (CH$_2$)$_2$), 48.46 (s, 1C, CH$_2$), 108.53 (s, C), 113.57-144.57 (m, 5C, phenyl ring), 177.49 (s, 2C, C=O). FABMS m/z: 252.27 ($C_{15}H_{12}N_2O_2^{\cdot+}$); m/z: ($C_9H_7N_2O_2^{\cdot+}$); m/z: 160.14 ($C_9H_6NO_2^{\cdot+}$); m/z: 77.10 ($C_6H_5^{\cdot+}$). Calculated: C 71.51 %, H

203

Orbital Elec. J. Chem., Campo Grande, 2(2): 201-208, 2010

4.79 %, and N 11.10 %, O 12.68 %. Found: C 71.39 %, H 4.63%, N 11.21%, O 12.77 %.

Phthalimide   formaldehyde   aniline   2-((phenylamino)methyl)isoindoline-1,3-dione

Scheme 2

Synthesis of metal complexes

Ethanolic solution of Mannich base (0.1M) was mixed with hot ethanolic solution of metal (II) chloride (0.05M) and digested on a water bath for 50 minutes. The content was concentrated and cooled. The solid product obtained was filtered, washed with ethanol and dried under vacuum.

Results and Discussion

Physical characteristics, micro analytical and magnetic susceptibility data of the complexes are given in Table 1. The analytical data of all the complexes correspond to the general formula ML_2X_2. Magnetic susceptibility values of the complexes at room temperature are consistent with octahedral geometry around the central metal ions. The chelates show no appreciable conductance, and this supports the hypothesis of their neutral nature. The electronic absorption spectra of the Mannich bases and their Co (II), Ni (II), Cu (II) and Zn (II) complexes were recorded at room temperature using DMSO as solvent. The electronic spectra of Co(II) complex showed two spin-allowed transitions at 17,876 and 21,714 cm^{-1} assignable to $^4T_{1g}(F) \rightarrow {}^4A_{2g}(F)$ and $^4T_{1g}(F) \rightarrow {}^4T_{1g}(P)$ transitions respectively, are in conformity with octahedral arrangements for Co(II) ion [13]. The appearance of a band at 19,244 cm^{-1} due to $^3A_{2g}(F) \rightarrow {}^3T_{1g}(P)$ transition favors an octahedral geometry [14] for the Ni(II) complex. The absence of any band below 10,000 cm^{-1} eliminates the possibility of a tetrahedral environment in this complex. Only one broad band is observed at 16,638 cm^{-1} in the electronic spectrum of the Cu(II) complex assigned to $^2E_g \rightarrow {}^2T_{2g}$ transition similar to octahedral [12] arrangement which is supported by its magnetic moment value (1.8 μB). Though three transitions are expected in this case, they are very close in energy and often appear in the form of one broad band envelope. No transitions were observed in the visible region for the Zn (II) complex consistent with the d^{10} configuration of the Zn^{2+} ion. This complex is also found to be diamagnetic as expected for the d^{10} configuration. The suggested structure for the complexes is shown in Figure 1.

204

Orbital Elec. J. Chem*., Campo Grande,* 2(2): 201-208, 2010

Table 1. Physical characterization, analytical, molar conductance and magnetic susceptibility data of the ligand and its complexes.

Compound	Color	Contents (found/calcd) %					Λ_m Ohm^{-1} cm^2 mol^{-1}	μ_{eff}, μ_B
		Metal	C	H	N	O		
Ligand-SBA	Brown	-	58.56/58.55	5.42/5.49	20.47/20.45	15.55/15.52	---	---
SBA -CoCl$_2$	Dark brown	10.91	44.46/44.45	4.10/4.10	15.56/15.53	11.85/11.87	11.1	4.77
SBA -NiCl$_2$	Light green	10.87	44.48/44.44	4.11/4.12	15.56/15.55	11.85/11.88	11.3	3.81
SBA- CuCl$_2$	Dark green	11.66	44.09/44.01	4.07/4.10	15.42/15.40	11.75/11.76	12.6	1.89
SBA-ZnCl$_2$	Colorless	11.96	43.94/43.90	4.06/4.05	15.37/15.38	11.71/11.73	10.2	---
Ligand-PFA	Yellow	-	71.41/71.42	4.77/4.79	11.14/11.10	12.67/12.68		
PFA-CoCl$_2$	Brown	7.93	54.92/54.90	4.34/4.35	11.30/11.28	21.52/21.53	11.9	4.70
PFA-NiCl$_2$	Light green	7.90	54.94/54.95	4.34/4.33	11.31/11.33	21.52/21.55	12.0	3.66
PFA-CuCl$_2$	Dark green	8.49	54.58/54.55	4.31/4.30	11.23/11.21	21.38/21.36	12.1	1.80
PFA-ZnCl$_2$	Colorless	8.72	54.44/54.46	4.30/4.33	11.20/11.17	21.33/21.36	10.2	---

Table 2. Important IR Absorption Bands (cm^{-1}) of SBA, PFA and of Co (II), Ni (II), Cu (II) and Zn (II) Complexes.

Compound	v_{NH}	$v_{C=O}$	v_{CNC}	v_3	v_4	v_1	v_2	v_5	v_6
SBA	3333, 3230	1691	1182	-	-	-	-	-	-
SBA -CoCl$_2$	3300	1631	1098	1142, 1005, 984	788, 631, 601	872	471	-	-
SBA -NiCl$_2$	3335	1631	1071	1170, 990	633, 604	828	543	-	-
SBA- CuCl$_2$	3313	1625	1100	1100, 1039, 996	778, 701	871	532	-	-
SBA-ZnCl$_2$	3390	1598	1087	-	-	1313	1018	1429	824
PFA	3447,3384	1765, 1708	1166	-	-	-	-	-	-
PFA-CoCl$_2$	3485	1635	1109	1151, 987	754, 612	852	490	-	-
PFA-NiCl$_2$	3548	1627	1101	-	-	1310	1052	1384	802
PFA-CuCl$_2$	3151	1622	1100	984	632	860	459	-	-
PFA-ZnCl$_2$	3335	1621	1100	1109	641	-	-	-	-

From the above spectral data the tentative assignment of the complexes are shown in figures 1 and 2.

Antimicrobial study

All the ligands and complexes were tested for *in vitro* antimicrobial activity. The antimicrobial activity values of the compounds against pathogenic gram-positive and gram-negative bacteria and fungi are presented in Tables 3 and 4. The compound SBA and PFA showed poor antibacterial activity, while Co (II) complexes showed good activity against *Pseudomonas aeuroginosa (PC), E. coli(EC), bacillus cereus, salmonella typhi, klebsilla pneumonia* bacteria. The antifungal activity of the compounds was studied with pathogenic fungi, and the results are given in Table 5. Ampotericin B is used as a reference. All the compounds showed significant antifungal activity, especially compound PFA-Co complex, which showed higher activity than others. It was found that most of the

205

Orbital Elec. J. Chem*., Campo Grande*, 2(2): 201-208, 2010

synthesized compounds possess antimicrobial properties. It is observed from these studies that metal chelates presented higher activity than the free ligand. Such increased activity of the metal chelates can be explained on the basis of Overtone's concept and chelation theory [15]. According to Overtone's concept of cell permeability, the lipid membrane that surrounds the cell favours the passage of only lipid soluble materials due to which liposolubility is an important factor that controls antimicrobial activity. On chelation, the polarity of the metal ion is reduced to a greater extent due to the overlap of the ligand orbital and partial sharing of the positive charge of the metal ion with donor groups. Further, it increases the delocalization of electrons over the whole chelate ring and enhances the lipophilicity of the complex. This increased lipophilicity enhances the penetration of the complexes into lipid membranes and blocking of metal binding sites on the enzymes of the microorganism.
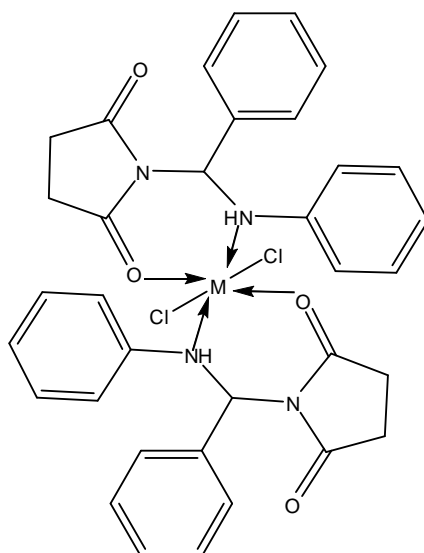

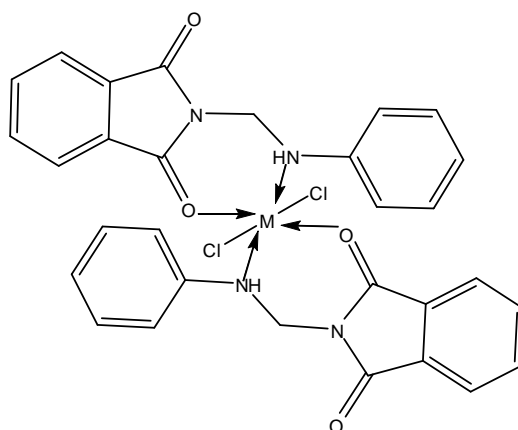**Figure 1**. 1-(phenyl(phenylamino)methyl)pyrrolidine-2,5-dione metal complexes.

Figure 2. 2-((phenylamino)methyl)isoindoline-1,3-dione metal complexes.

Table 3. Antibacterial activity zone of inhibition in mm against Pseudomonas aeruginosa(PA), E-coli(EC), salmonella typhi (ST), klebsilla pneumonia(KP), bacillus cereus (BC).

Compounds	ST	KP	EC	BC	PA
Streptomycin	29	26	33	23	30
SBA	-	2	-	-	-
SBA-CoCl$_2$	12	-	4	-	18
SBA-NiCl2	16	4	-	-	-
SBA-CuCl$_2$	-	8	-	-	-
PFA	3	-	3	-	-
PFA-CoCl$_2$	22	13	15	16	-
PFA-NiCl$_2$	-	-	-	-	-
PFA-CuCl$_2$	12	8	-	12	20
DMSO	-	-	-	-	-

Table 4. Antibacterial study of investigated compounds (MIC $\times$ 10^{-2} mol/L).

Compounds	MIC(µg/mL)	MBC(µg/mL)
SBA	KP-1.56	---
SBA-CoCl$_2$	ST- 1.56	---
SBA-CoCl$_2$	EC-12.5	---
SBA-CoCl$_2$	PA- 3.125	6.25
SBA-NiCl$_2$	ST- 3.125	6.25
SBA-NiCl$_2$	KP -6.25	---
PFA	ST-1.5	---
PFA	EC-1.52	---
PFA-CoCl$_2$	ST- 1.56	---
PFA-CoCl$_2$	KP- 12.5	---
PFA-CoCl$_2$	EC-6.25	12.5
PFA-CoCl$_2$	BC-1.525	3.125
PFA-CuCl$_2$	ST – 4.25	---
PFA-CuCl$_2$	KP-5.5	---
PFA-CuCl$_2$	BC-1.5	---
PFA-CuCl$_2$	PA-3.12	---

Table 5. Antifungal activity zone of inhibition in mm.

Compounds	A.O	A. F
Ampotericin B	20	16
SBA	-	-
SBA -CoCl$_2$	3	-
SBA –NiCl$_2$	-	-
SBA -CuCl$_2$	4	6
PFA	12	-
PFA -CoCl$_2$	18	12
PFA -NiCl$_2$	-	-
PFA -CuCl$_2$	2	-
DMSO	-	-

PA- *Pseudomonas aeuroginosa,*
EC- *E-coli,*
BC- *bacillus cereus,*
ST – *salmonella typhi*
KP- *klebsilla pneumonia*
A.O - *Aspergillus oryzae*
A.F - *Aspergillus fumigates*
MIC- minimum inhibitory concentration

207

Orbital Elec. J. Chem*., Campo Grande,* 2(2): 201-208, 2010

Two fold serial dilution method
50; 25; 12.5; 6.25; 3.125; 1.525; 0.7825; 0.3912.
----- No activity, No minimum bactericidal concentration (MBC)

References and Notes

[1]   Beyer, W.G. Manganese in Metabolism and Enzyme Function, New York: Academic Press, 1986.

[2]   Patel, I. A.; Thaker, B. T. *Indian J. Chem*. **1999**, *38A*, 427.

[3]   Tumer, M.; Koksal, H.; Sener, M. K.; Serin, S. *Transition Met. Chem*. **1999**, *24*, 414.

[4]   Al-Bari, M. A. A.; Khan, A.; Rahman, B. M.; Kudrat-E-Zahan, M.; Mossadik, A. M.; Islam, M. A U. *Research Journal of Agriculture and Biological Sciences* **2007**, *3*, 599.

[5]   Kant, R.; Chandrashekar, A. K.; Kumar, A. K. S. *Phosphorus, Sulfur, Silicon Relat. Elem.* **2008**, *183*, 1410.

[6]   Semenov, B. B.; Granik, V. G. *Pharm. Chem. J.* **2004**, *38*, 6.

[7]   Arend, M.; Westermann, B.; Risch, N. *Angew. Chem. Int. Ed*. **1998**, *37*, 1044.

[8]   Muller, R.; Goesmann, H.; Waldmann, H. *Angew. Chem. Int. Ed*. **1999**, *38*, 184.

[9]   Notz, W.; Tanaka, F.; Watanabe, S. I.; Chowdari, N. S.; Turner, J. M. Thayumanavan, R.; Barbas, C. F. *J. Org. Chem.* **2003**, *68*, 9624.

[10] Kowalski, K.; Zakrzewski, J. *Polyhedron* **1998**, 17, 2563.

[11] Sharmaan, C. L.; Mishra, D. V. *Can. J. Chem*. **1985**, *63*, 3027.

[12] Raman, N.; Raja, J. D.; Sakthivel, A. *Rus. J. Coord. Chem*. **2008**, *34*, 400.

[13] Krishna, C. H.; Mahapatra, C. M; Dush, K. C. *J. Inorg. Nucl. Chem*. **1977**, *39*, 1253.

[14] Kasim, A. N. M.; Venkappayya, D.; Prabhu, G. V. *J. Indian Chem. Soc*. **1999**, *76*, 67.

[15] Tweedy, B. G. *Phytopathology* **1964**, *55*, 910.